https://www.mdc-berlin.de/de/veroeffentlichungstypen/clinical-journal-club

Als gemeinsame Einrichtung von MDC und Charité fördert das Experimental and Clinical Research Center die Zusammenarbeit zwischen Grundlagenwissenschaftlern und klinischen Forschern. Hier werden neue Ansätze für Diagnose, Prävention und Therapie von Herz-Kreislauf- und Stoffwechselerkrankungen, Krebs sowie neurologischen Erkrankungen entwickelt und zeitnah am Patienten eingesetzt. Sie sind eingeladen, uns beizutreten. Bewerben Sie sich!

A 26-year-old man presented with sudden onset of severe pain in the legs and inability to move the left leg. On physical examination, he had complete loss of motor function in the left leg. Bedside ultrasonographic examination with color Doppler showed no blood flow in the distal aorta. Computed tomographic angiography of the abdomen revealed a saddle embolus at the aortoiliac junction (left). Emergency aortoiliac embolectomy was performed, and a gelatinous mass was removed. A subsequent transthoracic echocardiogram identified a heterogeneous mass in the left atrium (middle). On hospital day 2, cardiothoracic surgery was performed to remove the left atrial mass, and a villous, friable lesion was excised (right). Histopathology of the cardiac mass showed abundant mucopolysaccharide matrix with scattered nests of lepidic cells. What is the diagnosis?

Cardiac myxoma
Cardiac sarcoma
Intracardiac thrombus
Marantic endocarditis
Papillary fibroelastoma

Findings were consistent with a cardiac myxoma. A final diagnosis of acute abdominal aortic occlusion due to embolism of a left atrial myxoma was made. Genetic testing for the Carney complex, an inherited cancer syndrome associated with cardiac myxomas, was ordered but was not completed by the patient.

A myxoma is a primary heart (cardiac) tumor. This means that the tumor started within the heart. Most heart tumors start somewhere else.
Primary cardiac tumors such as myxomas are rare. About 75% of myxomas occur in the left atrium of the heart. They most often begin in the wall that divides the two upper chambers of the heart. They can occur in other intra-cardiac sites as well. Atrial myxomas are sometimes linked with valve obstruction stenosis and atrial fibrillation.

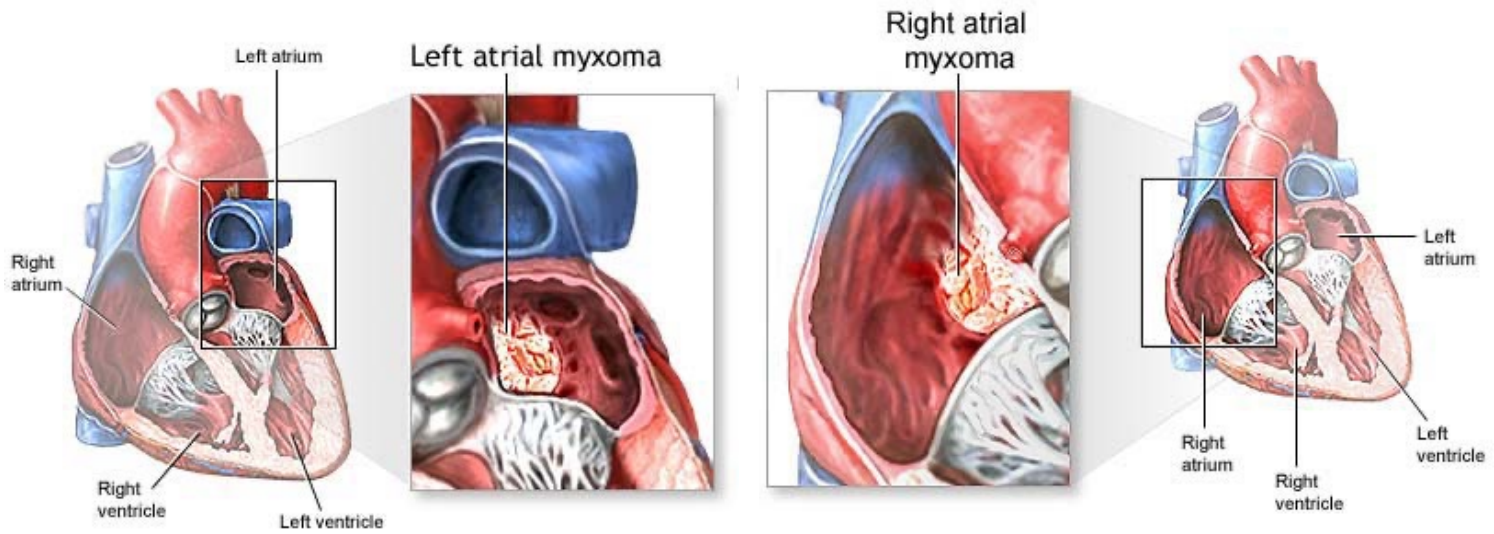

Der Carney-Komplex, kurz CNC, beschreibt ein Krankheitsbild mit multiplen Myxomen, hormonellen Regulationsstörungen, Pigmentflecken und teilweise malignen Neubildungen. Der CNC wird autosomal-dominant vererbt, wobei Keimbahnmutationen im Gen PRKAR1A für ca. 55 % aller Fälle verantwortlich sind. Dieses Gen kodiert die regulatorische Untereinheit 1-α der cAMP-abhängigen Proteinkinase A. Es handelt sich um ein Tumorsuppressorgen.

- Myxome des Myokards
- Herzinsuffizienz
- Embolien
- Ödeme
- Atemnot
- Herzinfarkt
- Leistungsabfall

Definition. Als Bronchiektase wird eine irreversible Ausweitung bzw. Aussackung eines Bronchus bezeichnet. Bronchiektasen treten bevorzugt in den dorsobasalen Lungenabschnitten auf und sind häufig von entzündlichen Vorgängen in der Bronchuswand und im umliegenden Gewebe begleitet.

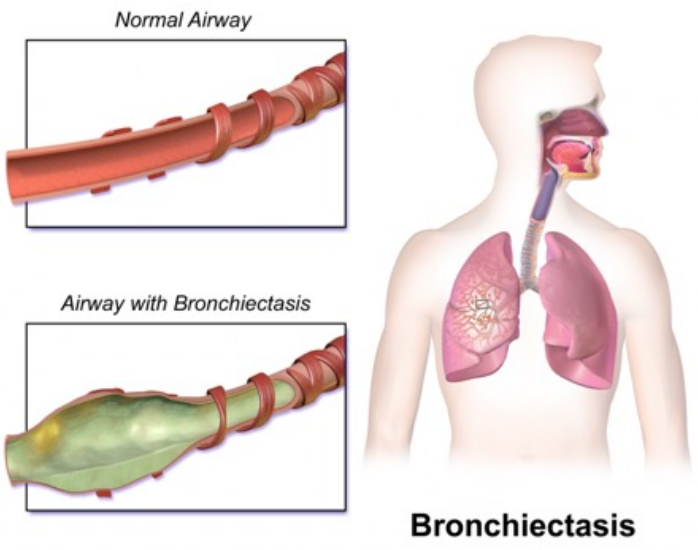

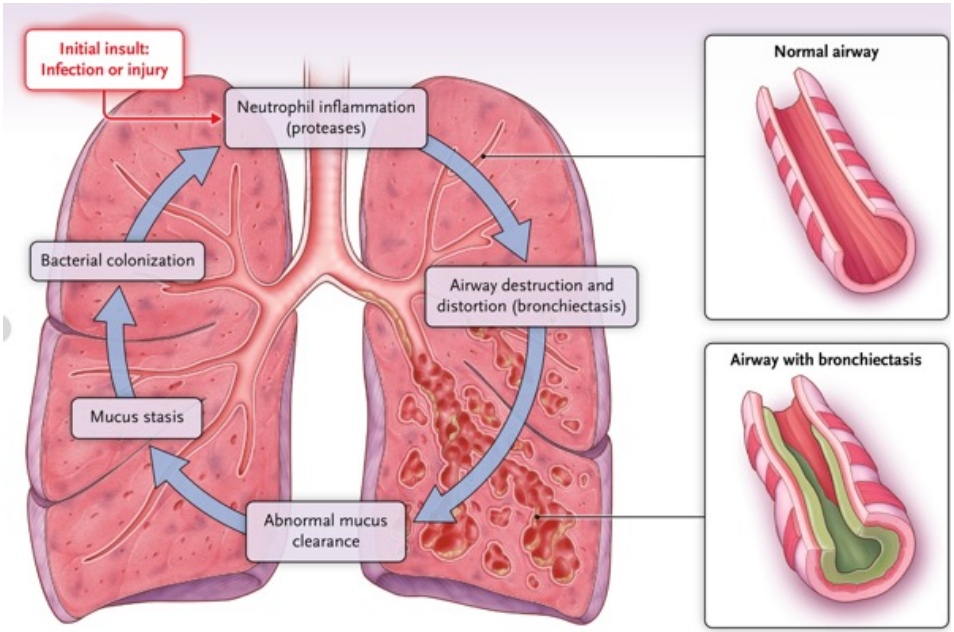

Defanging the Neutrophil to Treat Bronchiectasis

What Is Bronchiectasis?

Bronchiectasis is a chronic lung condition affecting approximately 0.5% of the population in high-income countries. Patients have permanently damaged airways, leading to symptoms of recurrent cough, sputum production, and respiratory tract infections. The most common cause is infectious disease, such as whooping cough, bacterial or viral pneumonia, and mycobacterial disease. Other causes include immune defects, connective-tissue disease (e.g., rheumatoid arthritis), primary ciliary dyskinesia, asthma, chronic obstructive pulmonary disease, allergic bronchopulmonary aspergillosis, inflammatory bowel disease, obstruction or foreign body, aspiration, and congenital or airway abnormality. The common end point is inflammation and permanent dilatation of the airways with impairment of the mucociliary escalator, which in turn impairs primary host defenses.

Neutrophils are a key secondary host defense. They differentiate and mature in the bone marrow, circulate in the blood, marginate on the endothelial layer, and extravasate from the blood vessel, whereupon they travel to sites of infection or inflamed tissue. At sites of infection, the neutrophil becomes activated and kills the pathogen by phagocytosis, release of reactive oxygen species.

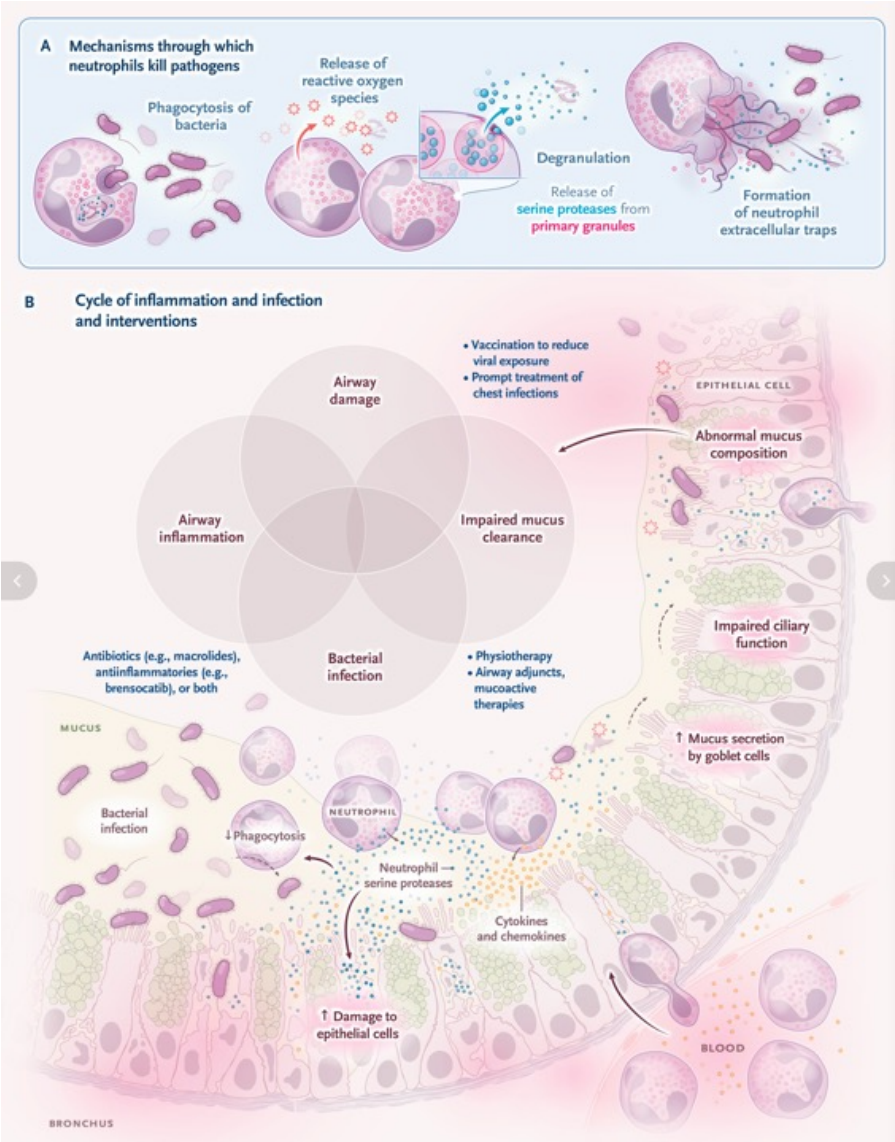

The Neutrophil — Defender and Offender.

Panel A shows the main mechanisms through which neutrophils kill pathogens. Panel B shows how free neutrophil elastase can perpetuate a cycle of infection and inflammation by damage to bronchial epithelial cells and increased apoptosis, increased mucus secretion by goblet cells, reduced ciliary beat frequency, increased levels of cytokines and chemokines, an increased number of neutrophils, and reduced neutrophil phagocytosis. The panel shows the pathogenesis of and interventions for bronchiectasis, in which a cycle of lung damage leads to events, including disrupted neutrophil function, that incur further lung damage. Both genetic and environmental factors may play a role in the development and progression of bronchiectasis. Currently, regular chest clearance with or without airway adjuncts is the mainstay of therapy for bronchiectasis. Annual vaccinations and prompt treatment of respiratory infections are advised to reduce the number of exacerbations and accelerate recovery from exacerbations. Long-term macrolide therapy and inhaled antibiotics (not licensed for use in bronchiectasis although used in clinical practice) are considered for patients with three or more exacerbations annually. Brensocatib represents a targeted antiinflammatory therapy for patients with bronchiectasis to reduce exacerbations and may attenuate the decline in lung function (which is measured by forced expiratory volume in 1 second [FEV_1]).

Brensocatib ist ein DPP-1-Inhibitor, der zur Zeit (2022) im Rahmen klinischer Studien zur Therapie von Bronchiektasen eingesetzt wird. Er gehört zur Klasse der Serinproteaseinhibitoren. Chronische Entzündungen des Lungengewebes unter der Mitwirkung von neutrophilen Granulozyten sind ein Pathomechanismus von Bronchiektasen. Neutrophile Granulozyten produzieren das Enzym neutrophile Elastase (ELA2, Elastase 2, Granulozytenelastase), das sich bei Patienten mit Bronchiektasen in Phasen einer Exazerbation in erhöhter Konzentration im Sputum nachweisen lässt. Eine übermäßige Aktivität der neutrophilen Elastase kann zu Gewebezerstörungen führen.
Brensocatib hemmt die Dipeptidylpeptidase I (DPP1), welche für die Aktivierung der neutrophilen Elastase benötigt wird. Dadurch wird der Umfang entzündlicher Gewebeveränderungen reduziert.

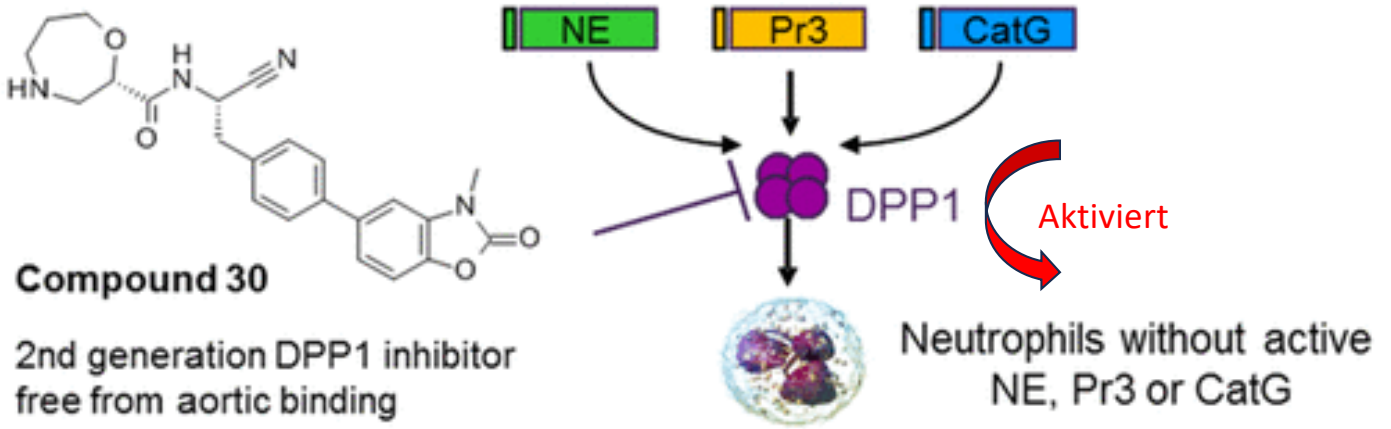

(when blocked by DPP1 inhibitor)

Neutrophil serine proteases, such as neutrophil elastase, are a key component of these processes. They are mainly stored within the primary granules. During the differentiation of neutrophils in the bone marrow, protease precursors within these granules are cleaved and thereby converted to functional enzymes by dipeptidyl peptidase 1 (DPP-1). Antiproteases, such as α_1-antitrypsin, secretory leukocyte protease inhibitor, elafin, and α_2-macroglobulin, keep these proteases in check at sites of infection. The main antiprotease is α_1-antitrypsin, produced mainly by the liver. When an imbalance between protease and antiprotease exists, as in cigarette smokers with severe α_1-antitrypsin deficiency, free neutrophil elastase and other proteases are in the airways. Because of the damaging effect of neutrophil elastase and other proteases on bronchial epithelial cells and alveoli, chronic bronchitis and panacinar emphysema develop in these persons at a young age.

How Does Brensocatib Work?

Brensocatib is an oral, selective, reversible inhibitor of DPP-1. Because DPP-1 has a pivotal role in the activation of the neutrophil serine proteases, its inhibition would be predicted to reduce the production of active neutrophil elastase and other proteases during neutrophil differentiation in the bone marrow. Indeed, Cipolla et al. reported lower levels of neutrophil elastase and other neutrophil proteases in the sputum of trial participants who received brensocatib than in those who received placebo. They also observed a reduction in neutrophil elastase activity in white cells. Chalmers et al. found prolonged time to first exacerbation over 24 weeks of treatment with brensocatib.

Phase 3 Trial of the DPP-1 Inhibitor Brensocatib in Bronchiectasis

In bronchiectasis, neutrophilic inflammation is associated with an increased risk of exacerbations and disease progression. Brensocatib, an oral, reversible inhibitor of dipeptidyl peptidase 1 (DPP-1), targets neutrophil serine proteases, key mediators of neutrophilic inflammation. In a phase 3, double-blind trial, we randomly assigned patients with bronchiectasis (in a 1:1:1 ratio for adults and a 2:2:1 ratio for adolescents) to receive brensocatib (10 mg or 25 mg once per day) or placebo. The primary end point was the annualized rate of adjudicated pulmonary exacerbations over a 52-week period. The secondary end points, listed in hierarchical testing order, were the time to the first exacerbation during the 52-week period; the percentage of patients remaining exacerbation-free at week 52; the change in forced expiratory volume in 1 second (FEV_1); the annualized rate of severe exacerbations; and change in quality of life.

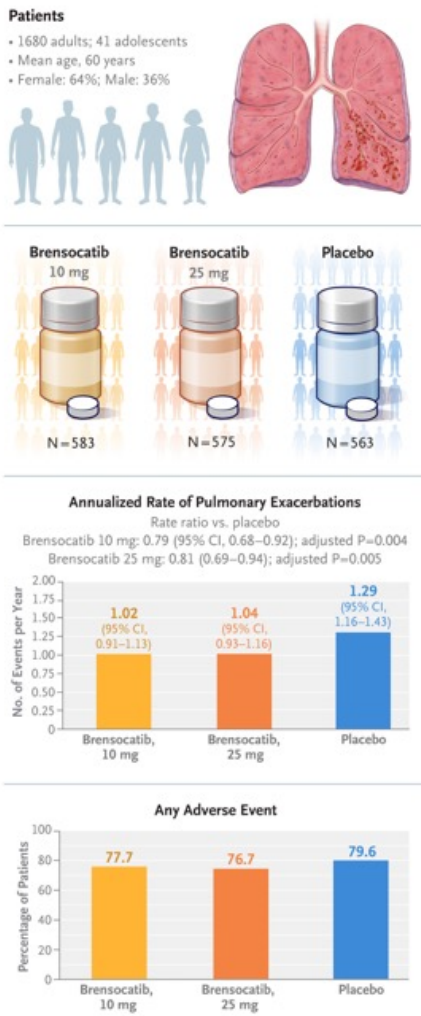

A consistent and established standard of care for bronchiectasis is lacking. International guidelines recommend airway clearance techniques, mucoactive agents, and antibiotics for the treatment of infection, but current approaches do not adequately address inflammation or slow disease progression.
Brensocatib is an oral, selective, competitive, and reversible inhibitor of DPP-1. In the phase 2 WILLOW trial involving adults with bronchiectasis, treatment with a 10-mg or 25-mg dose of brensocatib, administered once daily for 24 weeks, prolonged the time to the first exacerbation and led to a lower rate of exacerbations than placebo. We conducted an international, phase 3, double-blind, randomized, placebo-controlled trial (ASPEN) involving adult and adolescent patients with bronchiectasis to evaluate the efficacy and safety of 52 weeks of once-daily 10-mg or 25-mg brensocatib added to existing clinical management.

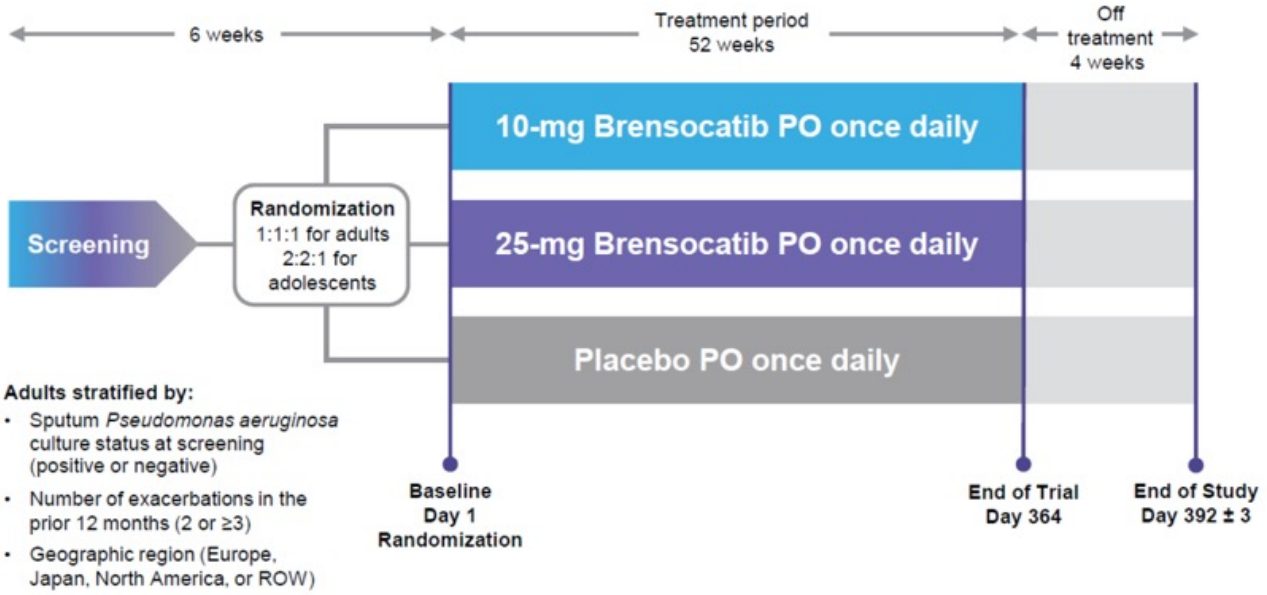

Characteristic	Brensocatib, 10 mg (N=583)	Brensocatib, 25 mg (N=575)	Placebo (N=563)
Age			
Mean — yr	59.8±15.9	60.6±15.8	60.0±15.4
Distribution — no. (%)			
≥75 yr	83 (14.2)	84 (14.6)	93 (16.5)
18 to 74 yr	483 (82.8)	475 (82.6)	462 (82.1)
<18 yr	17 (2.9)	16 (2.8)	8 (1.4)
Female sex — no. (%)	385 (66.0)	360 (62.6)	362 (64.3)
Race or ethnic group — no. (%)†			
White	431 (73.9)	430 (74.8)	405 (71.9)
Asian	63 (10.8)	64 (11.1)	64 (11.4)
More than one race or ethnic group	25 (4.3)	20 (3.5)	21 (3.7)
American Indian or Alaska Native	8 (1.4)	6 (1.0)	9 (1.6)
Black or African American	2 (0.3)	5 (0.9)	3 (0.5)
Native Hawaiian or Pacific Islander	1 (0.2)	0	1 (0.2)
Other	5 (0.9)	4 (0.7)	1 (0.2)
Unknown or not reported	48 (8.2)	46 (8.0)	59 (10.5)
Body-mass index‡	25.5±5.4	25.4±5.1	25.1±4.9
Most common causes of bronchiectasis — no. (%)§			
Idiopathic or other	331 (56.8)	354 (61.6)	321 (57.0)
Injury: pneumonia or childhood infection	173 (29.7)	156 (27.1)	174 (30.9)
Cilia abnormalities: primary ciliary dyskinesia	47 (8.1)	38 (6.6)	33 (5.9)
Long-term use of antibiotics — no. (%)	146 (25.0)	154 (26.8)	133 (23.6)
Macrolides	110 (18.9)	114 (19.8)	105 (18.7)
Inhaled antibiotics	41 (7.0)	40 (7.0)	36 (6.4)
Use of inhaled glucocorticoids — no. (%)	324 (55.6)	324 (56.3)	352 (62.5)
Pseudomonas aeruginosa–positive sputum sample — no. (%)	203 (34.8)	205 (35.7)	199 (35.3)
Exacerbations in previous 12 mo — no. (%)			
2¶	411 (70.5)	412 (71.7)	396 (70.3)
≥3	172 (29.5)	163 (28.3)	167 (29.7)
Bronchiectasis Severity Index score — points‖	7.1±3.5	7.1±3.6	7.1±3.6
Hospitalized for exacerbation in previous 24 mo — no. (%)	146 (25.0)	133 (23.1)	142 (25.2)
Postbronchodilator FEV_1 — % of predicted value**	74.3±23.4	74.3±24.6	71.9±22.2
Blood eosinophil count — no. (%)			
<300 cells/mm³	465 (79.8)	461 (80.2)	452 (80.3)
≥300 cells/mm³	115 (19.7)	111 (19.3)	106 (18.8)
Missing data	3 (0.5)	3 (0.5)	5 (0.9)
History of COPD — no. (%)	77 (13.2)	83 (14.4)	102 (18.1)
History of asthma — no. (%)	101 (17.3)	109 (19.0)	111 (19.7)
Smoking status — no. (%)††			
Never	419 (71.9)	412 (71.7)	380 (67.5)
Former	164 (28.1)	163 (28.3)	183 (32.5)
QOL-B RSS — points‡‡	59.8±17.0	61.9±17.2	60.0±16.8

Primary and Secondary End Points (Intention-to-Treat Population).

End Point	Brensocatib, 10 mg (N=583)	Brensocatib, 25 mg (N=575)	Placebo (N=563)
Primary end point			
Annualized rate of pulmonary exacerbations — no. of events/yr (95% CI)	1.02 (0.91 to 1.13)	1.04 (0.93 to 1.16)	1.29 (1.16 to 1.43)
Rate ratio (95% CI)	0.79 (0.68 to 0.92)	0.81 (0.69 to 0.94)	—
Adjusted P value	0.004	0.005	—
Secondary end points			
Hazard ratio for the time to the first exacerbation during the treatment period (95% CI)	0.81 (0.70 to 0.95)	0.83 (0.70 to 0.97)	—
Adjusted P value	0.02	0.04	—
Exacerbation-free during the treatment period — no. (%)†	283 (48.5)	279 (48.5)	227 (40.3)
Rate ratio for remaining exacerbation-free at week 52 (95% CI)‡	1.20 (1.06 to 1.37)	1.18 (1.04 to 1.34)	—
Adjusted P value§	0.02	0.04	—
Postbronchodilator FEV_1			
LS mean change from baseline to wk 52 — ml¶	−50±9	−24±10	−62±9
LS mean difference vs. placebo (95% CI) — ml	11 (−14 to 37)	38 (11 to 65)	—
Adjusted P value	0.38	0.04	—
Annualized rate of severe exacerbations (95% CI) — no. of events/yr	0.14 (0.10 to 0.18)	0.14 (0.11 to 0.18)	0.19 (0.14 to 0.24)
Rate ratio (95% CI)	0.74 (0.51 to 1.09)	0.74 (0.52 to 1.06)	—
Adjusted P value	NA	0.21	—
QOL-B RSS			
LS mean change from baseline to wk 52 — points‖	6.84±0.77	8.58±0.76	4.81±0.75
LS mean difference vs. placebo (95% CI) — points	2.03 (−0.08 to 4.14)	3.77 (1.68 to 5.85)	—

Exacerbations over the 52-Week Treatment Period, Time to the First Pulmonary Exacerbation, Patients Remaining Exacerbation-free, and Change in Postbronchodilator FEV_1 (Intention-to-Treat Population).

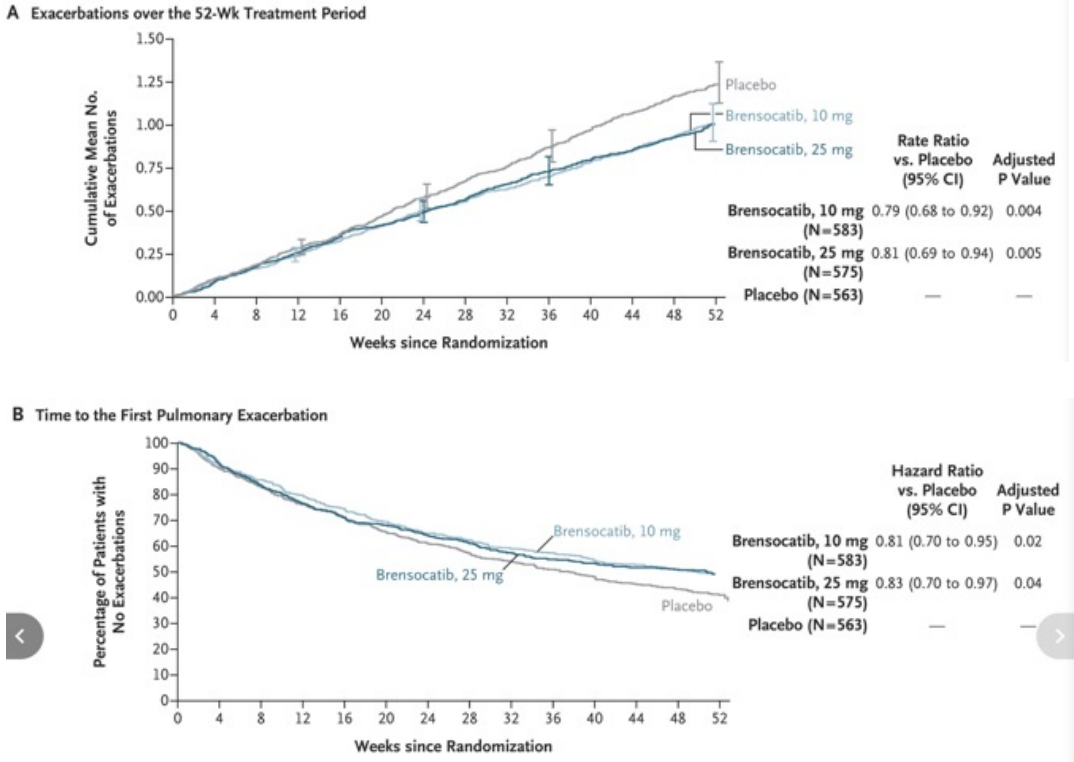

Safety Analyses.

Event	Brensocatib, 10 mg (N=582)	Brensocatib, 25 mg (N=574)	Placebo (N=563)
		number (percent)	
Any adverse event	452 (77.7)	440 (76.7)	448 (79.6)
Severe adverse event	74 (12.7)	67 (11.7)	90 (16.0)
Adverse event determined by an investigator to be related to brensocatib or placebo	72 (12.4)	85 (14.8)	73 (13.0)
Serious adverse event†	101 (17.4)	97 (16.9)	108 (19.2)
Serious adverse event determined by an investigator to be related to brensocatib or placebo	0	1 (0.2)	0
Adverse event resulting in death‡	3 (0.5)	4 (0.7)	7 (1.2)
Adverse event leading to discontinuation of brensocatib or placebo	25 (4.3)	22 (3.8)	23 (4.1)
Adverse event leading to trial withdrawal	14 (2.4)	16 (2.8)	16 (2.8)
Most common adverse events§			
Covid-19	92 (15.8)	120 (20.9)	89 (15.8)
Nasopharyngitis	45 (7.7)	36 (6.3)	43 (7.6)
Cough	41 (7.0)	35 (6.1)	36 (6.4)
Headache	39 (6.7)	49 (8.5)	39 (6.9)
Most common serious adverse events¶			
Bronchiectasis‖	47 (8.1)	48 (8.4)	67 (11.9)
Pneumonia	11 (1.9)	13 (2.3)	16 (2.8)
Any adverse event of special interest**	42 (7.2)	56 (9.8)	53 (9.4)
Hyperkeratosis	8 (1.4)	17 (3.0)	4 (0.7)
Periodontitis or gingivitis	8 (1.4)	12 (2.1)	15 (2.7)
Severe infection	4 (0.7)	7 (1.2)	4 (0.7)
Pneumonia	23 (4.0)	27 (4.7)	33 (5.9)

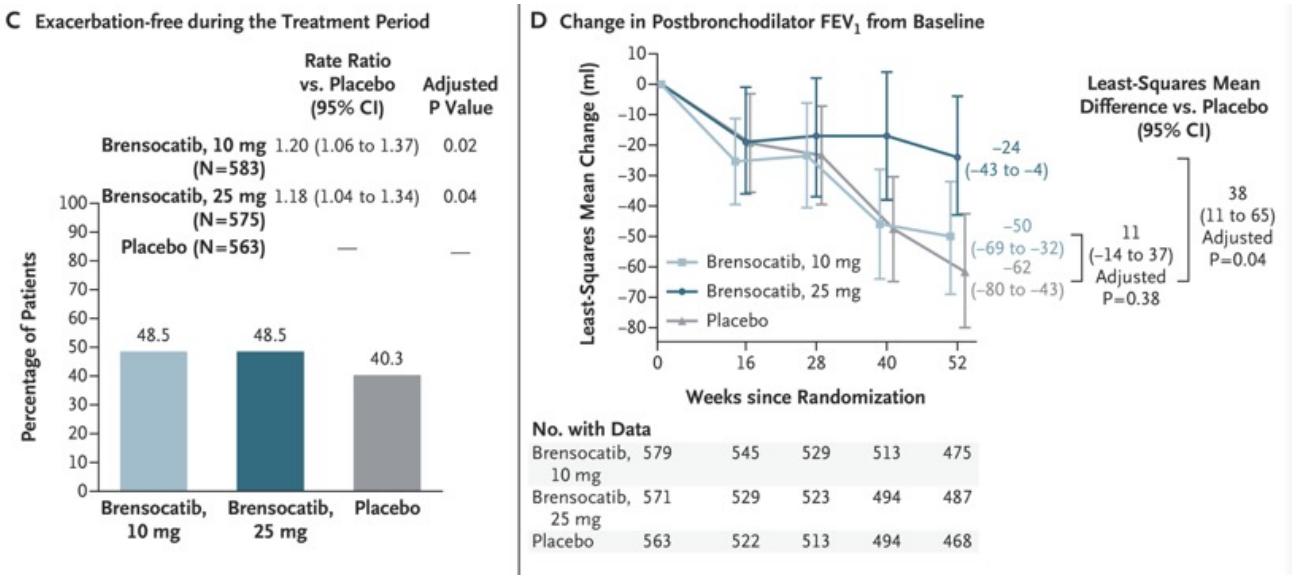

Panel C shows the percentage of patients who remained exacerbation-free during the treatment period according to trial group. These data are based on multiple imputation, because patients who discontinued brensocatib or placebo or withdrew from the trial early might have had a pulmonary exacerbation had they remained in the trial. The rate ratio for remaining exacerbation-free is reported here, although the odds ratio is the prespecified statistical inference in the statistical analysis plan. The reported P values are based on the odds ratio from the logistic-regression model, as prespecified in the statistical analysis plan, because these P values were used in the hierarchical testing. Panel D shows the least-squares mean change from baseline in the forced expiratory volume in 1 second (FEV_1), which was analyzed with the use of a linear repeated-measures model that included trial group, visit, trial-group-by-visit interaction, age group, and randomization stratification factors (*Pseudomonas aeruginosa*–positive sputum-culture status at screening, the number of exacerbations in the previous 12 months, and geographic region) as fixed effects and the baseline FEV_1 value as a covariate. P values (brensocatib vs. placebo) were calculated on the basis of the Wald test of the logistic-regression model. I bars indicate 95% confidence intervals.

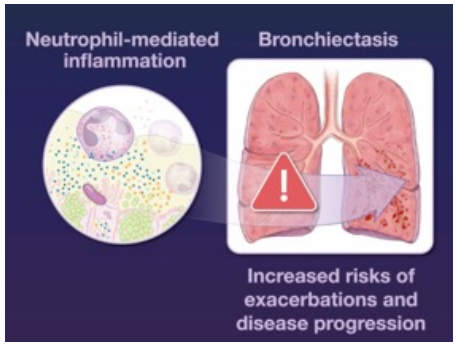
Neutrophil-mediated inflammation
Bronchiectasis
Increased risks of exacerbations and disease progression

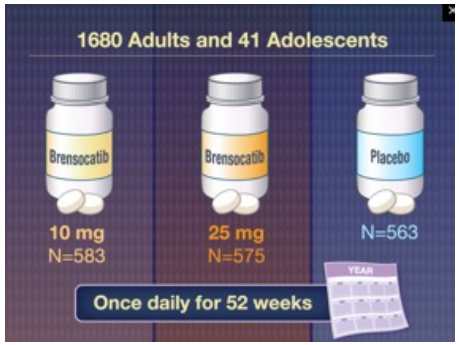
1680 Adults and 41 Adolescents
Brensocatib
Brensocatib
Placebo
10 mg
N=583
25 mg
N=575
N=563
Once daily for 52 weeks
YEAR

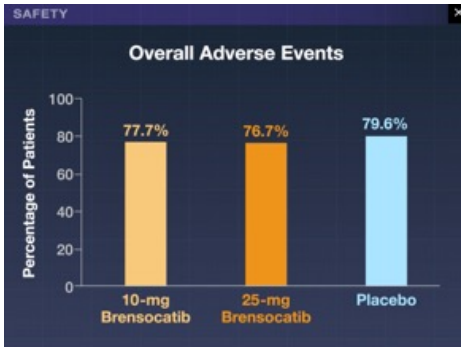
SAFETY
Overall Adverse Events
Percentage of Patients
100
80
60
40
20
0
77.7%
76.7%
79.6%
10-mg Brensocatib
25-mg Brensocatib
Placebo

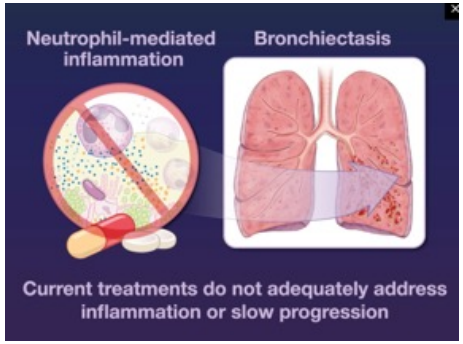
Neutrophil-mediated inflammation
Bronchiectasis
Current treatments do not adequately address inflammation or slow progression

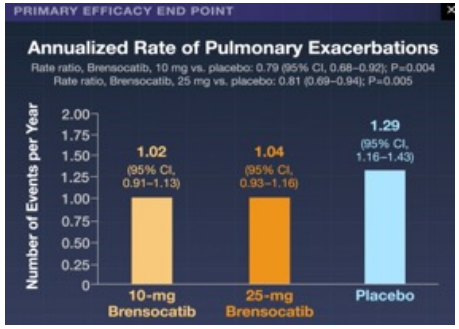
PRIMARY EFFICACY END POINT
Annualized Rate of Pulmonary Exacerbations
Rate ratio, Brensocatib, 10 mg vs. placebo: 0.79 (95% CI, 0.68–0.92); P=0.004
Rate ratio, Brensocatib, 25 mg vs. placebo: 0.81 (0.69–0.94); P=0.005
Number of Events per Year
2.00
1.75
1.50
1.25
1.00
0.75
0.50
0.25
0
1.02
(95% CI, 0.91–1.13)
1.04
(95% CI, 0.93–1.16)
1.29
(95% CI, 1.16–1.43)
10-mg Brensocatib
25-mg Brensocatib
Placebo

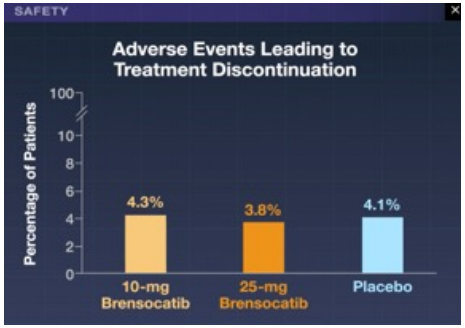
SAFETY
Adverse Events Leading to Treatment Discontinuation
Percentage of Patients
100
10
8
6
4
2
0
4.3%
3.8%
4.1%
10-mg Brensocatib
25-mg Brensocatib
Placebo

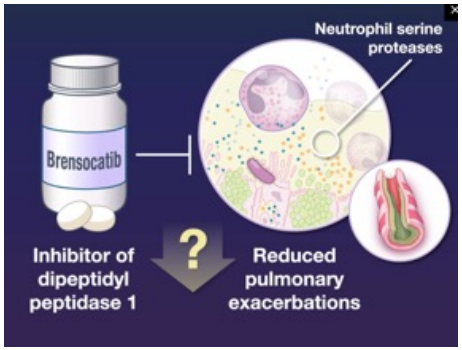
Neutrophil serine proteases
Brensocatib
Inhibitor of dipeptidyl peptidase 1
?
Reduced pulmonary exacerbations

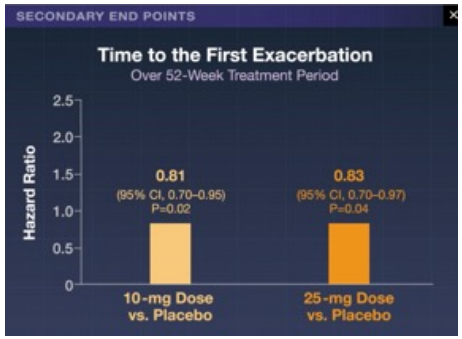
SECONDARY END POINTS
Time to the First Exacerbation
Over 52-Week Treatment Period
Hazard Ratio
2.5
2.0
1.5
1.0
0.5
0
0.81
(95% CI, 0.70–0.95)
P=0.02
0.83
(95% CI, 0.70–0.97)
P=0.04
10-mg Dose vs. Placebo
25-mg Dose vs. Placebo

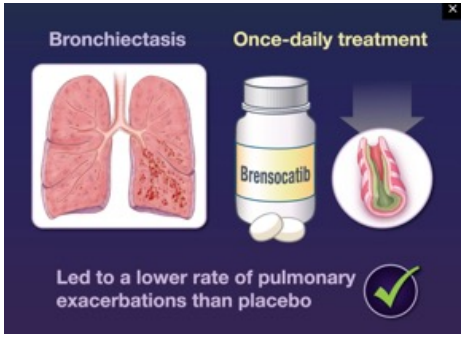
Bronchiectasis
Once-daily treatment
Brensocatib
Led to a lower rate of pulmonary exacerbations than placebo

Was ist Influenza? Die echte Grippe, auch Influenza genannt, ist eine akute Krankheit der Atemwege. Sie ist eine ernsthafte, mitunter auch lebensbedrohliche Krankheit, die durch Grippeviren ausgelöst wird. Erkältungen oder „grippale Infekte“ dagegen werden von anderen Erregern verursacht.

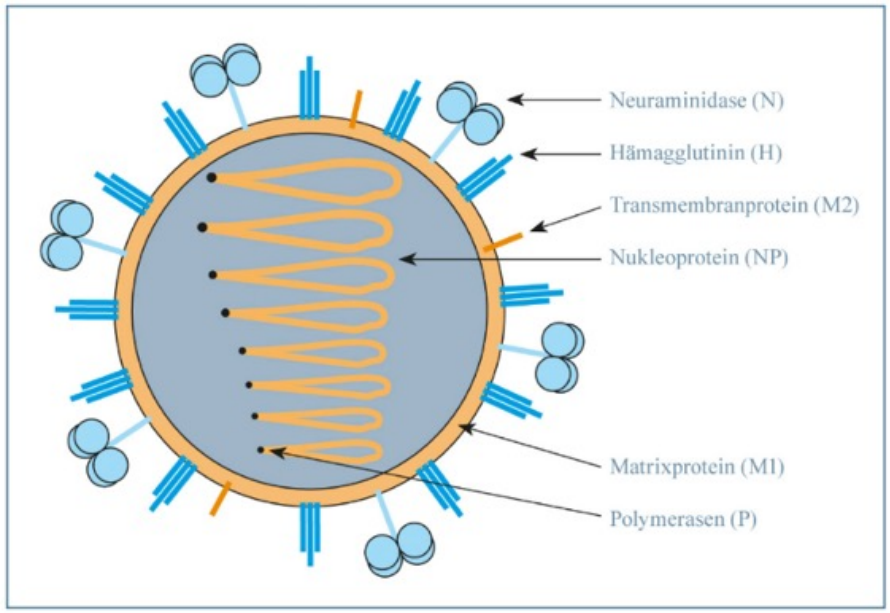

Baloxavir marboxil hemmt ein Enzym des Influenza-Virus, die CAP-abhängige Endonuklease PA, wodurch der Virus seine RNA-Replikation nicht fortsetzen kann. Dieser Wirkmechanismus ist einzigartig unter den antiviralen Medikamenten gegen Influenza.

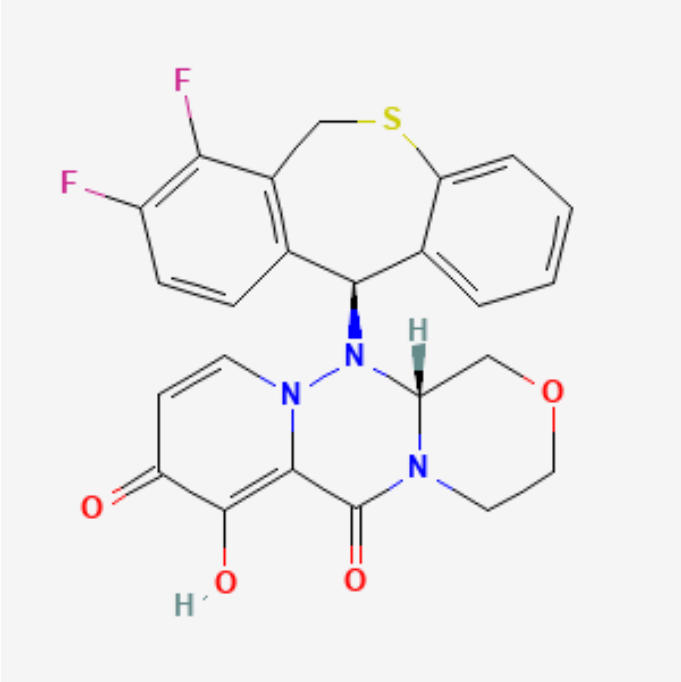

Efficacy of Baloxavir Treatment in Preventing Transmission of Influenza

Baloxavir marboxil (baloxavir) rapidly reduces influenza virus shedding, which suggests that it may reduce transmission. Studies of treatment with neuraminidase inhibitors have not shown sufficient evidence that they prevent transmission to contacts. We conducted a multicountry, phase 3b trial to assess the efficacy of single-dose baloxavir treatment to reduce influenza transmission from index patients to household contacts. Influenza-positive index patients 5 to 64 years of age were randomly assigned in a 1:1 ratio to receive baloxavir or placebo within 48 hours after symptom onset. The primary end point was transmission of influenza virus from an index patient to a household contact by day 5. The first secondary end point was transmission of influenza virus by day 5 that resulted in symptoms.

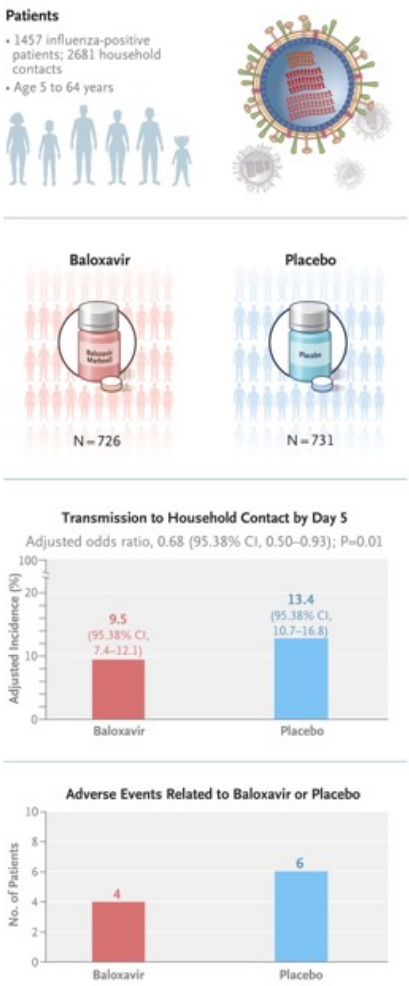

Baloxavir marboxil (baloxavir), an influenza virus cap-dependent endonuclease inhibitor ("cap" refers to a 7-methyl guanosine that is added to the 5′ end of the host messenger RNA strand), is administered orally as a single dose and has shown efficacy as treatment and postexposure prophylaxis for influenza. In phase 3 studies, baloxavir was shown to rapidly reduce influenza virus titers and stop shedding of infectious virus faster than oseltamivir, findings that suggest the potential for baloxavir to reduce transmission. Approximately one third of influenza virus transmission occurs within households, and the risk of transmission from infected index patients to their household contacts can be as high as 38%. Therefore, households offer a unique opportunity to evaluate the effect of baloxavir for "treatment to reduce transmission" more efficiently than in other settings. We conducted the CENTERSTONE trial, a phase 3b, double-blind, randomized, placebo-controlled trial, to evaluate the efficacy of baloxavir in the prevention of influenza virus transmission in households.

Eligible index patients were 5 to 64 years of age, had a positive polymerase-chain-reaction (PCR) test or antigen test for influenza, had a negative PCR or antigen test for severe acute respiratory syndrome coronavirus 2 (SARS-CoV-2), underwent screening within 48 hours after symptom onset, and lived in a household with at least one eligible household contact. The required number of eligible, unvaccinated household contacts, was changed from at least two to at least one after trial commencement to permit households with only two occupants or those in regions where the number of influenza vaccinations may have increased during the Covid-19 pandemic to participate. Household contacts underwent screening within 24 hours after the index patient had undergone randomization and were eligible for enrollment if all the contacts in the household tested negative for influenza and SARS-CoV-2, at least one contact in the household had not received an influenza vaccine within 6 months.

Randomization and Treatment

Eligible index patients were randomly assigned in a 1:1 ratio to receive either a single oral dose of baloxavir or matching placebo, within 2 hours after randomization. Randomization was performed with the use of an interactive Web-response system. In patients 12 years of age or older, baloxavir was administered in tablet form at a dose of 40 mg for those weighing less than 80 kg or 80 mg for those weighing 80 kg or greater. In patients younger than 12 years of age, baloxavir was administered in an oral suspension at a dose of 2 mg per kilogram of body weight for those weighing less than 20 kg or 40 mg for those weighing 20 kg or greater.

End Points

The primary efficacy end point was transmission of influenza virus from an index patient to a household contact by day 5 after randomization, as determined by a positive PCR test for influenza and a virus type and subtype consistent with those of the index patient. All household contacts were tested for influenza on or before day 5, regardless of whether they had symptoms.

Enrollment, Randomization, and Follow-up.

Patients (randomized to baloxavir or placebo)

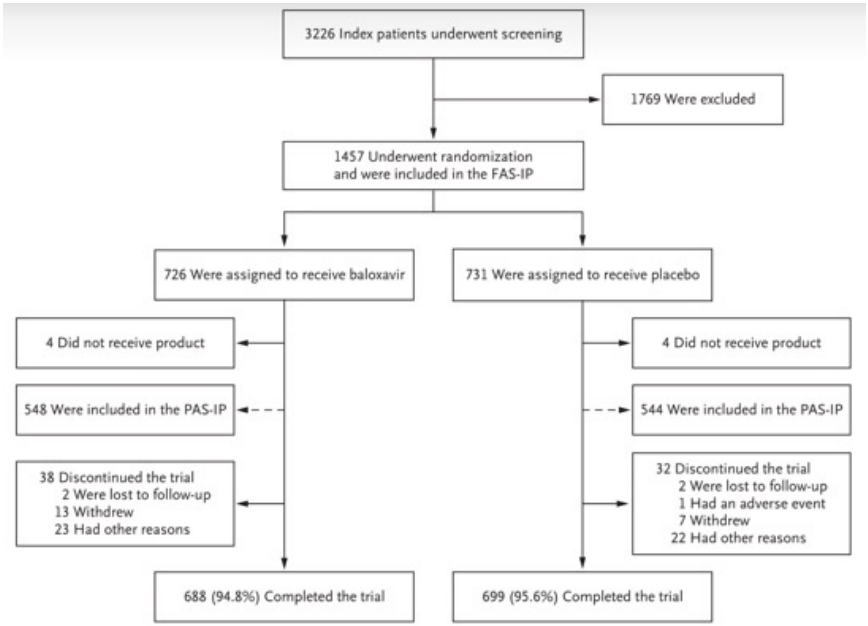

Household contacts (were tested for influenza virus)

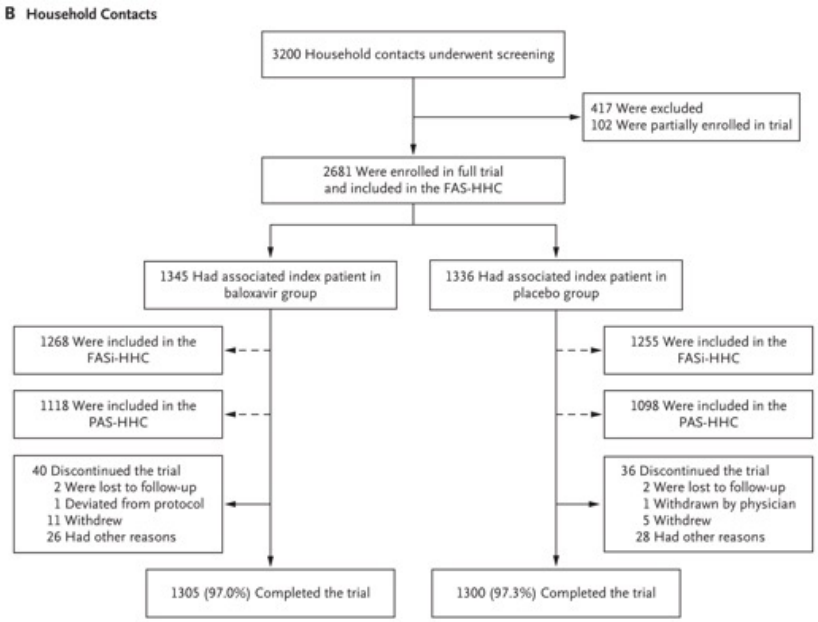

Characteristic	Index Patients in Baloxavir Group (N=548)	Index Patients in Placebo Group (N=544)	Index Patient in Baloxavir Group (N=1118)	Index Patient in Placebo Group (N=1098)
Age — yr				
Mean	30.8±15.2	31.8±15.9	35.4±18.6	35.1±18.3
Median	30.0	30.0	36.0	35.5
Age group — no. (%)				
Index patients				
<12 yr	44 (8.0)	46 (8.5)	—	—
12 to 30 yr	245 (44.7)	235 (43.2)	—	—
>30 yr	259 (47.3)	263 (48.3)	—	—
Household contacts				
2 to <12 yr	—	—	121 (10.8)	118 (10.7)
≥12 yr	—	—	997 (89.2)	980 (89.3)
Sex — no. (%)				
Male	248 (45.3)	266 (48.9)	525 (47.0)	486 (44.3)
Female	300 (54.7)	278 (51.1)	593 (53.0)	612 (55.7)
Geographic region — no. (%)				
Europe	243 (44.3)	250 (46.0)	418 (37.4)	444 (40.4)
Asia	139 (25.4)	139 (25.6)	284 (25.4)	289 (26.3)
United States	141 (25.7)	135 (24.8)	373 (33.4)	334 (30.4)
Rest of the world	25 (4.6)	20 (3.7)	43 (3.8)	31 (2.8)
Maximum duration of influenza symptoms — no. (%)				
≤24 hr	292 (53.3)	288 (52.9)	NA	NA
>24 to 48 hr	256 (46.7)	256 (47.1)	NA	NA
No. of household contacts in the PAS-HHC†				
Mean	2.04±1.09	2.02±1.09	NA	NA
Median	2	2	NA	NA
Influenza season — no. (%)‡				
2019–2020	92 (16.8)	87 (16.0)	257 (23.0)	230 (20.9)
2020–2021	0	0	0	0
2021–2022	41 (7.5)	41 (7.5)	88 (7.9)	98 (8.9)
2022–2023	184 (33.6)	182 (33.5)	346 (30.9)	341 (31.1)
2023–2024	231 (42.2)	234 (43.0)	427 (38.2)	429 (39.1)
Influenza virus type — no. (%)§				
Type A¶	450 (82.1)	451 (82.9)	907 (81.1)	899 (81.9)
Type B‖	93 (17.0)	91 (16.7)	201 (18.0)	193 (17.6)
Type A and B	5 (0.9)	2 (0.4)	10 (0.9)	6 (0.5)
Influenza virus A subtype — no./total no. (%)§				
H1N1pdm09	220/455 (48.4)	228/453 (50.3)	451/917 (49.2)	454/905 (50.2)
H3N2	213/455 (46.8)	202/453 (44.6)	420/917 (45.8)	404/905 (44.6)
H1N1pdm09 and H3N2	2/455 (0.4)	2/453 (0.4)	3/917 (0.3)	3/905 (0.3)
Unknown	20/455 (4.4)	19/453 (4.2)	43/917 (4.7)	42/905 (4.6)
Missing	0/455	2/453 (0.4)	0/917	2/905 (0.2)

Primary and First Secondary End Points.

End Point	HHCs of Index Patient in Baloxavir Group (N=1118)	HHCs of Index Patient in Placebo Group (N=1098)
Primary end point: transmission of influenza virus by day 5		
HHCs with an end-point event — no. (%)	94 (8.4)	131 (11.9)
Adjusted incidence of transmission (95.38% CI) — %†	9.5 (7.4 to 12.1)	13.4 (10.7 to 16.8)
Adjusted odds ratio (95.38% CI)†‡	0.68 (0.50 to 0.93)	—
P value†	0.01	—
Adjusted relative risk reduction (95.38% CI) — % ‡§	29 (12 to 45)	—
First secondary end point: transmission of influenza virus by day 5 that resulted in symptoms¶		
HHCs with an end-point event — no. (%)	56 (5.0)	72 (6.6)
Adjusted incidence of transmission (95.38% CI) — %†	5.8 (4.1 to 8.2)	7.6 (5.7 to 10.2)
Adjusted odds ratio (95.38% CI)†‡	0.75 (0.50 to 1.12)	—
P value†	0.16	—
Adjusted relative risk reduction (95.38% CI) — %‡§	24 (−2 to 46)	—

Other Secondary End Points at the Household (HH) or HHC Level.

End Point	HHs or HHCs of Index Patient in Baloxavir Group	HH or HHCs of Index Patient in Placebo Group
Transmission of influenza virus by day 5 at the HH level		
HHs with ≥1 HHC with an end-point event — no./total no. (%)	85/548 (15.5)	106/544 (19.5)
Odds ratio (95% CI)	0.76 (0.56 to 1.05)	—
Relative risk reduction (95% CI) — %	20 (−4 to 38)	—
Transmission of influenza virus by day 5 that resulted in symptoms at the HH level†		
HHs with ≥1 HHC with an end-point event — no./total no. (%)	47/548 (8.6)	65/544 (11.9)
Odds ratio (95% CI)	0.69 (0.46 to 1.03)	—
Relative risk reduction (95% CI) — %	28 (−3 to 49)	—
Transmission of influenza virus by day 9 at the HHC level‡		
Evaluable contact cases — no./total no.	1081/1118	1038/1098
HHCs with an end-point event — no./total no. (%)	101/1081 (9.3)	141/1038 (13.6)
Adjusted incidence of transmission (95% CI) — %§	10.8 (8.4 to 13.7)	15.4 (12.2 to 19.2)
Adjusted odds ratio (95% CI)§	0.66 (0.48 to 0.91)	—
Adjusted relative risk reduction (95% CI) — %¶	30 (13 to 44)	—
Transmission of influenza virus by day 9 that resulted in symptoms at the HHC level†‡		
Evaluable contact cases — no./total no.	1079/1118	1037/1098
HCCs with an end-point event — no./total no. (%)	57/1079 (5.3)	73/1037 (7.0)
Adjusted incidence of transmission (95% CI) — % §	6.2 (4.4 to 8.5)	8.3 (6.1 to 11.0)
Adjusted odds ratio (95% CI)§	0.73 (0.49 to 1.09)	—
Adjusted relative risk reduction (95% CI) — %¶	26 (1 to 47)	—
Any infection with influenza virus by day 9 at the HHC level‖		
Evaluable contact cases — no./total no.	1071/1118	1040/1098
HHCs with an end-point event — no./total no. (%)	130/1071 (12.1)	173/1040 (16.6)
Adjusted incidence of transmission (95% CI) — %§	14 (11.4 to 17.1)	18.7 (15.4 to 22.5)
Adjusted odds ratio (95% CI)§	0.71 (0.54 to 0.94)	—
Adjusted relative risk reduction (95% CI) — %¶	25 (8 to 37)	—
Any infection with influenza virus by day 9 that resulted in symptoms at the HHC level†**		
Evaluable contact cases — no./total no.	1069/1118	1039/1098
Household contacts with an end-point event — no./total no. (%)	61/1069 (5.7)	80/1039 (7.7)
Adjusted incidence of transmission (95% CI) — %§	6.4 (4.6 to 8.9)	8.7 (6.5 to 11.6)
Adjusted odds ratio (95% CI)§	0.72 (0.49 to 1.06)	—
Adjusted relative risk reduction (95% CI) — %¶	26 (3 to 46)	—

Development of Resistance in Baloxavir-Treated Index Patients.

Patients and Substitution	Influenza A(H1N1pdm09)	Influenza A(H3N2)	Influenza B	Total†
All baloxavir-treated index patients — no.	69	88	53	208
Any PA I38X or T20K substitution at baseline — no. (%)	0	0	0	0
Any PA I38X or T20K substitution that emerged during follow-up — no. (%)‡	5 (7.2)	10 (11.4)	0	15 (7.2)
Baloxavir-treated index patients <12 yr of age — no.	4	18	3	25
Any PA I38X or T20K substitution that emerged during follow-up — no. (%)‡	1 (25.0)	3 (16.7)	0	4 (16.0)
PA I38N — no. (%)	1 (25.0)	0	0	1 (4.0)
PA I38T — no. (%)	0	3 (16.7)	0	3 (12.0)
PA I38T and I38I — no. (%)	0	1 (5.6)§	0	1 (4.0)
Baloxavir-treated index patients ≥12 yr of age — no.	65	70	50	183
Any PA I38X or T20K substitution that emerged during follow-up — no. (%)‡	4 (6.2)	7 (10.0)	0	11 (6.0)
PA I38M — no. (%)	0	1 (1.4)	0	1 (0.5)
PA I38T — no. (%)	3 (4.6)	6 (8.6)	0	9 (4.9)
PA I38T and I38I — no. (%)	1 (1.5)	0	0	1 (0.5)

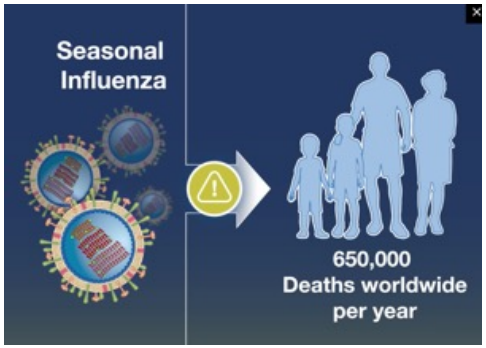
Seasonal Influenza
650,000 Deaths worldwide per year


CENTERSTONE TRIAL
• Phase 3b
• Randomized
• Double-blind
• Placebo-controlled
• 1457 Influenza-positive patients
• Age 5 to 64 years
• 2681 Household contacts
• Enrolled across 5 influenza seasons

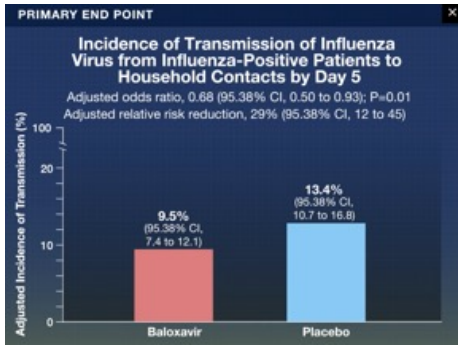
PRIMARY END POINT
Incidence of Transmission of Influenza Virus from Influenza-Positive Patients to Household Contacts by Day 5
Adjusted odds ratio, 0.68 (95.38% CI, 0.50 to 0.93); P=0.01
Adjusted relative risk reduction, 29% (95.38% CI, 12 to 45)
Adjusted Incidence of Transmission (%)
100
20
10
0
9.5% (95.38% CI, 7.4 to 12.1)
13.4% (95.38% CI, 10.7 to 16.8)
Baloxavir
Placebo

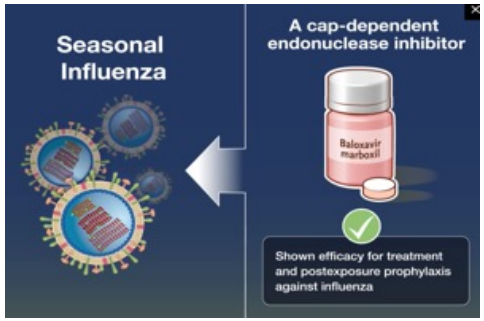
Seasonal Influenza
A cap-dependent endonuclease inhibitor
Baloxavir marboxil
Shown efficacy for treatment and postexposure prophylaxis against influenza

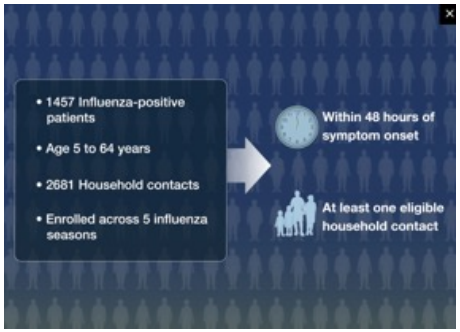
• 1457 Influenza-positive patients
• Age 5 to 64 years
• 2681 Household contacts
• Enrolled across 5 influenza seasons
Within 48 hours of symptom onset
At least one eligible household contact

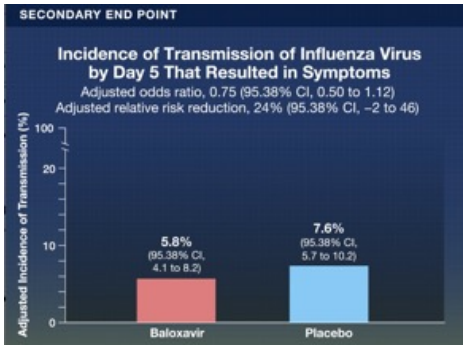
SECONDARY END POINT
Incidence of Transmission of Influenza Virus by Day 5 That Resulted in Symptoms
Adjusted odds ratio, 0.75 (95.38% CI, 0.50 to 1.12)
Adjusted relative risk reduction, 24% (95.38% CI, −2 to 46)
Adjusted Incidence of Transmission (%)
100
20
10
0
5.8% (95.38% CI, 4.1 to 8.2)
7.6% (95.38% CI, 5.7 to 10.2)
Baloxavir
Placebo


Single-dose treatment with oral baloxavir led to a significantly lower incidence of transmission
Baloxavir marboxil
Laboratory-confirmed influenza to household contacts than placebo


CENTERSTONE TRIAL
Prevent influenza transmission to household contacts

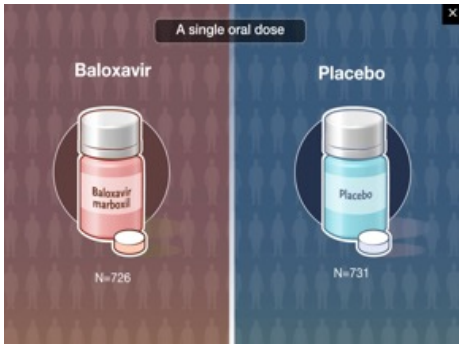
A single oral dose
Baloxavir
Placebo
Baloxavir marboxil
Placebo
N=726
N=731

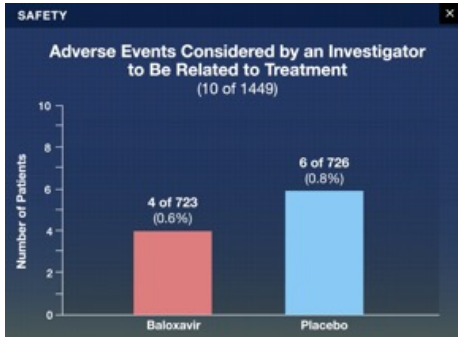
SAFETY
Adverse Events Considered by an Investigator to Be Related to Treatment
(10 of 1449)
Number of Patients
10
8
6
4
2
0
4 of 723 (0.6%)
6 of 726 (0.8%)
Baloxavir
Placebo

Klonale Hämatopoese unklarer Bedeutung (CHIP) bezeichnet eine Erkrankung, bei der erworbene Mutationen in den Blutzellen auftreten, ohne dass es zu einer malignen Erkrankung des Blutes kommt. CHIP ist mit dem Alterungsprozess assoziiert und kann das Risiko für die Entwicklung von hämatologischen Neoplasien, sowie kardiovaskulären und anderen Erkrankungen erhöhen.

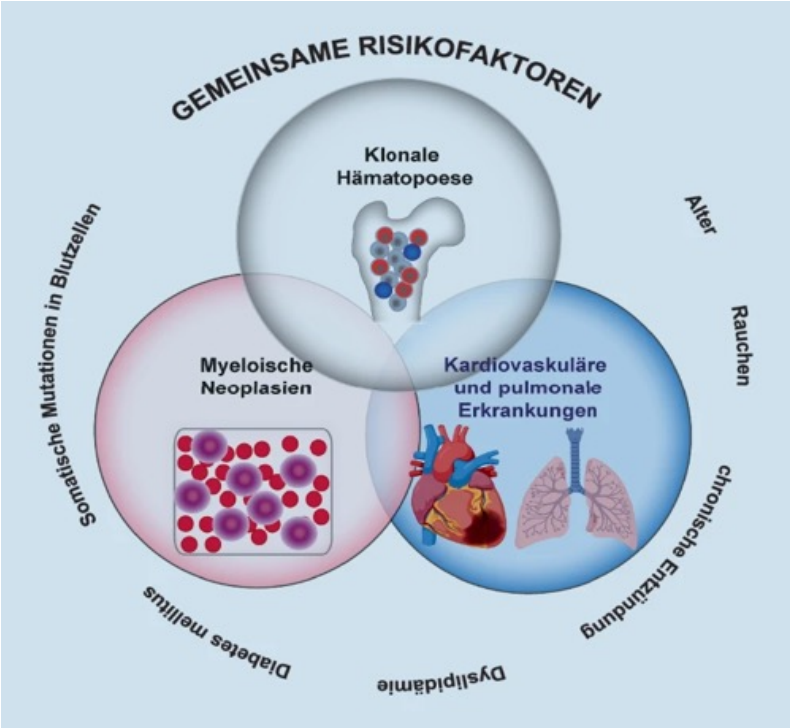

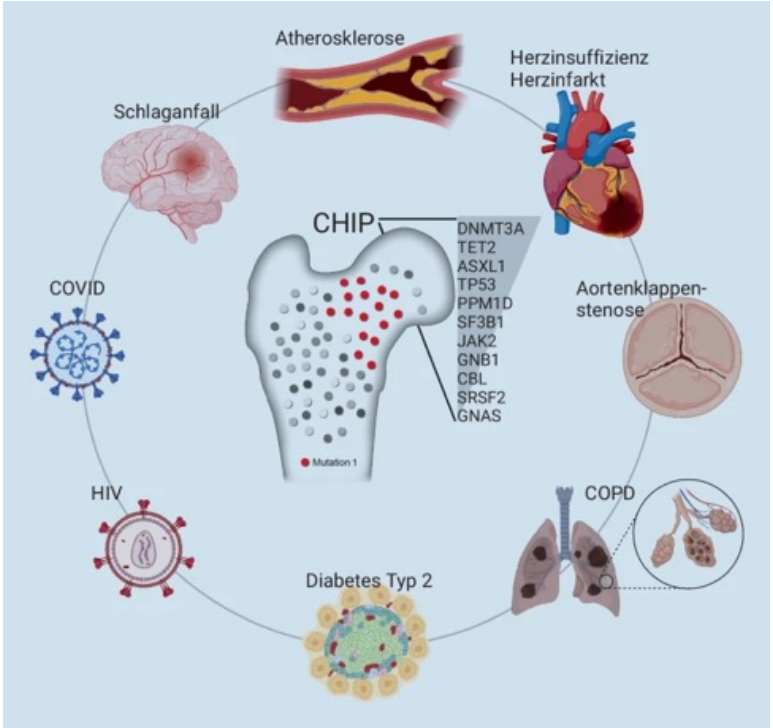

DNMT3A ist ein Gen, das für das Enzym DNA-Methyltransferase 3 alpha (DNMT3A) codiert, welches eine wichtige Rolle bei der DNA-Methylierung spielt. DNMT3A-Mutationen sind häufig in hämatologischen Neoplasien, insbesondere in akuter myeloischer Leukämie (AML), zu finden. Diese Mutationen können mit einer Vielzahl von klinischen und prognostischen Parametern bei AML-Patienten assoziiert sein.

Klonale Hämatopoese:

Das Auftreten von Mutationen in den Blutzellen, die zu einer klonalen Expansion, also einer Vermehrung der mutierten Zellen, führen.

Unbekannte Bedeutung:

CHIP wird als "unbekannte Bedeutung" bezeichnet, da die Mutationen nicht zu einer malignen Erkrankung führen und die Auswirkungen auf die Gesundheit in vielen Fällen noch unklar sind.

Alterungsprozess:

CHIP tritt häufiger bei älteren Menschen auf, was darauf hindeutet, dass es mit dem Alterungsprozess und der Ansammlung von Mutationen im Körper zusammenhängt.

Risikofaktor:

CHIP kann das Risiko für die Entwicklung von hämatologischen Neoplasien, kardiovaskulären Erkrankungen und anderen Erkrankungen erhöhen.

Keine Behandlung:

Solange sich CHIP nicht zu Blutkrebs entwickelt, ist keine spezifische Behandlung erforderlich, aber es ist wichtig, das Risiko für andere Erkrankungen zu berücksichtigen und die Gesundheit zu überwachen.

Zusammenhang mit anderen Erkrankungen:

CHIP wurde mit folgenden Erkrankungen in Verbindung gebracht:

Hämatologische Neoplasien:

CHIP kann das Risiko für die Entwicklung von Myelodysplastischem Syndrom (MDS) und akuter myeloischer Leukämie (AML) erhöhen.

Kardiovaskuläre Erkrankungen:

CHIP wurde mit einem erhöhten Risiko für Atherosklerose, koronare Herzkrankheit und Herzinsuffizienz in Verbindung gebracht.

Andere Erkrankungen:

CHIP kann auch das Risiko für chronisch-obstruktive Lungenerkrankung (COPD), Infektionen und Diabetes erhöhen.

Wichtige Hinweise:

- Es ist wichtig, dass Personen mit CHIP regelmäßig von einem Arzt überwacht werden, um das Risiko für andere Erkrankungen zu reduzieren.
- Die Behandlung von CHIP hängt von den individuellen Risikofaktoren und der Erkrankung ab.
- Aktuelle Forschung konzentriert sich auf die Entwicklung von Therapien, die die klonale Expansion mutierter Blutzellen reduzieren können.

Die Tet-Methylcytosin-Dioxygenase 2, kurz TET2, ist ein Enzym, das die Umsetzung von Methylcytosin zu 5-Hydroxymethylcytosin katalysiert. Es gehört zur Familie der TET-Enzyme ("ten-eleven translocation") und fungiert als Tumorsuppressor. Mutationen des TET2-Gens lassen sich bei vielen malignen hämatologischen Erkrankungen nachweisen. Somatische Mutationen von TET2 treten häufig bei myelodysplastischen Syndromen (MDS) und myeloproliferativen Erkrankungen (MPN) auf. Sie haben bei einigen Tumorformen einen hohen prognostischen Wert. So sind beispielsweise Nonsense- oder Frameshift-Mutationen von TET2 bei der zytogenetisch normalen akuten myeloischen Leukämie (CN-AML) mit einem schlechteren Outcome verbunden. Keimzellmutationen von TET2 führen bei homozygotem Vorkommen bei den betroffenen Kindern zu einer Immundefizienz und Lymphomen.

Tumor-Infiltrating Clonal Hematopoiesis

Clonal hematopoiesis of indeterminate potential (CHIP) is an age-related condition associated with increased mortality among patients with cancer. CHIP mutations with high variant-allele frequencies can be detected in tumors, a phenomenon we term tumor-infiltrating clonal hematopoiesis (TI-CH). The frequency of TI-CH and its effect on tumor evolution are unclear. We characterized CHIP and TI-CH in 421 patients with early-stage non–small-cell lung cancer (NSCLC) from the TRACERx study and in 49,351 patients from the MSK-IMPACT pan-cancer cohort. We studied the association of TI-CH with survival and disease recurrence and evaluated the functional effect of *TET2*-mutant CHIP on the biologic features of lung tumors.

Conclusions

TI-CH increased the risk of disease recurrence or death among patients with NSCLC and the risk of death from any cause among patients with solid tumors. TI-CH remodeled the tumor immune microenvironment and accelerated tumor organoid growth, findings that support a role for an aging-related hematologic clonal proliferation in cancer evolution.

Clonal hematopoiesis of indeterminate potential (CHIP) is a prevalent age-associated condition involving the expansion of blood cells derived from a somatically mutated hematopoietic stem cell without hematologic disorders. CHIP increases the risk of hematologic cancers and chronic inflammatory diseases, such as cardiovascular disease, chronic obstructive pulmonary disease, and chronic liver disease. CHIP is also associated with an increased incidence of lung cancer as well as an increased risk of death among patients with solid tumors.

CHIP-derived immune cells have been detected in solid-tumor tissues from patients with CHIP, with an enrichment in non–small-cell lung cancer (NSCLC), where they have the potential to alter the local microenvironment and influence tumor evolution. Although more than 20% of patients with cancer have CHIP, the effect of tumor-infiltrating immune cells with CHIP mutations on tumor progression and patient outcomes remains poorly understood.

Here, we define the presence of CHIP mutations with high variant-allele frequencies (VAFs) within tumors as tumor-infiltrating clonal hematopoiesis (TI-CH). We determined the prevalence of TI-CH in 421 patients with early-stage NSCLC and 49,351 patients across 75 cancer types from a real-world cohort, studied its associations with patient outcomes, and evaluated its functional effect using preclinical models of lung cancer.

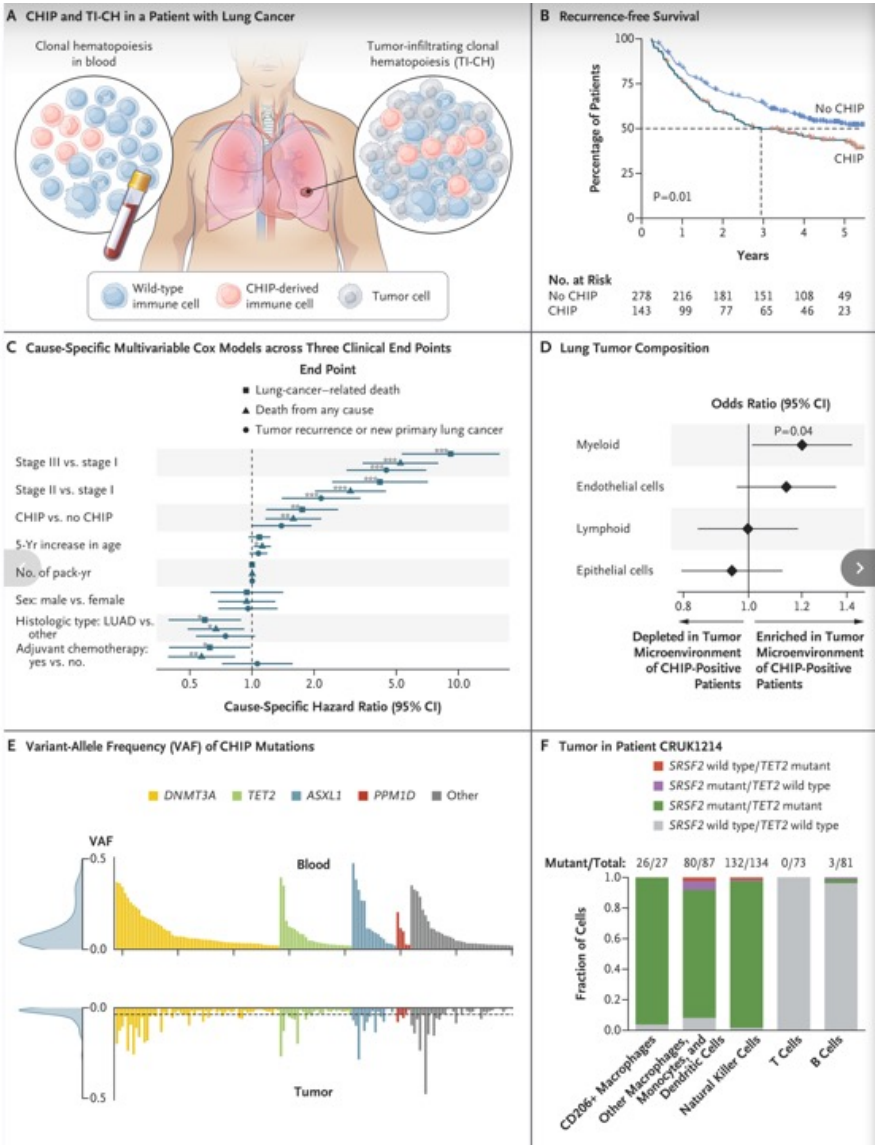

CHIP and TI-CH in Patients with Non–Small-Cell Lung Cancer (NSCLC) Enrolled in the TRACERx Study.

Panel A shows a schematic representation of clonal hematopoiesis of indeterminate potential (CHIP) and tumor-infiltrating clonal hematopoiesis (TI-CH) in a patient with lung cancer. Panel B shows Kaplan–Meier probability estimates of recurrence-free survival among patients without CHIP and those with CHIP in the TRACERx (Tracking Non–Small-Cell Lung Cancer Evolution through Therapy) study. The P value was calculated with the log-rank test. Panel C shows cause-specific multivariable Cox models across three clinical end points: lung-cancer–related death, death from any cause, and tumor recurrence or new primary lung cancer. Age in years was used as a continuous variable and divided by 5 so that the hazard ratio represents the change in risk for a 5-year increase. One asterisk indicates a P value of less than 0.05, two asterisks a P value of less than 0.01, and three asterisks a P value of less than 0.001. CI denotes confidence interval, and LUAD lung adenocarcinoma. Panel D shows age-adjusted logistic-regression analysis for the association between the presence of CHIP and cellular densities (higher vs. lower than the cohort average for each cell type) in the lung tumor microenvironment. Panel E shows a bar plot representing the variant allele frequency (VAF) of CHIP mutations in blood samples (top) and tumor samples (bottom) from 143 patients with CHIP. Each column corresponds to a patient. The bars are colored according to the mutated gene. For patients with more than one CHIP mutation, the highest VAF was selected. Density distributions of VAFs in blood samples (top) and tumor samples (bottom) are depicted on the left. Panel F shows single-cell genotyping of different immune-cell populations isolated from a primary lung tumor in a patient with *TET2*-mutant and *SRSF2*-mutant TI-CH. Cells are color coded according to their genotypes within each cell population.

Characteristics of Patients with Primary Stage I through III NSCLC in the TRACERx Study and MSK-IMPACT Cohort.

Characteristic	TRACERx Study (N=421)		MSK-IMPACT Cohort (N=2602)	
	No CHIP (N=278)	CHIP (N=143)	No CHIP (N=1685)	CHIP (N=917)
Median age (IQR) — yr	68 (62–74)	73 (66–78)	67 (60–73)	72 (66–77)
Sex — no. (%)				
Female	130 (47)	58 (41)	843 (50)	441 (48)
Male	148 (53)	85 (59)	524 (31)	286 (31)
Missing data	—	—	318 (19)	190 (21)
Smoking status				
Current smoker — no. (%)	125 (45)	55 (38)	63 (4)	28 (3)
Median pack-yr (IQR)	42 (30–54)	45 (30–57)		
Former smoker — no. (%)	130 (47)	81 (57)	484 (29)	270 (29)
Median pack-yr (IQR)	36 (19–52)	40 (21–62)		
Never smoked — no. (%)	23 (8)	7 (5)	152 (9)	51 (6)
Missing data — no. (%)	—	—	986 (59)	568 (62)
Race — no. (%)†				
White	267 (96)	137 (96)	868 (52)	497 (54)
Asian	2 (1)	0	86 (5)	28 (3)
Black	4 (1)	3 (2)	46 (3)	19 (2)
Other or missing data	5 (2)	3 (2)	685 (41)	373 (41)
Histologic type — no. (%)				
Lung adenocarcinoma	160 (58)	80 (56)	1264 (75)	685 (75)
Lung squamous-cell carcinoma	84 (30)	50 (35)	222 (13)	132 (14)
Other	34 (12)	13 (9)	199 (12)	100 (11)
Main oncogenic driver — no. (%)				
TP53 mutation	176 (63)	103 (72)	742 (44)	407 (44)
KRAS mutation	87 (31)	40 (28)	484 (29)	294 (32)
STK11 mutation	37 (13)	26 (18)	201 (12)	117 (13)
EGFR mutation	22 (8)	7 (5)	387 (23)	193 (21)
Oncogenic isoforms‡	15 (5)	4 (3)	70 (4)	16 (2)
Median follow-up (95% CI) — yr	4.6 (4.5–4.8)	4.9 (4.5–5.1)	2.4 (2.3–2.6)	2.4 (2.2–2.7)
Tumor-infiltrating clonal hematopoiesis — no. (%)	—	60 (42)	—	333 (36)

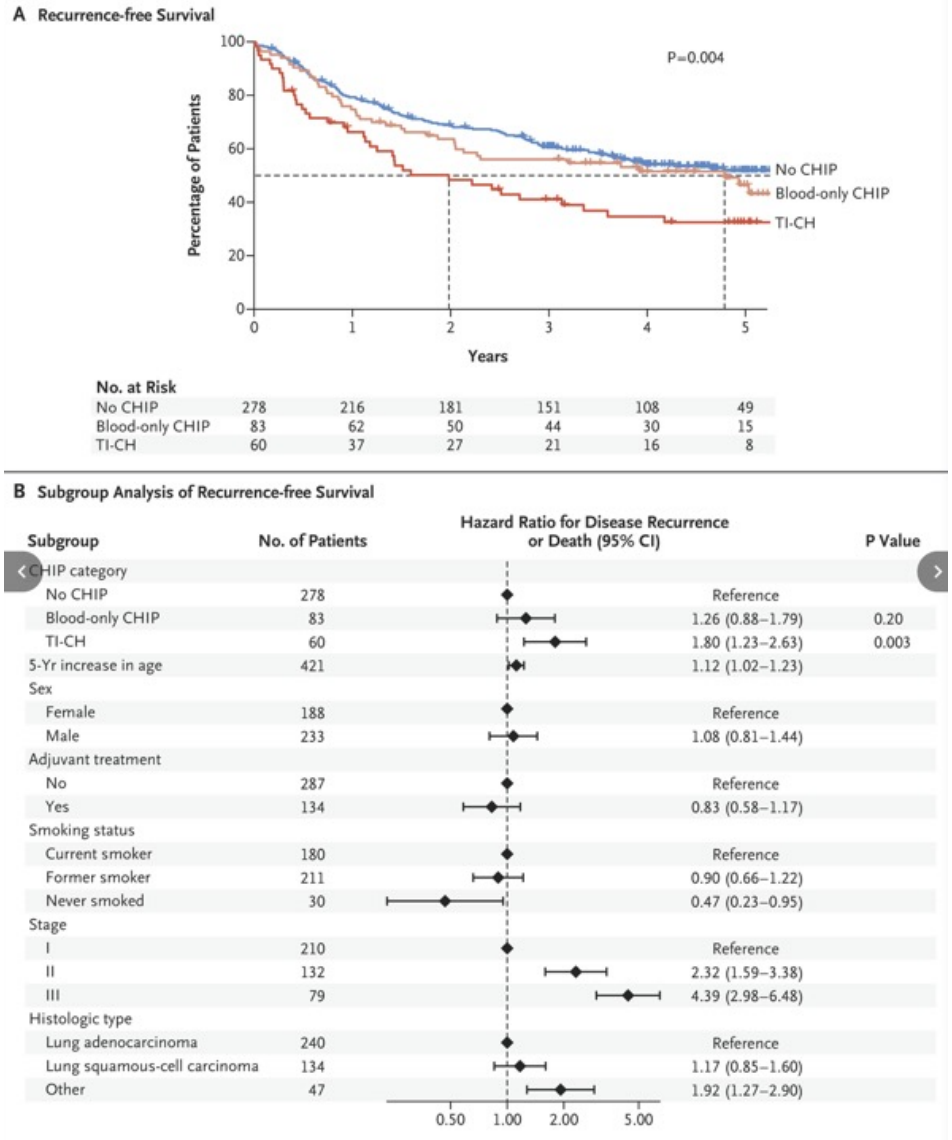

TI-CH and Patient Outcome in NSCLC.

Panel A shows Kaplan–Meier probability estimates of recurrence-free survival among patients without CHIP (blue), patients with blood-only CHIP (orange), and patients with TI-CH (red) in the TRACERx study. The P value was calculated with the log-rank test. Panel B shows a multivariable Cox model for recurrence-free survival among patients enrolled in the TRACERx study; the model accounted for baseline clinical characteristics and CHIP category (no CHIP, blood-only CHIP, and TI-CH). Hazard ratios and 95% confidence intervals are depicted. Age in years was used as a continuous variable and divided by 5 so that the hazard ratio represents the change in risk for a 5-year increase. P values that were derived from the multivariable analysis are shown only for the CHIP categories (the factor of interest).

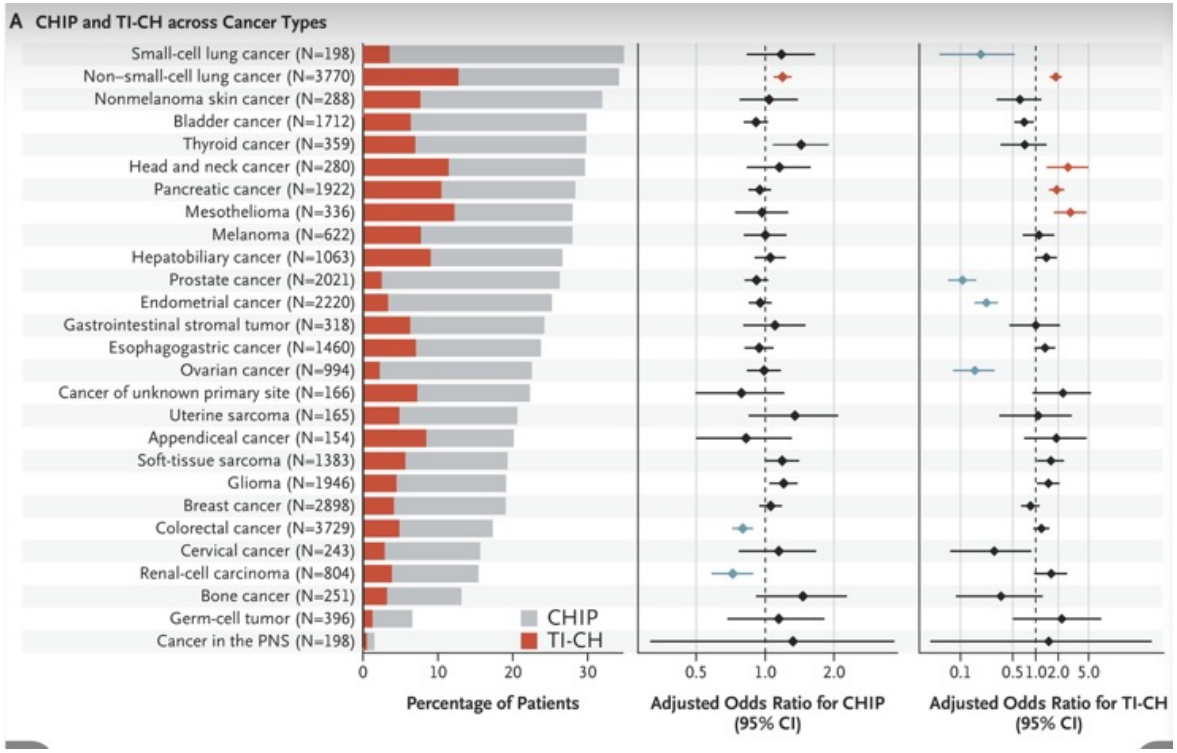

TI-CH in the MSK-IMPACT Pan-Cancer Cohort.

Panel A, left, shows the percentages of patients with CHIP (gray) and with TI-CH (red) across cancer types from the 31,556 patients with primary tumor samples. Only cancer types found in more than 150 patients are represented. Panel A, right, shows adjusted odds ratio and 95% confidence intervals for the presence of CHIP and TI-CH in each cancer type as compared with the others. Odds ratios were derived from multivariable logistic regressions, with adjustment for age, sex, ethnic group, smoking status, and previous treatment (for CHIP and TI-CH) and for tumor purity and the VAF of CHIP mutations in blood (for TI-CH). Benjamini–Hochberg correction for multiple testing was applied, with enrichments ($Q<0.05$) highlighted in red for positive associations and blue for negative associations.

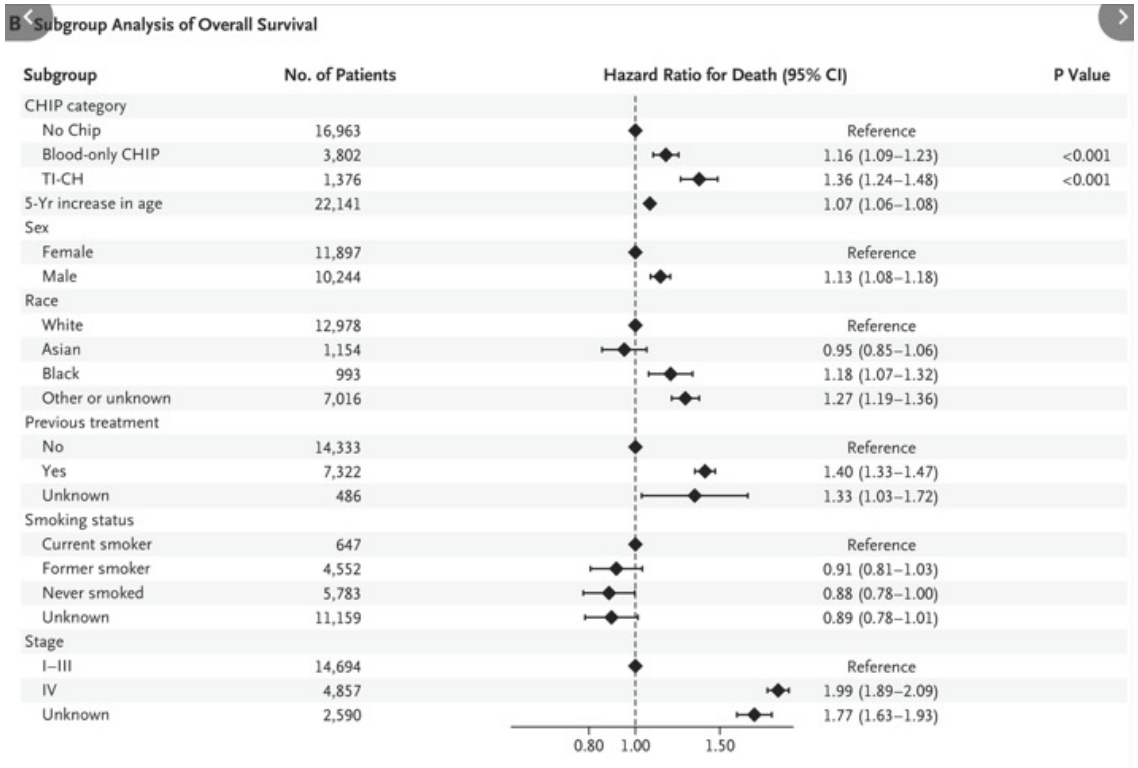

Panel B shows a multivariable Cox model for the risk of death among 22,141 patients with primary tumor samples analyzed and overall-survival data available. Hazard ratio and 95% confidence intervals are depicted. Age in years was used as a continuous variable and divided by 5 so that the hazard ratio represents the change in risk for a 5-year increase. P values that were derived from the multivariable analysis are shown only for the CHIP categories (the factor of interest). MSK-IMPACT denotes Memorial Sloan Kettering–Integrated Mutation Profiling of Actionable Cancer Targets, and PNS peripheral nervous system.

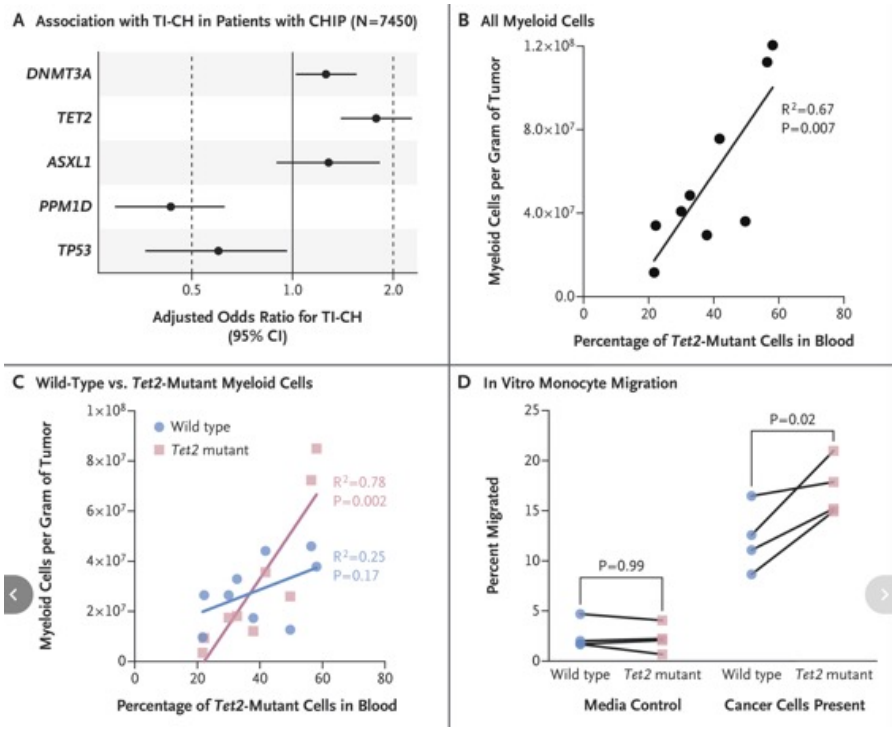

The Functional Effect of *TET2*-Mutant CHIP in NSCLC.

Panel A shows adjusted odds ratios and 95% confidence intervals derived from a multivariable logistic regression for the presence of TI-CH in 7450 patients with CHIP in the MSK-IMPACT pan-cancer cohort, with adjustment for age, sex, ethnic group, previous treatment, smoking status, tumor purity, and the VAF of CHIP mutations in blood. CHIP mutations were categorized as *DNMT3A*, *TET2*, *ASXL1*, *PPM1D*, *TP53*, or other gene mutations, with the "other" category used as the reference level. Panels B and C show the correlation between the percentage of *Tet2*-mutant cells in blood and overall myeloid cell infiltration in the tumor microenvironment (Panel B) or *Tet2*-mutant as compared with wild-type myeloid cell infiltration in the tumor microenvironment (Panel C) in mice, with the use of nine biologic replicates. Panel D shows the percentage of *Tet2*-mutant or wild-type monocytes that migrated to the bottom chamber in the presence or absence of 3LL lung tumor cells (blood from one to four mice was pooled per data point).

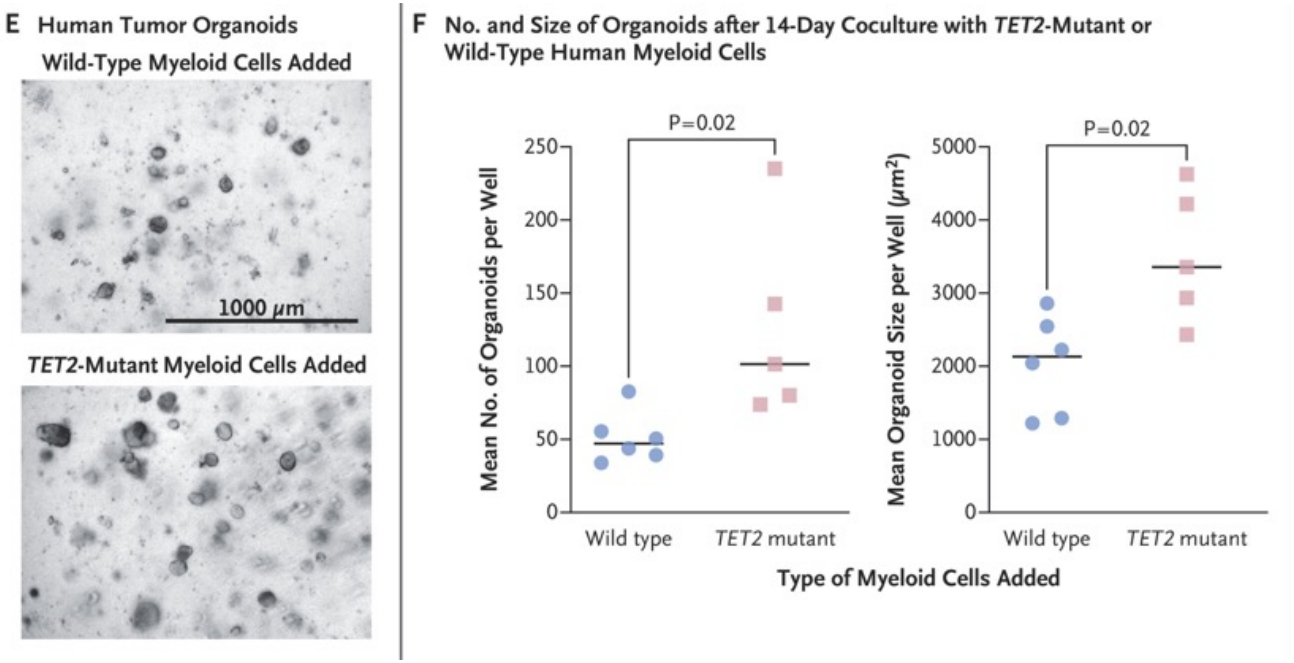

Panel E shows representative bright-field images of patient-derived tumor organoids after 14-day coculture with *TET2*-mutant or wild-type human myeloid cells. Panel F shows the number and size of tumor organoids after 14-day coculture with *TET2*-mutant or wild-type human myeloid cells (five or six biologic replicates across three independent experiments). The horizontal bars indicate median values.

Discussion

Cancer evolution, once regarded as a stepwise accumulation of oncogenic mutations, is now seen as a multifactorial process that is affected by the tissue microenvironment, local and systemic immune responses, environmental exposures, and aging. Recent studies have highlighted the influence of the aging hematopoietic system on the development of lung cancer. Here, age-associated TI-CH emerges as an important facet influencing cancer progression.

TI-CH is a pan-cancer phenomenon that is observed in 26% of patients with CHIP, representing more than 6% of all solid-tumor cases, and is associated with adverse patient outcomes. The likelihood of having TI-CH varies across cancer types, with enrichment in NSCLC, head and neck cancer, pancreatic cancer, and mesothelioma. With respect to NSCLC, approximately 40% of patients with CHIP had TI-CH, which independently increased their risk of death or recurrence. Across CHIP mutations, *TET2* emerged as an independent predictor of TI-CH. In a NSCLC model, *Tet2*-mutant CHIP resulted in increased infiltration of myeloid cells into tumors, mimicking observations in human disease. *Tet2*-mutant monocytes preferentially migrated toward tumor cells and accumulated as macrophages within murine tumors. In a finding consistent with published evidence that *TET2* mutations can functionally remodel myeloid responses, *TET2*-mutant myeloid cells showed enhanced protumorigenic capacity in tumor organoid cocultures as compared with wild-type myeloid cells.

Metachromatic leukodystrophy (MLD) is a rare, inherited disorder where the body can't properly break down fatty substances called sulfatides, leading to their buildup in nerve cells and the destruction of the myelin sheath. This damage disrupts nerve function and causes progressive loss of motor and cognitive abilities.

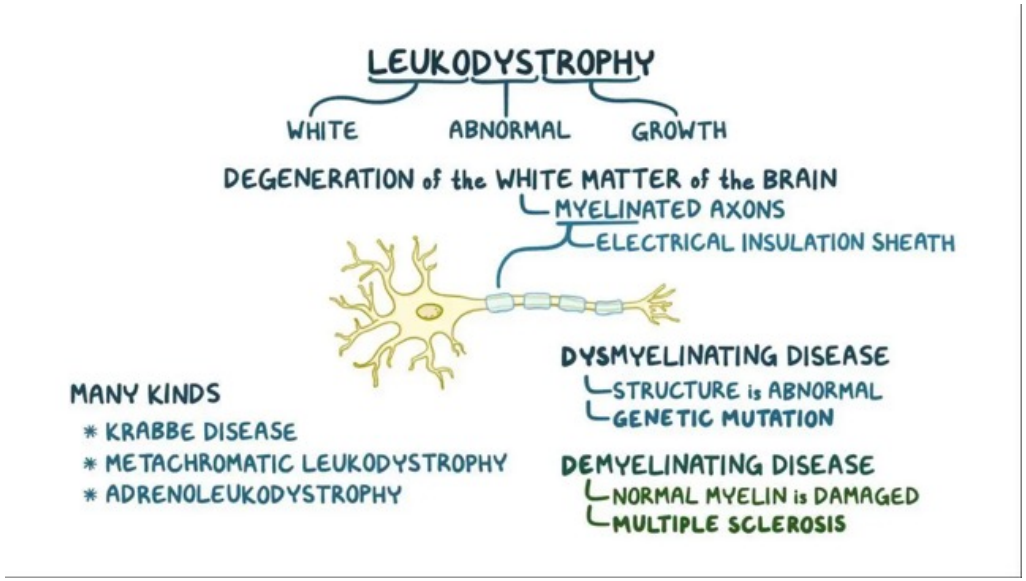

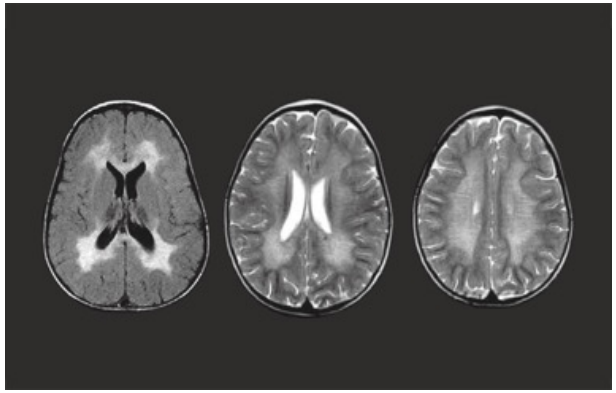

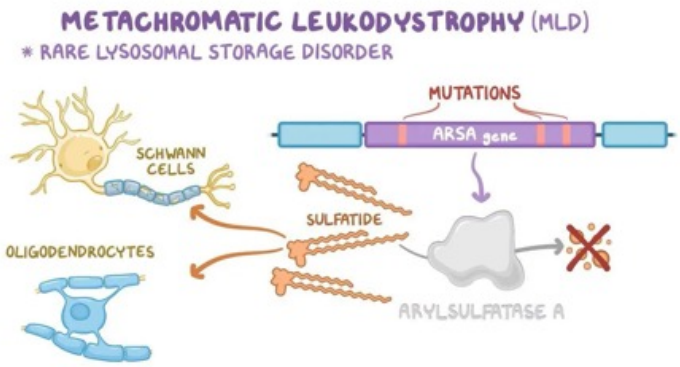

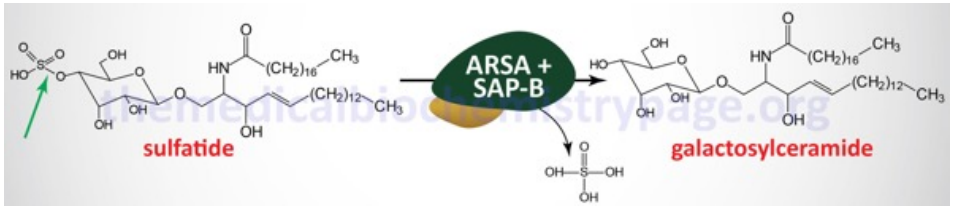

What is MLD?

- MLD is a lysosomal storage disease, meaning it's caused by a defect in the process of breaking down and recycling cellular waste in lysosomes.
- Specifically, MLD is caused by a deficiency of the enzyme arylsulfatase A (ARSA), which is responsible for breaking down sulfatides.
- Without this enzyme, sulfatides accumulate, especially in the brain, spinal cord, and peripheral nerves, damaging the myelin sheath.
- Myelin is a fatty substance that insulates and protects nerve fibers, allowing them to transmit signals efficiently.
- When myelin is damaged, nerve impulses can't travel properly, leading to a variety of symptoms.

Causes and Inheritance:

- MLD is an autosomal recessive genetic disorder, meaning a person needs to inherit two copies of the mutated gene, one from each parent, to develop the condition.
- Mutations in the ARSA gene or, less commonly, in the PSAP gene, which codes for a protein that activates ARSA, can cause MLD.

Symptoms:

- Symptoms vary depending on the age of onset and severity of the condition.
- **Late Infantile MLD:** This is the most severe form, typically appearing between 12 and 18 months of age. Symptoms include developmental delays, loss of previously acquired skills, muscle weakness, and seizures.
- **Juvenile MLD:** This form typically appears between 3 and 10 years of age, and symptoms include loss of previously acquired skills, motor problems, and cognitive decline.
- **Adult MLD:** This form typically appears after 16 years of age, with symptoms including cognitive and behavioral problems, and motor difficulties.
- Regardless of the subtype, MLD eventually leads to progressive deterioration of intellectual and motor function, with individuals losing their ability to walk, talk, and eventually becoming unresponsive.

Diagnosis:

- MLD can be diagnosed through a combination of methods, including blood tests to measure ARSA enzyme activity, genetic testing to identify mutations in the ARSA or PSAP gene, and brain imaging techniques such as MRI to visualize white matter changes.
- Newborn screening programs in some countries may also detect MLD.

(atidarsagene autotemcel)

Libmeldy: autologous CD34^{+} cells encoding the *ARSA* gene

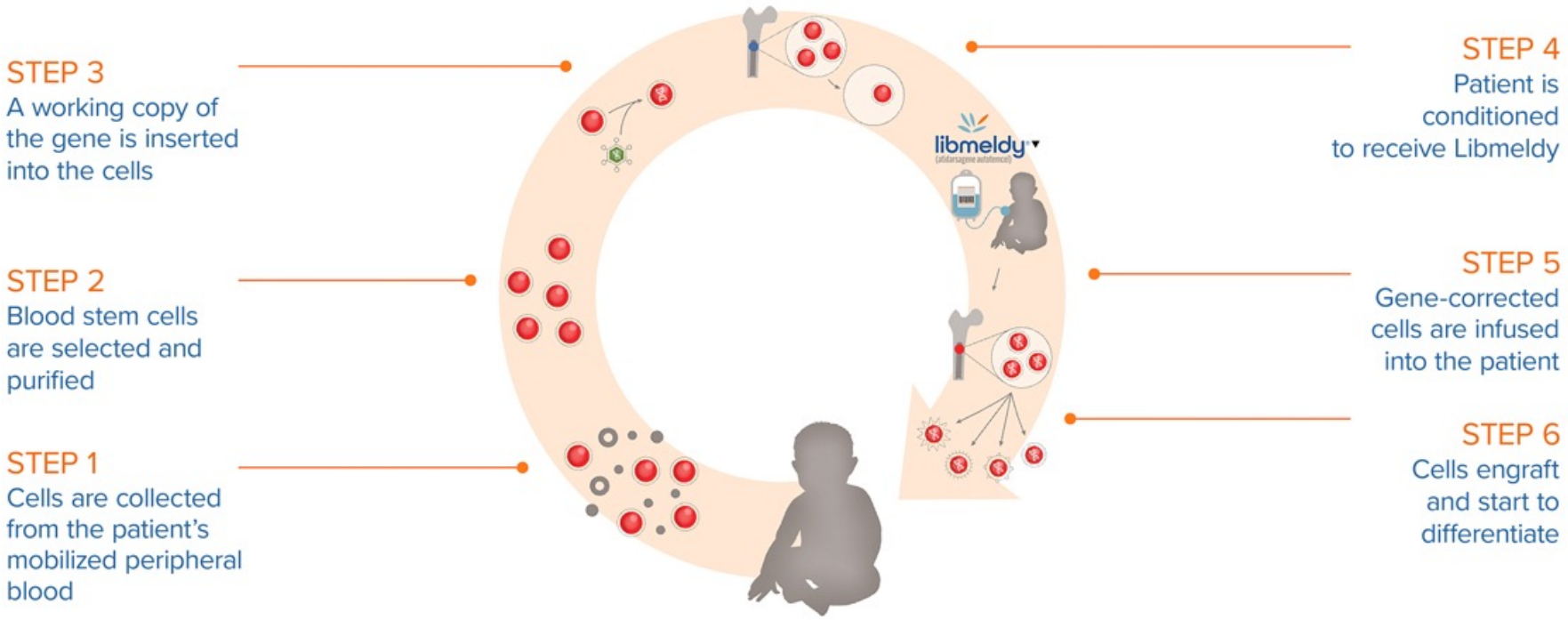

CD34 gene transfer, a type of gene therapy, aims to cure neurological diseases by delivering a functional copy of a gene to affected cells, potentially correcting a genetic defect. This is often achieved using lentiviral vectors (LVs) to modify CD34+ hematopoietic stem and progenitor cells (HSPCs), which can then be infused back into the patient. The modified cells can differentiate into microglia, the brain's immune cells, and express new therapeutic proteins, potentially correcting the underlying neurological issue.

1. Identifying the Genetic Defect:
   - Many neurological diseases, particularly those of genetic origin, stem from a faulty gene or a missing one.
   - Gene therapy aims to address this by providing a functional copy of the gene or correcting the faulty one.

2. Utilizing CD34+ Cells:
   - CD34+ cells are a type of stem cell, specifically hematopoietic stem and progenitor cells (HSPCs), which can differentiate into various blood cell types.
   - They are easily collected from bone marrow, peripheral blood, or umbilical cord blood.
   - These cells are ideal for gene transfer because they can be modified ex vivo (outside the body), transduced with a therapeutic gene, and then reinfused.

3. The Lentiviral Vector (LV):
   - LVs are a type of viral vector that can deliver genetic material into cells without causing disease.
   - They are engineered to carry the therapeutic gene and are used to modify the CD34+ cells.

4. Gene Transfer and Modification:
   - The LV delivers the therapeutic gene into the CD34+ cells, where it can be integrated into the cell's genome.
   - This modifies the cells' genetic makeup, allowing them to produce the correct protein or correct the malfunctioning gene.

5. Differentiation and Therapeutic Effect:
   - Once reinfused, the modified CD34+ cells can differentiate into microglia, the brain's immune cells.
   - These modified microglia can then express the therapeutic protein, potentially correcting the neurological condition.

6. Potential for Neurological Cure:
   - By delivering a functional gene to the brain's immune cells, this process can potentially repair or correct the underlying genetic defect in neurological diseases.
   - This can lead to a cure or at least significant improvement in symptoms for certain neurological disorders.

Example: Mucopolysaccharidosis Type IIIA (MPSIIIA):
   - One study showed that lentiviral vector-mediated ex vivo gene therapy, using CD34+ cells, can correct the genetic defect in MPSIIIA, a lysosomal storage disease causing cognitive decline.
   - The study demonstrated that modifying CD34+ cells with a lentiviral vector encoding the SGSH gene and reinfusing them into MPSIIIA mice resulted in neurological correction.

In essence, CD34 gene transfer leverages the power of stem cells and viral vectors to deliver a functional copy of a gene to the brain's immune cells, potentially leading to a cure or significant improvement in neurological diseases.

Long-Term Effects of Atidarsagene Autotemcel for Metachromatic Leukodystrophy

Metachromatic leukodystrophy (MLD) is an ultrarare, severe lysosomal storage disorder caused by a deficiency of arylsulfatase A (ARSA). We treated patients who had MLD with atidarsagene autotemcel (arsa-cel), a hematopoietic stem-cell–based gene therapy, in two prospective open-label clinical studies and expanded-access programs. We compared their outcomes with those of untreated patients (natural history cohort). The primary end point was survival free from severe motor impairment (the time from birth to the first occurrence of loss of locomotion and of sitting without support or death from any cause).

Conclusions

Among patients with presymptomatic late-infantile or early-juvenile MLD and those with early-symptomatic early-juvenile MLD, the risk of severe motor impairment or death was significantly lower among those who received treatment with arsa-cel than in a natural history cohort that did not receive treatment.

Atidarsagene autotemcel (arsa-cel, also known as OTL-200) is an autologous hematopoietic stem-cell (HSC)–based gene therapy consisting of CD34+ hematopoietic stem and progenitor cells (HSPCs) transduced ex vivo with a lentiviral vector encoding human *ARSA* complementary DNA, with constitutive ARSA expression driven by a human phosphoglycerate kinase promoter. Arsa-cel is the only approved treatment for early-onset MLD. Allogeneic HSC transplantation has shown a benefit in patients with late-onset MLD who are presymptomatic or minimally symptomatic at the time of transplantation, but it is not effective in patients with early-onset MLD, even those who are presymptomatic. Before the approval of arsa-cel, no treatment options were available for early-onset MLD beyond supportive care.

Here, we present the results from an integrated analysis of safety and efficacy data from 39 patients with early-onset MLD who were treated with arsa-cel, with a median follow-up of 6.76 years (maximum, 12.19), as compared with data from 49 untreated patients with MLD. Data from these 88 patients constitute the dataset reviewed in the Biologics License Application for arsa-cel.

Patient Characteristics and Duration of Follow-up in the Integrated Summary of Efficacy.

„historical“ controls

Variable	Arsa-cel*			Untreated†	
	Presymptomatic Late-Infantile MLD (N=18)	Presymptomatic Early-Juvenile MLD (N=8)	Early-Symptomatic Early-Juvenile MLD (N=11)	Late-Infantile MLD (N=26)	Early-Juvenile MLD (N=17)
Sex — no. (%)					
Female	5 (28)	2 (25)	5 (45)	14 (54)	9 (53)
Male	13 (72)	6 (75)	6 (55)	12 (46)	8 (47)
Median age at diagnosis (range) — mo	6.6 (0.4–12.3)	12.6 (0.0–44.1)	64.6 (24.9–131.7)	30.5 (18.6–44.0)	53.2 (30.9–91.3)
Median age at symptomatic disease onset (range) — mo	NA	NA	64 (29–83)	15 (9–26)	47 (18–75)
Median age at arsa-cel treatment or at first contact (range) — mo‡	10.3 (7.6–17.7)	16.1 (11.3–48.9)	69.0 (30.5–139.7)	18.8 (14.5–27.9)	52.6 (19.2–74.1)
Median duration of follow-up (range) — yr	6.7 (2.4–12.2)	3.8 (1.1–9.6)	7.4 (0.6–9.4)	4.4 (0.6–18.8)	5.6 (0.4–20.7)
Median age at last contact or death (range) — yr	7.4 (3.2–13.4)	6.1 (2.1–12.0)	12.6 (5.1–19.1)	6.2 (2.7–20.4)	10.3 (2.8–25.3)

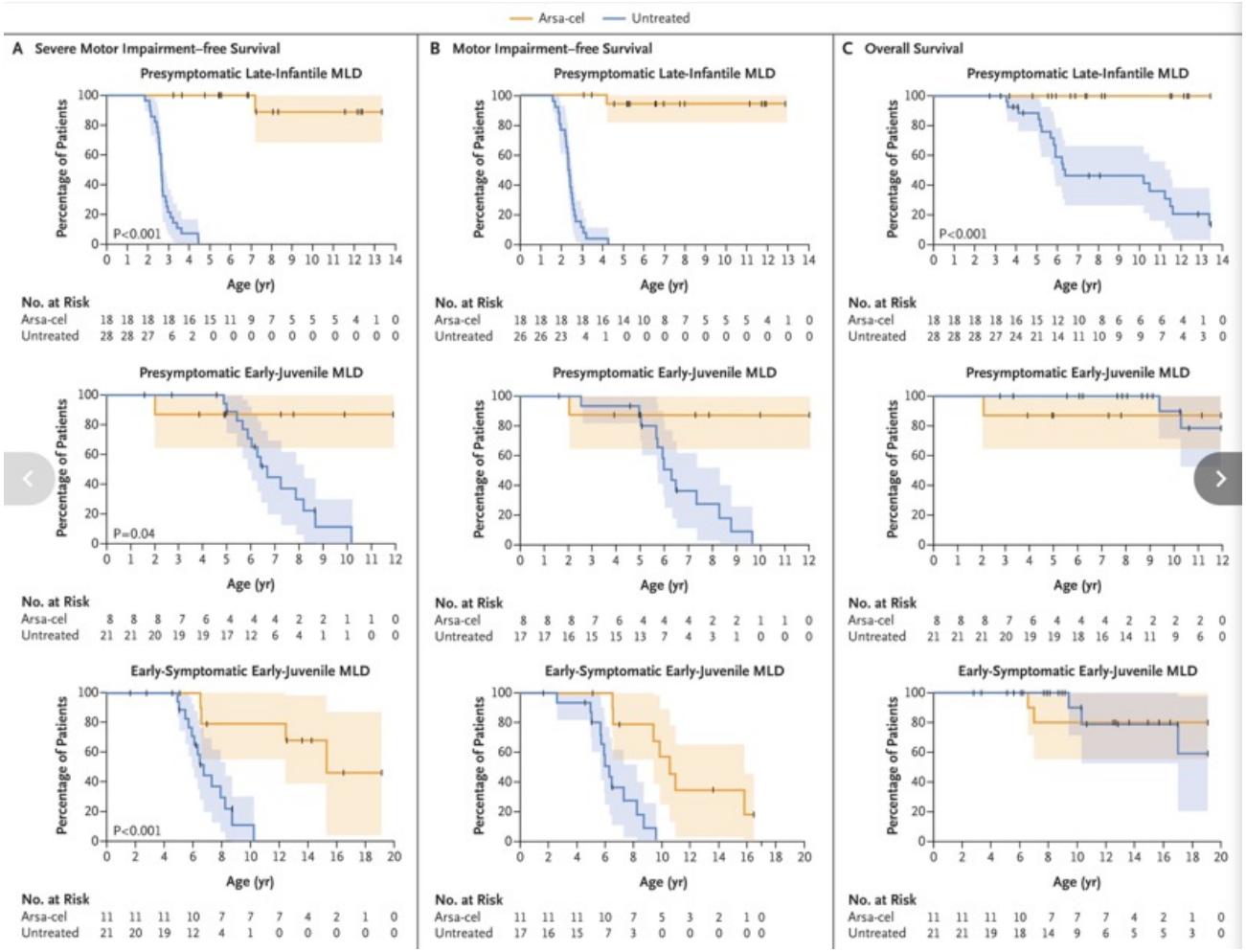

Severe Motor Impairment–free Survival, Motor Impairment–free Survival, and Overall Survival.

Shown are Kaplan–Meier estimates of survival free from severe motor impairment among atidarsagene autotemcel (arsa-cel)–treated patients with presymptomatic late-infantile metachromatic leukodystrophy (MLD), those with presymptomatic early-juvenile MLD, and those with early-symptomatic early-juvenile MLD (Panel A); survival free from motor impairment in the three groups (Panel B); and overall survival in the three groups (Panel C), as compared with natural history data from untreated patients with matched MLD subtypes. Survival free from severe motor impairment was defined as the time from birth to the first of loss of locomotion and of sitting without support (a Gross Motor Function Classification for Metachromatic Leukodystrophy [GMFC-MLD] level of ≥5, on a scale that ranges from level 0 [normal function] to level 6 [the loss of all gross motor function]) or death from any cause; otherwise, data were censored at the date of the last GMFC-MLD assessment. Survival free from motor impairment was defined as the time from birth to the loss of the ability to walk (a GMFC-MLD level of ≥3 confirmed at all subsequent assessments) or death from any cause; otherwise, the data were censored at the date of the last GMFC-MLD assessment. Tick marks indicate censored data. P values were calculated from an unstratified log-rank test. The widths of the confidence intervals (shaded areas) have not been adjusted for multiplicity and should not be used in place of hypothesis testing.

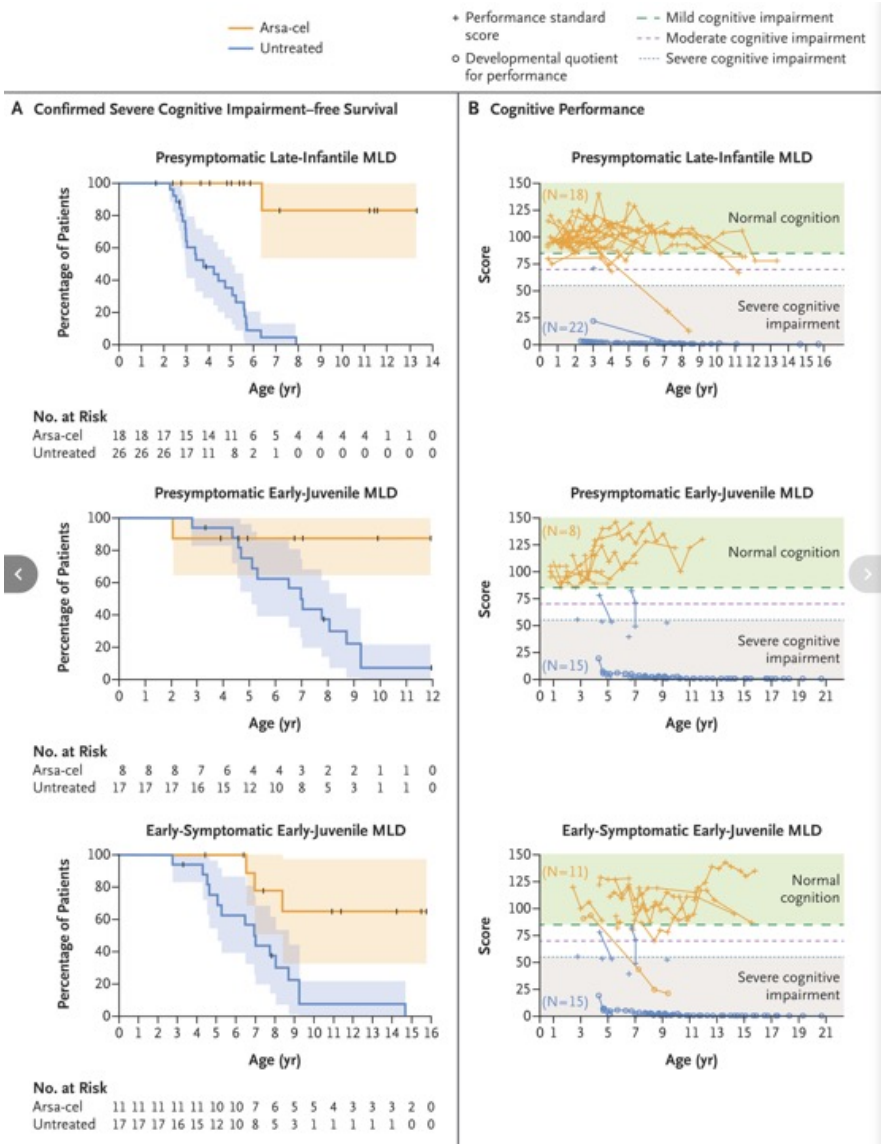

Integrated Efficacy Analyses of Cognitive Performance.

Shown are Kaplan–Meier estimates of survival free from confirmed severe cognitive impairment among arsa-cel–treated patients with presymptomatic late-infantile MLD, those with presymptomatic early-juvenile MLD, and those with early-symptomatic early-juvenile MLD (Panel A), as well as plots of the performance standard score and the developmental quotient for performance according to chronological age among arsa-cel–treated patients with presymptomatic late-infantile MLD, those with presymptomatic early-juvenile MLD, and those with early-symptomatic early-juvenile MLD (Panel B), as compared in each case with natural history data from untreated patients with matched MLD subtypes. Survival free from confirmed severe cognitive impairment was defined as the time from birth to the first occurrence of confirmed severe cognitive impairment (a performance standard score of ≤55 and no subsequent scores of >55) or death from any cause; otherwise, the data were censored (indicated by tick marks) at the time of the last neuropsychological assessment. Survival free from confirmed severe cognitive impairment was a post hoc modification to the prespecified end point of survival free from severe cognitive impairment. Cognitive performance was evaluated according to standardized assessments that were used to calculate a performance standard score or developmental quotient for performance (Table S3). Developmental quotients are shown for patients who had their last assessment performed with the use of a tool designed for a younger age than their chronological age. Reference lines for mild (performance standard score of ≥70 to <85), moderate (score of >55 to <70), and severe (score of ≤55) cognitive impairment are based on standard score categories. Normal cognition was defined as a standard score of ≥85. The widths of the confidence intervals in Panel A (shaded areas) have not been adjusted for multiplicity and should not be used in place of hypothesis testing.

Discussion

This study showed a beneficial effect of treatment with arsa-cel in patients with MLD that has been durable — up to 12 years for the earliest treated patient. Moreover, the duration of follow-up is among the longest reported for a lentiviral vector–based gene therapy; 13 patients have been followed for at least 8 years and 7 patients have been followed for at least 10 years after treatment.

The use of a historical prospective cohort of untreated patients with MLD as the comparison group is appropriate in this study because the rapid disease progression of early-onset MLD is well characterized, and the results from the natural history cohort are consistent with those from published literature. The natural history data were obtained over a period of 21 years, which overlaps with the 11-year (2010 to 2021) clinical development program of arsa-cel. The inclusion of untreated siblings of treated patients also lends validity to the use of this cohort, since siblings with early-onset MLD typically have a similar natural history of the disease course.

The results of our study showed that arsa-cel led to a durable, disease-modifying effect in patients with early-onset MLD, especially in children treated before symptoms developed, a finding that contrasts with the rapid decline to severe neurologic disability that has been observed in untreated patients with MLD.

FcRn, auch bekannt als neonataler Fc-Rezeptor, ist ein Rezeptor, der eine wichtige Rolle spielt im Transfer von mütterlichen IgG an das Fetus

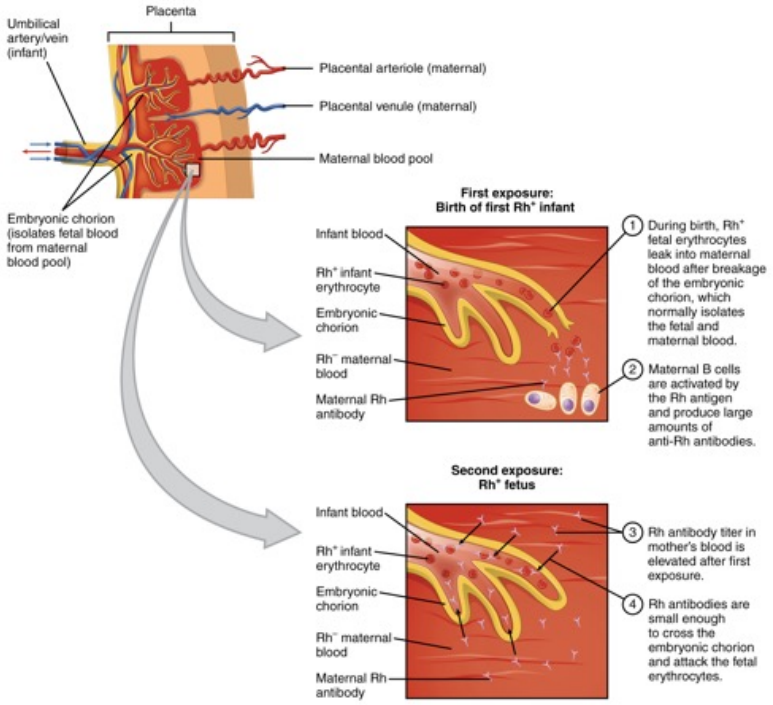

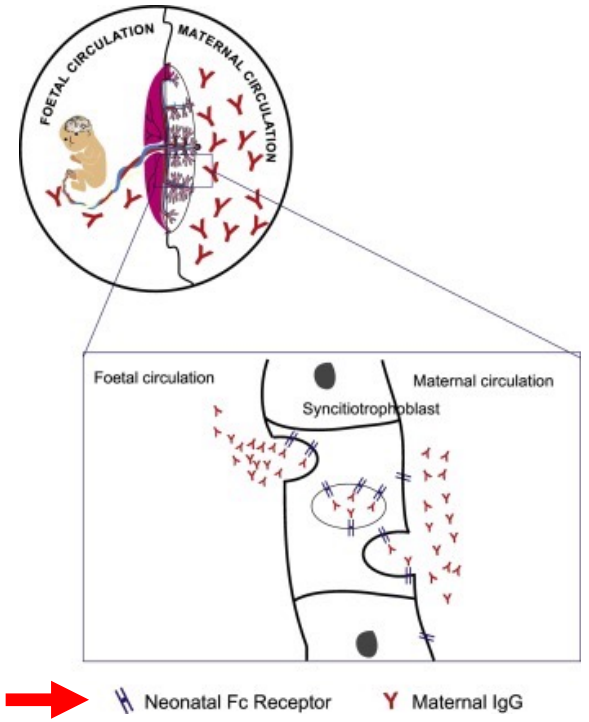

Erythroblastosis fetalis, auch bekannt als hämolytische Erkrankung des Fetus und Neugeborenen (HDFN), ist eine Erkrankung, bei der die Mutter Antikörper gegen das Blut ihres Kindes bildet, das bestimmte Antigene (wie Rh-Faktor) hat, die von der Mutter fehlen

RhoGAM ist ein Medikament, das bei Rh-negativen Frauen eingesetzt wird, um eine Rh-Immunisierung zu verhindern, die bei Rh-positiven Kindern oder nach einer Fehlgeburt auftreten kann. RhoGAM ist eine Form von Rh-Immunglobulin, die dabei hilft, die Bildung von Antikörpern gegen Rh-positive Blutkörperchen bei Rh-negativen Personen zu verhindern.

FcRn, auch bekannt als neonataler Fc-Rezeptor, ist ein Rezeptor, der an den Fc-Teil von Immunoglobulin G (IgG) bindet. Er spielt eine wichtige Rolle im Transfer von mütterlichen IgG an das Fetus und in der Aufrechterhaltung der IgG-Konzentration im Körper. FcRn ist auch an der Bindung von Albumin beteiligt und spielt eine Rolle im Recycling von IgG.

Hauptfunktion:

Transport von IgG:

FcRn ist verantwortlich für den Transport von mütterlichem IgG durch die Plazenta an den Fetus, wodurch das Neugeborene passiv immunisiert wird.

Recycling von IgG:

FcRn bindet IgG in saurem pH-Wert (z.B. in Endosomen) und schützt es vor intrazellulärem Abbau. Anschließend transportiert er das IgG zurück in den Blutkreislauf, wodurch die IgG-Konzentration im Körper aufrechterhalten wird.

Bindung von Albumin:

FcRn bindet nicht nur IgG, sondern auch Albumin, und spielt möglicherweise eine Rolle in der Albumin-Homöostase.

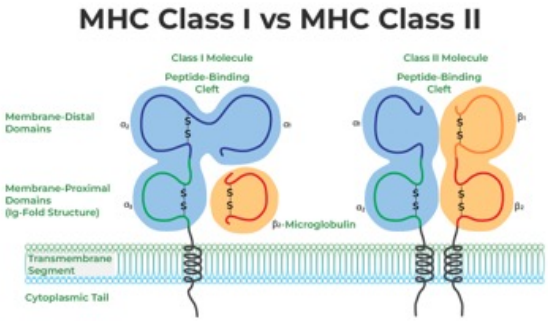

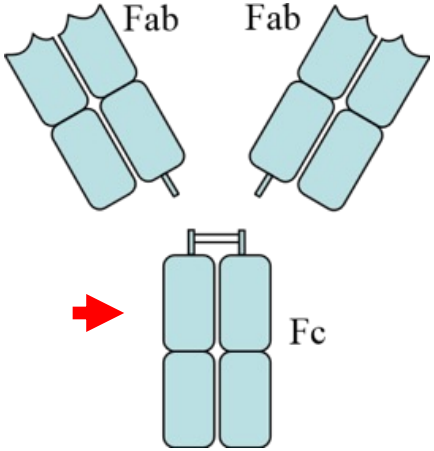

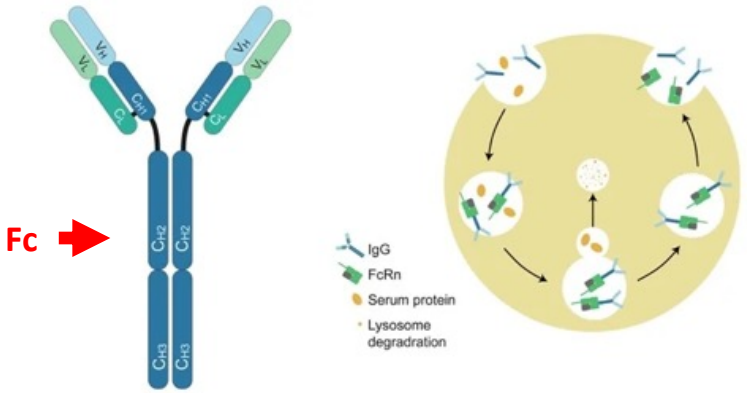

Neonatal Fc Receptor — Biology and Therapeutics

Autoimmune diseases represent a major health care problem, affecting more than 5% of the world's population and involving virtually every organ system. A major pathogenic mechanism involves IgG autoantibodies that recognize self-antigens and induce pathologic effects by way of diverse pathways. IgG is the most abundant antibody type in the bloodstream (with a concentration of 10 g per liter), second only to albumin (with a concentration of 40 g per liter); the high concentrations of IgG and albumin are due to their plasma half-life of 21 days, which exceeds that of any other circulating protein. There is substantial interest in the development of therapeutic approaches to treat IgG-mediated autoimmune diseases that target B cells and plasma cells and the IgG they produce. These strategies include biologic agents that deplete B cells by targeting cell-surface proteins such as CD19 or CD20. Long-lived IgG-producing plasma cells can be targeted by means of their expression of CD38. Alternatively, B cells can be deprived of the B-cell activating factor required for their survival, or activation can be prevented with the use of Bruton's tyrosine kinase inhibitors. Unlike glucocorticoid agents, which are broadly suppressive and modestly decrease the levels of IgG, the levels and activity of IgG are more directly altered by the use of intravenous immune globulin, plasmapheresis, or immunoadsorption, which are toxic, invasive, or of limited availability. Recently, a new class of therapeutics that disable the neonatal Fc receptor (FcRn), which protects IgG from degradation, has emerged to treat IgG-mediated autoimmune disease. Here, we review how advances in our understanding of the biologic features of FcRn led to this new therapeutic approach.

History of FcRn Biology

Our understanding of FcRn derives from foundational studies in the late 19th century by Paul Ehrlich, who used rodent models to investigate the passive transport of immunity from mothers to their offspring through milk. This concept was revived in the mid-20th century by various investigators who showed that transmission of immunity through mother's milk in rodents occurred in the small intestine and was restricted to neonatal life. Transmission was dependent on the Fc, but not the antigen-binding or the Fab region of IgG, and was a saturable process because, at higher IgG concentrations, antibodies were degraded and not transported. Brambell et al. proposed that a selective, receptor-mediated process internalizes and then carries luminal IgG across intestinal epithelial cells into tissues. This transport process (or transcytosis) in rodents involved fluid-phase (or pinocytic) uptake into apical intracellular vesicles, where the IgG bound cell membranes at acidic, but not neutral, pH.

Structure of IgG and Interaction with FcRn.

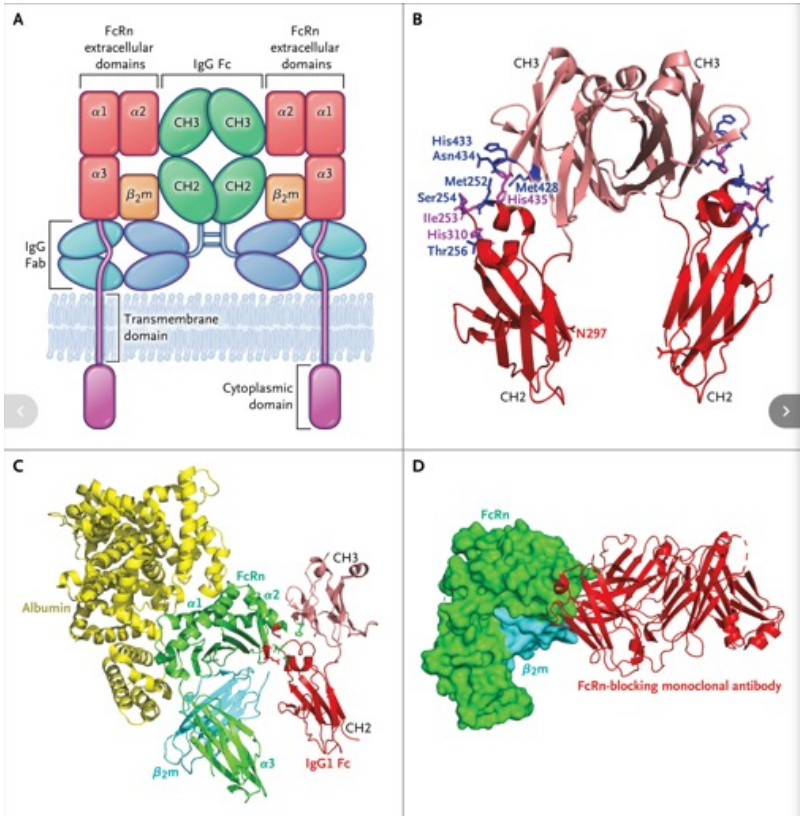

KEY POINTS

FcRn Interactions in IgG-Mediated Therapies

- The neonatal Fc receptor (FcRn) is a developmentally regulated, major histocompatibility complex class I –related molecule that binds IgG and albumin in a pH-dependent manner.
- FcRn protects IgG and albumin from destruction and enables the long half-lives of these circulating proteins.
- FcRn transports IgG across polarized cells and is important for IgG movement across barrier surfaces such as the placenta.
- FcRn regulates IgG function in innate and adaptive immune activities associated with professional antigen-presenting cells; such regulation is involved in protection from infection and cancer and in the development of autoimmune diseases.
- Understanding the biologic features of FcRn has enabled the development of therapeutics that block FcRn–IgG interactions to disrupt placental transport of IgG, cause IgG degradation, and decrease activation of cellular immunity as a new avenue for IgG-mediated treatment of autoimmune and alloimmune diseases.
- Augmentation of IgG–FcRn interactions can be used to extend the half-life of IgG-based therapeutics or enable their transport across epithelia for vaccination or delivery of therapeutic drugs.

Expression and Regulation of FcRn

Originally considered a protein restricted to neonatal life, FcRn is now understood to be expressed by many somatic cell types in adults, a finding that was based originally on the functional expression of FcRn in rat hepatocytes and its presence in the human placenta. FcRn is broadly expressed in adult human parenchymal cells of epithelial and endothelial origin and in hematopoietic cells.

Functions of FcRn

There are three broad categories of FcRn function: a transporter of IgG across polarized cells such as epithelia, a protector of IgG and albumin from catabolism, and a regulator of cellular pathways of immunity associated with myeloid cells. Each pathway may contribute to the pathogenesis of autoimmune diseases and thus influence the therapeutic effects of FcRn blockade.

FcRn as a Transporter

FcRn is expressed in virtually all polarized human epithelial cell types that separate two tissue interfaces, and it is associated with IgG transport across the cell. Foundational studies using human intestinal epithelial-cell monolayers showed that transcytosis mediates bidirectional transport of IgG.

FcRn as a Protection Receptor

On the basis of findings in animal models that the half-life of IgG was inversely related to its serum concentration and dependent on the Fc domain, Brambell drew critical parallels to IgG transport across the epithelium in neonatal rodent models. They hypothesized that a related “protection” receptor was also involved in preventing IgG catabolism.

FcRn as a Regulator of Cellular Immunity

Human monocytes, macrophages, dendritic cells, and neutrophils express high levels of FcRn and various classical FcγRs. The low-affinity activating human FcγRs (FcγRIIa and FcγRIII) bind IgG as a soluble or cell-associated immune complex; the latter occurs, for example, when a microbe or cell, such as a platelet or red cell, is bound by an antibody or autoantibody, respectively.

When FcRn encounters IgG as an immune complex containing a bound antigen, FcRn and its associated immune complex are diverted away from recycling pathways to intracellular compartments involved in class I HLA and class II HLA antigen-processing pathways for activation of CD8+ and CD4+ T cells, respectively. This action can lead to increased B-cell responses and IgG production. These FcRn-regulated cellular pathways are involved in tissue responses that are associated with autoimmune diseases, as shown in models of inflammatory bowel disease and rheumatoid arthritis, or immune responses to cancer. By their nature, these pathways probably sustain autoimmunity and may be amenable to therapeutic blockade with anti-FcRn agents.

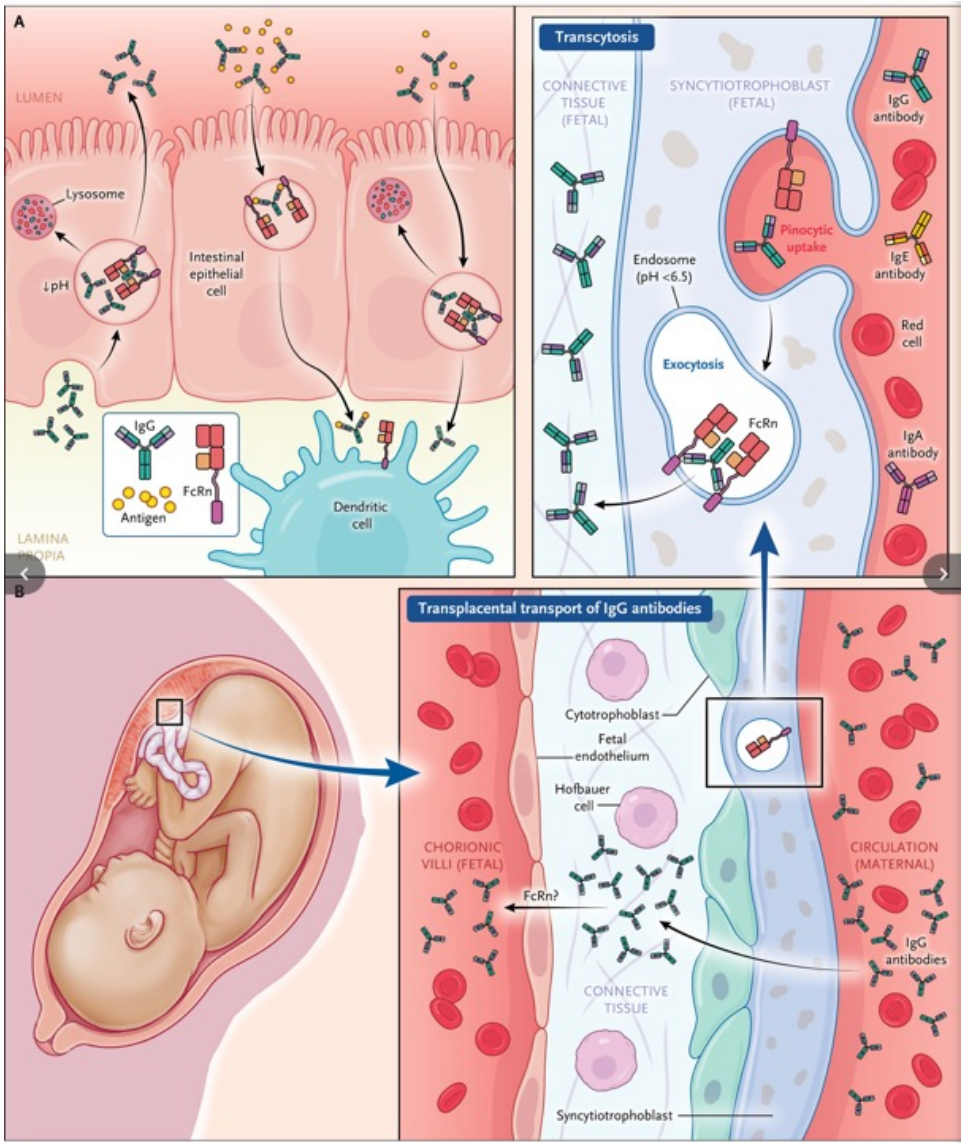

FcRn in Transcytosis and Transplacental Transfer of IgG.

Panel A depicts transcytosis across polarized epithelial cells in adults. In intestinal epithelial cells abutting the lumen of the gut, pinocytosis of IgG from the tissues allows internalization into intracellular acidic vesicles. There, it binds FcRn and is transported to the opposite cell surface facing the lumen, where the FcRn-bound IgG is released. At this point, the IgG antibody can bind luminal antigens, such as those from bacteria, and the reverse cycle of transcytosis takes place, enabling delivery of antigens bound to IgG for uptake by tissue dendritic cells that also express FcRn. Panel B depicts transplacental transfer of maternal IgG to the fetus. In humans, the maternal and fetal circulation are separated by a polarized layer of epithelium (the syncytiotrophoblast). There, maternal IgG is transported from the maternal bloodstream into the stroma and subsequently transmitted across the fetal endothelium to the fetal bloodstream. FcRn is responsible for this transport in the syncytiotrophoblast and possibly in the endothelium. Panel B is adapted from Pyzik et al.[4]

FcRn as a Therapeutic Target for IgG-Mediated Autoimmune Disease

The evidence that FcRn plays a role in the pathogenesis of autoimmune disorders was first provided by genetic models. Mice lacking β2-microglobulin, and thus functional FcRn, are less susceptible to the development of a spontaneous lupus-like autoimmune syndrome. Mice deficient in β2-microglobulin or FcRn are resistant to a bullous pemphigoid disorder caused by injection of anti-hemidesmosome antibodies. FcRn-deficient mice are resistant to antibody-induced autoimmune arthritis. Moreover, the efficacy of intravenous immune globulin in these autoimmune disease models is dependent on FcRn. The first evidence that an IgG-mediated autoimmune disease could be targeted by pharmacologic blockade of FcRn with a therapeutic antibody was provided in an active and a passive model of myasthenia gravis. These studies and others laid the foundation for developing therapeutics that target FcRn to treat IgG-mediated autoimmune disease.

Therapeutic Agents to Block FcRn

Several approaches have been pursued to obtain therapeutic blockade of FcRn by selectively targeting the IgG binding interface. The first involves engineering a human IgG1 Fc domain with five mutations that increase binding to FcRn at acidic and neutral pH values. The crystal structure of this mutated Fc in a complex with human FcRn shows that it binds like a natural Fc fragment but, because it lacks Fab domains, does not abut the membrane of endosomes. In combination with the increased affinity for FcRn binding conferred by mutations, this mutated Fc outcompetes endogenous IgG antibodies for FcRn-mediated protection. It is thus a high-affinity antibody fragment that acts as a decoy and induces IgG degradation (e.g., the FcRn antagonist efgartigimod).

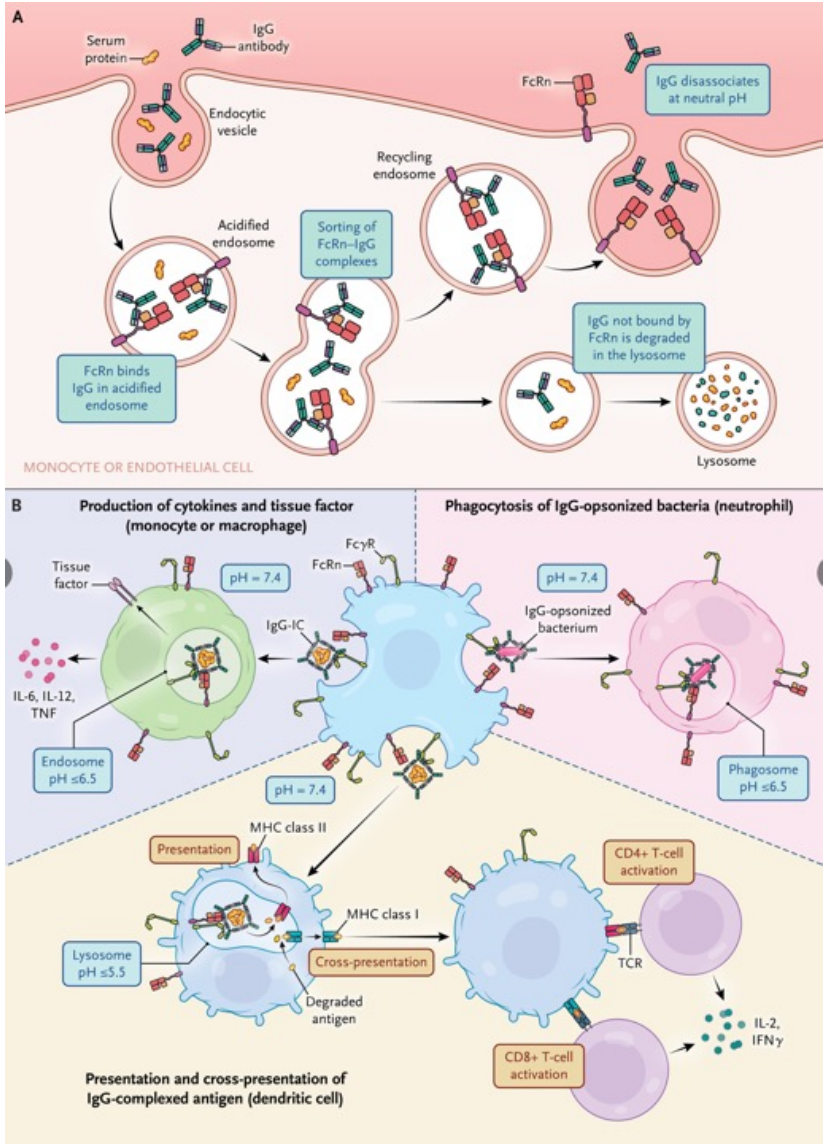

FcRn in Immune Activities.

Panel A depicts the recycling and protection of IgG from catabolism. Fluid-phase uptake of IgG by endothelial and monocytic cells allows binding to FcRn in acidified intracellular endosomal vesicles. These vesicles recycle the FcRn-bound IgG to the plasma membrane, where IgG dissociates from FcRn at the neutral pH of the extracellular milieu. IgG that is not bound by FcRn is transferred to lysosomes for degradation. Panel A is adapted from Roopenian et al.[5] Panel B depicts the immune activities of FcRn. When FcRn on a professional antigen-presenting cell, such as a monocytic or myeloid cell, binds IgG as an immune complex with antigen, several FcRn-regulated functions may be engaged. These include the production of cytokines and other mediators, such as tissue factor, which is associated with the induction of thrombosis; phagocytosis of the IgG-opsonized microbe or cell; and the internalization and transport of the IgG-bound antigens to intracellular compartments where the processing of IgG-associated proteins enables the generation of peptides. These peptides bind to class I and class II HLA molecules for stimulation of CD8+ and CD4+ T cells and their downstream consequences. These cellular pathways occur in cooperation with classical Fcγ receptors. Panel B is adapted from Pyzik et al.[4]

Therapeutic Blockade of FcRn in Clinical Practice

A major benefit of anti-FcRn therapies is that circulating IgG levels provide a pharmacodynamic biomarker. Inhibition of FcRn decreases all IgG subtypes and autoantibodies within the first week of administration, a change that typically plateaus at a reduction of 50 to 70% after multiple doses, depending on the dose and schedule of administration. All FcRn blockers cause prolonged IgG depletion notwithstanding their pharmacokinetic half-lives of 1 to 4 days. Pretreatment levels of gamma globulin may not return for 1 to 3 months after completion of therapy. Preexisting protective antibodies to tetanus toxoid, varicella zoster, or pneumococcus are also decreased by FcRn blockade but return to baseline with global IgG recovery.

Trials are currently under way to examine the therapeutic efficacy of these approaches in many clinical indications. The clearest benefits of FcRn inhibition are seen in cases of myasthenia gravis caused by IgG autoantibodies to the acetylcholinesterase receptor. Findings from studies of the use of intravenous immune globulin in the treatment of myasthenia gravis suggest that a 20 to 30% reduction in autoantibody levels may be a threshold for observing clinical improvement.

Recently, FcRn inhibition has been used to inhibit maternal–fetal transfer of IgG anti-D and anti-Kell antibodies in severe, early-onset hemolytic disease of the fetus and newborn (HDFN). Nipocalimab, at weekly doses intended to completely block FcRn, led to dramatic responses in 7 of 13 fetuses, 8 of which had had siblings that died in previous pregnancies. The 7 fetuses with responses received no other antenatal treatment, in particular no intrauterine transfusions, and only 1 postnatal transfusion, unlike their preceding, severely affected siblings.

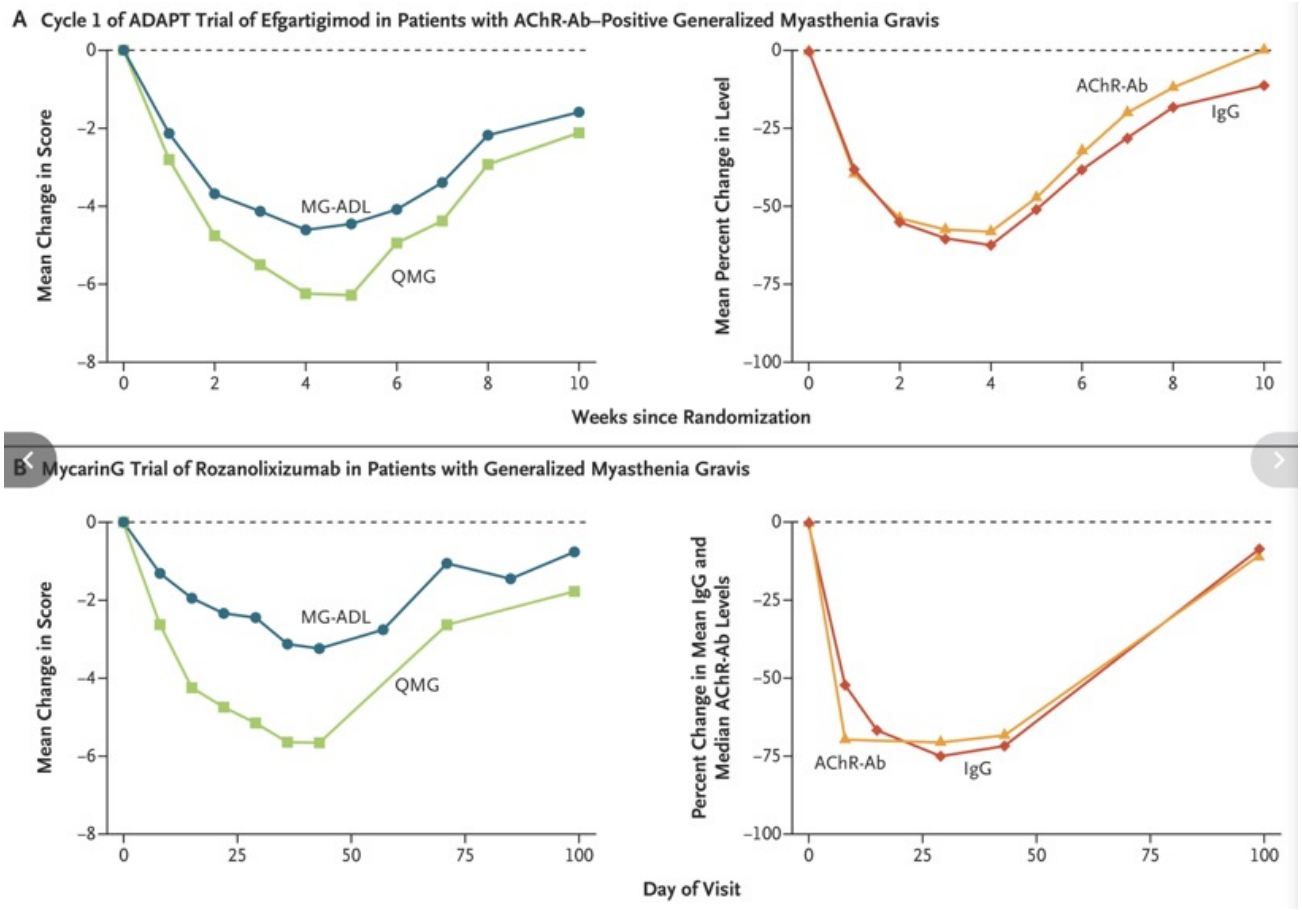

MG-ADL and QMG Scores and IgG and AChR-Ab Levels in ADAPT and MycarinG Trials.

Panel A shows the mean change in the Myasthenia Gravis–Activities of Daily Living (MG-ADL) score (blue circles; higher scores indicate more severe disease) and the Quantitative Myasthenia Gravis (QMG) score (green squares; higher scores indicate more severe disease) and the levels of IgG (red diamonds) and acetylcholine esterase receptor antibody (AChR-Ab; orange triangles) from baseline during cycle 1 of the ADAPT trial of efgartigimod (at a dose of 10 mg per kilogram of body weight per week for 4 weeks) in patients with AChR-Ab–positive generalized myasthenia gravis.[67] The mean changes in MG-ADL and QMG scores reflect decreases (indicating clinical improvement) from baseline. Changes in AChR-Ab and IgG levels are reported as percent decreases from baseline. Panel B shows the mean changes in the MG-ADL score and the QMG score and the percent changes in levels of IgG and AChR-Ab from baseline to day 43 of the treatment period and through the final visit of the MycarinG trial of rozanolixizumab at a dose of 10 mg per kilogram of body weight per week for 6 weeks in patients with generalized myasthenia gravis.[68] The mean changes in MG-ADL and QMG scores reflect decreases from baseline. The changes in levels of AChR-Ab and IgG are reported as percent decreases from baseline; a decrease of 2 or more in the MG-ADL score and a decrease of 3 or more in the QMG score are considered clinically important. In all graphs, each point represents 46 to 69 observations.

Efgartigimod ist ein humanisiertes IgG1-Fc-Fragment, das an den neonatalen Fc-Rezeptor bindet und dessen Wechselwirkung mit IgG hemmt, wodurch das IgG-Recycling reduziert und der Abbau von IgG und pathologischen Autoantikörpern gesteigert wird, ohne andere Immunglobuline und Albuminspiegel zu verändern.

IgG-Mediated Autoimmune Diseases under Evaluation for Anti-FcRn Therapies.

Category or Organ System and Disease	Representative Autoantigens	Major IgG Subclasses
Peripheral and central nervous system		
CIDP†	Myelin-associated antigens — contactin-1, contactin-associated protein 1, neurofascin-155	IgG1, IgG3, and IgG4
Myasthenia gravis‡	Acetylcholine receptor, muscle-specific kinase	IgG1, IgG3, and IgG4
Autoimmune encephalitis	N-methyl-D-aspartate receptor, leucine-rich glioma-inactivated 1, contactin-associated protein-like 2, γ-aminobutyric acid-B receptor	IgG1 and IgG3
Guillain–Barré syndrome	Gangliosides (GM1, GD1a, GT1a, GT1b, and GQ1b)	Various subclasses
Myelin oligodendrocyte glycoprotein antibody-associated disease and neuromyelitis optica spectrum disorder	Myelin oligodendrocyte glycoprotein, aquaporin-4	IgG1
Stiff-person syndrome	Glutamic acid decarboxylase, glycine receptor, amphiphysin, gephyrin, dipeptidyl peptidase-like protein 6	IgG1
Skin		
Pemphigus vulgaris	Desmoglein 1 and desmoglein 3	IgG1 and IgG4
Pemphigus foliaceus	Desmoglein 1	IgG1 and IgG4
Bullous systemic lupus erythematosus	Collagen VII	IgG2 and IgG3
Bullous pemphigoid	Type XVII collagen (BP180), bullous pemphigoid antigen (BP230)	IgG1 and IgG4, occasionally IgG2 and IgG3
Hematologic system		
Immune thrombocytopenic purpura§	Platelet glycoproteins (GPIIb/IIIa, GPIb/IX)	IgG1 and IgG3
Warm autoimmune hemolytic anemia	Erythrocyte membrane proteins (Rh complex, band 3, glycophorin A)	IgG1 and IgG3
Rheumatologic diseases		
Rheumatoid arthritis	Citrullinated proteins (vimentin, fibrinogen, enolase)	Various subclasses, particularly IgG1
Autoimmune inflammatory myopathies (dermatomyositis, polymyositis, necrotizing myopathy)	Nuclear helicase Mi-2, transcription intermediary factor 1-γ, melanoma differentiation-associated protein 5, nuclear matrix protein 2, aminoacyl-tRNA-synthetases (especially histidyl-tRNA synthetase), signal recognition particle, HMG-coA-reductase, and other myositis-specific autoantigens	IgG1 and IgG3
Sjögren's syndrome	Ro Sjögren's syndrome (SS)–related antigen A, lupus antigen (La) SS antigen B	IgG1 and IgG3
Systemic lupus erythematosus	Double-stranded DNA, Smith antigen (small nuclear ribonucleoproteins)	IgG1 and IgG3
Fetal and newborn conditions		
Fetal and neonatal alloimmune thrombocytopenia	Human platelet antigen	IgG1
HDFN	Fetal red-cell antigens (RhD, RhC, Kell)	Various subclasses, particularly IgG1 and IgG3
Renal diseases		
Lupus nephritis	DNA, RNA, histones, and other nuclear antigens	Various subclasses, often IgG1 and IgG3
Primary membranous nephropathy¶	Phospholipase A2 receptor, thrombospondin type-1 domain-containing protein 7A	IgG4
Organ transplantation — antibody-mediated rejection	Donor-specific human leukocyte antigen	Various subclasses
Gastrointestinal diseases — autoimmune pancreatitis¶	Lactoferrin, carbonic anhydrase II	IgG4
Infectious disease-induced autoimmunity — Covid-19–mediated postural orthostatic tachycardia syndrome	Autoantigens not yet fully characterized	Not strongly linked to a specific immunoglobulin subtype
Endocrine disorders		
Graves' disease	Thyroid-stimulating hormone receptor	IgG1
Thyroid eye disease	Thyroid-stimulating hormone receptor, type 1 insulin-like growth factor receptor	IgG1
Idiopathic diseases — fibromyalgia	Autoantigens not clearly defined	No specific immunoglobulin subtype associated

Conclusion

Insights from foundational studies that deciphered the transport of immunity from a mother to her offspring has led in the ensuing years to delineation of FcRn as a critical factor in determining the transport, lifespan, and activity of its two ligands, IgG and albumin. This understanding has enabled, and now validated, FcRn as a therapeutic target in the treatment of IgG-mediated alloimmune and autoimmune diseases. Manipulation of FcRn, whether by inhibition or augmentation, may prove to be an important part of the therapeutic armamentarium in the prevention and treatment of infectious diseases, autoimmunity, and cancer.

Cutaneous Leishmaniasis

The Images in Clinical Medicine *featured in this issue of the* Journal *spotlight some of the effects of the climate crisis on clinical health.*

A previously healthy 3-year-old boy was brought to the emergency department with a 6-week history of painless bumps and ulcers on his left leg. He initially had itchy insect bites on his foot, and then bumps and ulcers had developed slowly on his leg. The boy had recently immigrated from Venezuela after a months-long journey by land with his family. On physical examination, ulcerated plaques with rolled borders and satellite papules were observed on the left lower leg, buttocks, and back. Three biopsy samples were obtained from one of the lesions. Histopathological analysis was notable for severe lymphohistiocytic infiltration with no organisms identified by routine microbiologic stains. Polymerase-chain-reaction testing of a tissue sample identified *Leishmania guyanensis*. A diagnosis of cutaneous leishmaniasis was made. Leishmaniasis is caused by a protozoa parasite that is transmitted by phlebotomine sandfly bites. Cutaneous leishmaniasis is the most common manifestation of the disease and may result in disfiguring scars. Climate change is affecting the spread of leishmaniasis by altering the geographic distribution and size of sandfly populations. People experiencing poverty and migration are at highest risk for acquiring the infection. After a 28-day course of miltefosine, the skin lesions resolved.

Pavement Burns

The Images in Clinical Medicine *featured in this issue of the* Journal *spotlight some of the effects of the climate crisis on clinical health.*

A 56-year-old man with a history of alcohol use disorder was transferred to a burn center for management of burns on his feet. The patient had walked barefoot on asphalt for 1 minute while he was intoxicated. The injury had occurred during the 2021 Pacific Northwest heat dome, a heat wave during which maximum air temperatures reached 42°C (108°F), approximately 21°C (38°F) above historical averages. On physical examination, the patient was in severe pain. He had unroofed blisters with oozing and erythema on the soles of both feet, on the plantar surfaces of the toes of the right foot, and on the heel of the left foot. An intact blister was also present on the right heel. A diagnosis of second-degree pavement burns was made. Extreme heat events increase the risk of contact burns from hot surfaces in the environment. Young children, older adults, unhoused persons, and persons with substance use disorder are at elevated risk for these types of burns. The patient was admitted to the burn unit. He received treatment with an analgesic agent, wound débridement, bacitracin, and an antimicrobial foam dressing. At an 18-day follow-up visit, the patient's burns were healing without complications.

Case 12-2025: A 56-Year-Old Woman with Sore Throat and Rash

A 56-year-old woman was evaluated in the emergency department of this hospital because of sore throat and rash.
The patient had been in her usual state of health until 2 days before the current presentation, when sore throat and pruritus on the chest developed. There was a history of depression with psychosis, and she resided in a homeless shelter. Despite pruritus, the patient did not inspect the skin on her chest.
On the day of the current presentation, while the patient was looking in the mirror in a public bathroom, she noticed a rash on her face, which prompted her to look at the rest of her skin. She saw that the rash also involved the chest, abdomen, and legs. She presented to the emergency department of this hospital for evaluation.
In the emergency department, the patient reported ongoing pruritus and sore throat. She noted that several residents at the homeless shelter had appeared to be scratching themselves in the week before the current presentation, and she had heard an employee at the shelter discussing lice and scabies with another shelter resident. There was no known exposure to new soaps, detergents, or lotions. She did not sleep outside or spend time in the woods. She was not sexually active. She had no fever, malaise, headache, confusion, changes in strength or sensation, dyspnea, or cough. In addition to her history of depression with psychosis, she had a history of dyslipidemia and metabolic dysfunction–associated steatohepatitis. Medications included risperidone and benztropine. There were no known adverse reactions to medications. She did not smoke tobacco, drink alcohol, or use illicit drugs.
The temporal temperature was 38.4°C, the blood pressure 134/72 mm Hg, the pulse 83 beats per minute, the respiratory rate 16 breaths per minute, and the oxygen saturation 96% while the patient was breathing ambient air. She was alert and cooperative. Diffuse pink papules were present on the forehead, nose, cheeks, and chin. An ulcer was present on the anterior upper gum. Excoriated papules and vesicles were seen on the back, chest, and abdomen, with involvement of the inframammary and inguinal folds. Pink papules were noted on the dorsal aspect of the hands and the palms (not shown). The lung sounds were normal. Labs showed 5 % atypical lymphocytes but were otherwise normal.

Clinical Photographs.

Diffuse pink papules are present on the forehead, nose, cheeks, and chin (Panel A). An ulcer is present on the anterior upper gum (Panel B). Excoriated papules and vesicles are shown on the back (Panel C), chest (Panel D), and abdomen (Panel E), with involvement of the inframammary and inguinal folds (Panel F). The patient's hands are shown in Panel B and at the top of Panel F.

Chicken pox that I know:

Homelessness and Dermatologic Disease

Persons experiencing homelessness are disproportionately affected by dermatologic conditions, possibly owing to limited access to hygiene facilities, exposure to communal living environments, and barriers to health care access.[1] The use of shared spaces and bedding increases the risk of parasitic infestations. In persons experiencing homelessness, chronic conditions such as eczema, psoriasis, and seborrheic dermatitis are often severe and untreated.

Parasitic Infestations

Scabies

Scabies is a parasitic infestation caused by the mite *Sarcoptes scabiei* var. *hominis*, which burrows into the skin to lay eggs. Subtypes include classic, nodular, and crusted (Norwegian) scabies. Patients with classic scabies present with burrows, erythematous papules, and excoriations that typically involve the interdigital web spaces, wrists, ankles, axillae, genitals, and periumbilical regions.

This patient's rash involved the face, which is not consistent with the typical scabies rash distribution. Severe scabies reactions can cause widespread eruptions similar to that seen in this patient, but vesicles would be an uncommon manifestation.

Crab Lice

The crab louse, *Pthirus pubis*, is an obligate parasite that attaches to hair shafts, primarily in the pubic region, axillae, eyelashes, and beard. Findings associated with crab lice infestation include pruritus, erythematous papules, nits (eggs) on hair shafts, and rarely, maculae ceruleae (blue-gray macules caused by bilirubin breakdown).

Body Lice

The body louse, *Pediculus humanus corporis*, is a parasite that typically resides in clothing seams and moves to the skin to feed. Patients with body lice infestation present with diffuse pruritic papules and excoriations; secondary bacterial infections can develop. Body lice infestation — unlike scabies and infestations of crab lice and head lice — is strongly associated with homelessness, with the prevalence ranging from 19.1 to 68.0% among persons experiencing homelessness.

Avoiding Anchoring Bias

Although parasitic infestations are prevalent among persons experiencing homelessness, there is a risk of anchoring on the patient's residence in a homeless shelter where other residents might have had pruritus. Anchoring bias — the cognitive tendency to lock onto salient features of a patient's initial presentation without adjusting after additional information is obtained — can hinder diagnostic accuracy.

Drug Reactions

A drug reaction should be considered in any patient with a diffuse rash. Many drug-related eruptions can be classified as severe cutaneous adverse reactions to medication, including life-threatening conditions such as the Stevens–Johnson syndrome, toxic epidermal necrolysis, and drug reaction with eosinophilia and systemic symptoms (DRESS) syndrome.

Viral Infections

Measles

Patients with measles present with a morbilliform rash consisting of macules and papules that coalesce into patches and plaques. The rash typically begins on the face and spreads in a cephalocaudal manner. Koplik spots (bluish-white papules on the buccal mucosa) are a hallmark feature of measles. Systemic symptoms include a high temperature, cough, coryza, and conjunctivitis.

Rubella

Like measles, rubella is more common in unvaccinated persons. Rubella resembles measles in terms of the rash, but the systemic symptoms are milder. Postauricular and occipital lymphadenopathy is a distinguishing feature of rubella. This patient's rash, with macules and papules that did not coalesce, was not consistent with rubella, nor was the presence of vesicles and enanthem.

Acute HIV Infection

Acute retroviral syndrome develops in up to 80% of patients with a new human immunodeficiency virus (HIV) infections typically occurring 2 to 6 weeks after exposure to the virus. Symptoms last days to weeks and include fever, myalgia, pharyngitis, lymphadenopathy, and night sweats.

Herpes Simplex Virus Infection

Patients with herpes simplex virus (HSV) infection typically present with localized vesicular lesions that progress to pustules and crusts. Oral or genital mucosal involvement is common, and the morphologic appearance can vary depending on the HSV subtype and means of acquisition. Although vesicular lesions were present in this patient, the diffuse nature of her rash would be atypical of both primary HSV infection and HSV reactivation. Disseminated HSV infection can occur in immunocompromised persons, causing a systemic illness that is characterized by fever, headache, neurologic findings, and other end-organ disease.

Mpox

Patients with mpox typically present with a localized vesiculopustular rash with a stereotyped progression. Established lesions are often deep-seated, well-circumscribed, and umbilicated. The rash can affect the face, hands, feet, chest, genitals, and perianal region. Although the rash is usually localized, it can be diffuse in some cases.

Varicella–Zoster Virus Infection

Varicella–zoster virus (VZV) infection is a highly contagious herpesvirus infection that causes two distinct clinical syndromes: varicella (chickenpox) and herpes zoster (shingles). Varicella is caused by primary VZV infection, whereas herpes zoster results from VZV reactivation. After primary infection occurs, VZV establishes latency in the dorsal-root ganglia and can reactivate later in life.

Primary VZV infection typically affects children. Widespread childhood vaccination has reduced both the incidence and the severity of disease, given that breakthrough cases in vaccinated persons tend to be milder. The rash associated with varicella is polymorphic, including erythematous macules, papules, vesicles, and crusts at various stages at the same time. Lesions typically spread in a cephalocaudal manner, starting on the scalp and face and progressing to the trunk, arms, and legs. Additional symptoms include fever and malaise. The rash is accompanied by pruritus, as opposed to pain.

VZV reactivation typically occurs in adults, with increasing age being the most important risk factor. The rash associated with herpes zoster develops in a dermatomal distribution, starting with painful vesicular lesions that proceed through numerous stages but appear and evolve synchronously within the dermatome affected. In the context of disseminated disease, which can be seen in immunocompromised persons, the rash can be widespread.

This patient did not have known risk factors for immunocompromise and did not describe the rash as painful, so a diagnosis of disseminated herpes zoster was unlikely. Varicella is rare in adults, but it can occur and is associated with severe disease and complications such as hepatitis and pneumonitis. Therefore, prompt recognition of the diagnosis and initiation of treatment is important. In this patient, the presence of vesicles, enanthem, and polymorphic lesions, as well as elevated hepatic-enzyme levels, is most consistent with primary VZV infection.

To establish the diagnosis, I would unroof and scrape a prominent vesicular lesion to obtain a specimen for VZV-specific nucleic acid testing or direct fluorescent antibody testing. Given that disseminated HSV infection is also a possibility, I would send a specimen for HSV-specific nucleic acid testing or direct fluorescent antibody testing. A biopsy of the rash would be appropriate if pathological examination of the specimen could be performed within a short time frame, allowing for the rapid initiation of antiviral therapy and limiting the spread of disease.

Dr. John Trinidad's Diagnosis

Primary varicella–zoster virus infection (Chicken Pox oder Windpocken).

Diagnostic Testing

Examination of a punch-biopsy specimen of the skin on the right side of the chest revealed vesicular and acantholytic changes involving the epidermis and hair-follicle epithelium. There was marked epidermal necrosis; keratinocytes had prominent viral cytopathic effects, including multinucleation, nuclear molding, and chromatin margination. Immunohistochemical staining for VZV showed strong nuclear and cytoplasmic positivity. In contrast, immunohistochemical staining for HSV-1 and HSV-2 was negative. Nucleic acid testing for VZV DNA performed on the skin-biopsy specimen confirmed the presence of VZV, whereas nucleic acid testing for HSV-1 and HSV-2 DNA was negative. Bacterial culture of the biopsy specimen grew *Cutibacterium acnes* (formerly *Propionibacterium acnes*), a component of normal skin flora that resides predominantly in sebaceous glands. Mycobacterial and fungal cultures were negative. Serologic testing showed no detectable VZV IgM or IgG, and screening for HIV-1 antigens and for HIV-1 and HIV-2 antibodies was also negative. Overall, these findings are diagnostic of VZV infection.

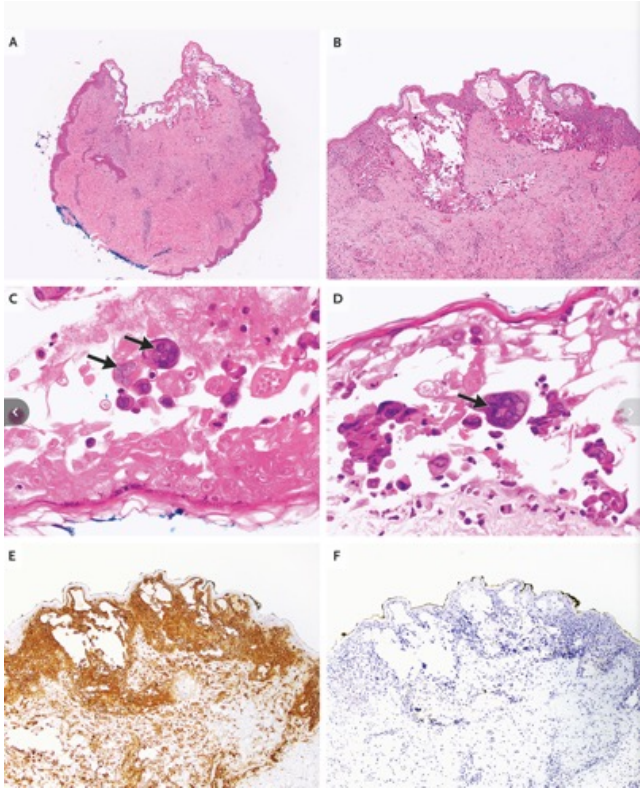

Biopsy Specimen of the Skin on the Right Side of the Chest. Hematoxylin and eosin staining shows vesicular and acantholytic changes involving the epidermis and hair-follicle epithelium (Panels A and B). Keratinocytes have prominent viral cytopathic effects, including multinucleation, nuclear molding, and chromatin margination (Panels C and D, arrows). Immunohistochemical staining for varicella–zoster virus shows strong nuclear and cytoplasmic positivity (Panel E), whereas immunohistochemical staining for herpes simplex virus is negative (Panel F).

Discussion of Management

Many of us have experienced chickenpox as an uncomfortable but relatively inconsequential rite of passage during childhood. However, we are obliged to remember that this highly transmissible infection can lead to serious complications.

Effective infection control follows three steps: identify, isolate, and inform. Given that primary VZV infection conveys a high level of lifelong immunity to a second episode of clinical disease, chickenpox has long been uncommon among adults in the United States. The incidence among children has plummeted with widespread uptake of the varicella vaccine, which after two doses is approximately 95% effective in preventing clinical disease, although not subclinical infection. Many clinicians therefore may be relatively unfamiliar with the clinical presentation of chickenpox, and we must remember to consider it in any patient presenting with a compatible rash. In this patient, there was an approximately 24-hour delay in recognition. Although more than 95% of adults born in the United States before 1980 have had chickenpox and are protected from a second episode, some have not had primary VZV infection and have not been vaccinated against it. The occurrence of a second episode of chickenpox, albeit very rare, is well-described, even in ostensibly immunocompetent persons.

Case Records Editors' Note — Lessons Learned

1. Persons experiencing homelessness are disproportionately affected by dermatologic conditions. Although parasitic infestations are prevalent in this population, anchoring on infestations as the cause of diffuse rash can delay the diagnosis of viral infection.
2. Primary VZV infection is uncommon in adults but should be considered in immunocompetent patients who have a diffuse rash that is compatible with varicella.

Final Diagnosis

Primary varicella–zoster virus infection.

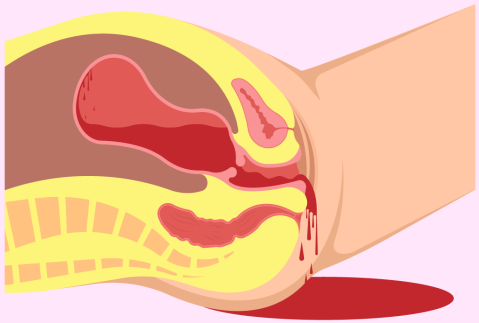

Postpartum haemorrhage

Uterine atony

Placental debris

Abnormal placentation

Uterine inversion

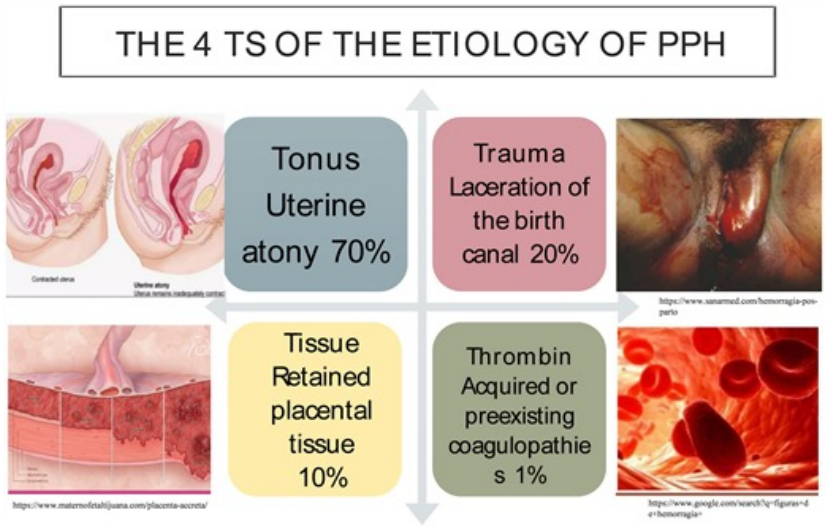

FIGO. Guidelines: prevention and treatment of postpartum hemorrhage in low-resource settings. Int. J. Gynecol. Obstet. v. 117, n. 2, p. 108-18, may 2012.

Causes of and risk factors for postpartum haemorrhage: a systematic review and meta-analysis

Summary

Background An understanding of the causes of postpartum haemorrhage is needed to provide appropriate treatment and services. Knowledge of the risk factors for postpartum haemorrhage can help address modifiable risk factors. We did a systematic review and meta-analysis to identify and quantify the various causes and risk factors for postpartum haemorrhage.

Methods In this systematic review and meta-analysis, we did a systematic literature search in MEDLINE, Embase, Web of Science, Cochrane Library, and Google Scholar for cohort studies of postpartum haemorrhage from Jan 1, 1960, to Nov 30, 2024 without language restrictions. At least two authors independently undertook study selection, data extraction, and quality assessment. Population-based cohort studies available in English were eligible. Rates of postpartum haemorrhage causes as well as crude and adjusted odds ratios (ORs) for risk factors were pooled using a random-effects model. Risk factors were classified as having weak, moderate, or strong association based on the pooled ORs: weak (OR >1 to 1·5), moderate (OR >1·5 to 2), and strong (OR >2). This study is registered with PROSPERO, CRD42023479686.

Findings We synthesised data from 327 studies, including 847 413 451 women with no restriction on age, race, or ethnicity. Most studies were of high methodological quality. The pooled rates of the five commonly reported causes of postpartum haemorrhage were uterine atony (70·6% [95% CI 63·9–77·3]; n=834 707 women, 14 studies), genital tract trauma (16·9% [9·3–24·6]; n=18 449 women, six studies), retained placenta (16·4% [12·3–20·5]; n=235 021 women, nine studies), abnormal placentation (3·9% [0·1–7·6]; n=29 638 women, two studies), and coagulopathy (2·7% [0·8–4·5]; n=236 261, nine studies). The pooled rate of women with multiple postpartum haemorrhage causes was 7·8% (95% CI 4·7–10·8; n=666, two studies). Risk factors with a strong association with postpartum haemorrhage included anaemia, previous postpartum haemorrhage, caesarean birth, female genital mutilation, sepsis, no antenatal care, multiple pregnancy, placenta praevia, assisted reproductive technology use, macrosomia with a birthweight of more than 4500 g, and shoulder dystocia. Risk factors with moderate association with postpartum haemorrhage included BMI ≥30 kg/m², COVID-19 infection, gestational diabetes, polyhydramnios, pre-eclampsia, and antepartum haemorrhage. Risk factors with weak association with postpartum haemorrhage included Black and Asian ethnicity, BMI 25–29·9 kg/m², asthma, thrombocytopenia, uterine fibroids, antidepressant use, induction of labour, instrumental birth, and premature rupture of membranes.

Interpretation The finding that uterine atony is the commonest cause of postpartum haemorrhage supports the WHO recommendation for all women giving birth to be given prophylactic uterotonics. Knowledge of risk factors with a strong association with postpartum haemorrhage can help to identify women at high risk of postpartum haemorrhage who could benefit from enhanced prophylaxis and treatment. The importance of multiple concurrent causes of postpartum haemorrhage supports the use of treatment bundles.

Oxytocin ist das am häufigsten verwendete Uterotonikum, gefolgt von Ergometrin, Methylergometrin, Carboprost und Misoprostol

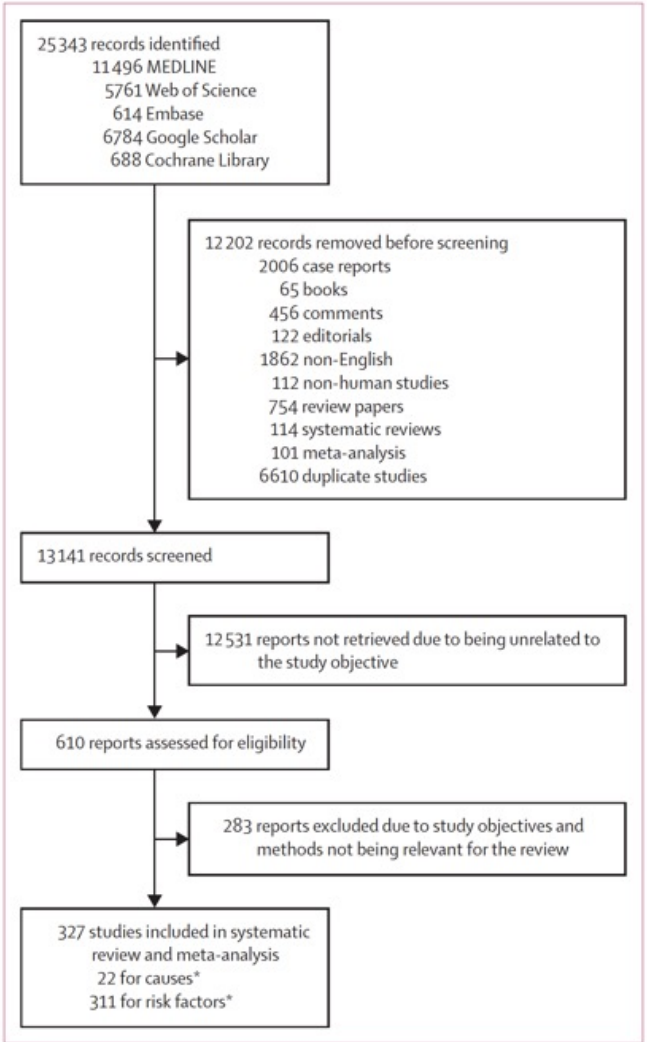

Figure 1: **Study selection**
*Six of the included studies had data for both causes and risk factors.

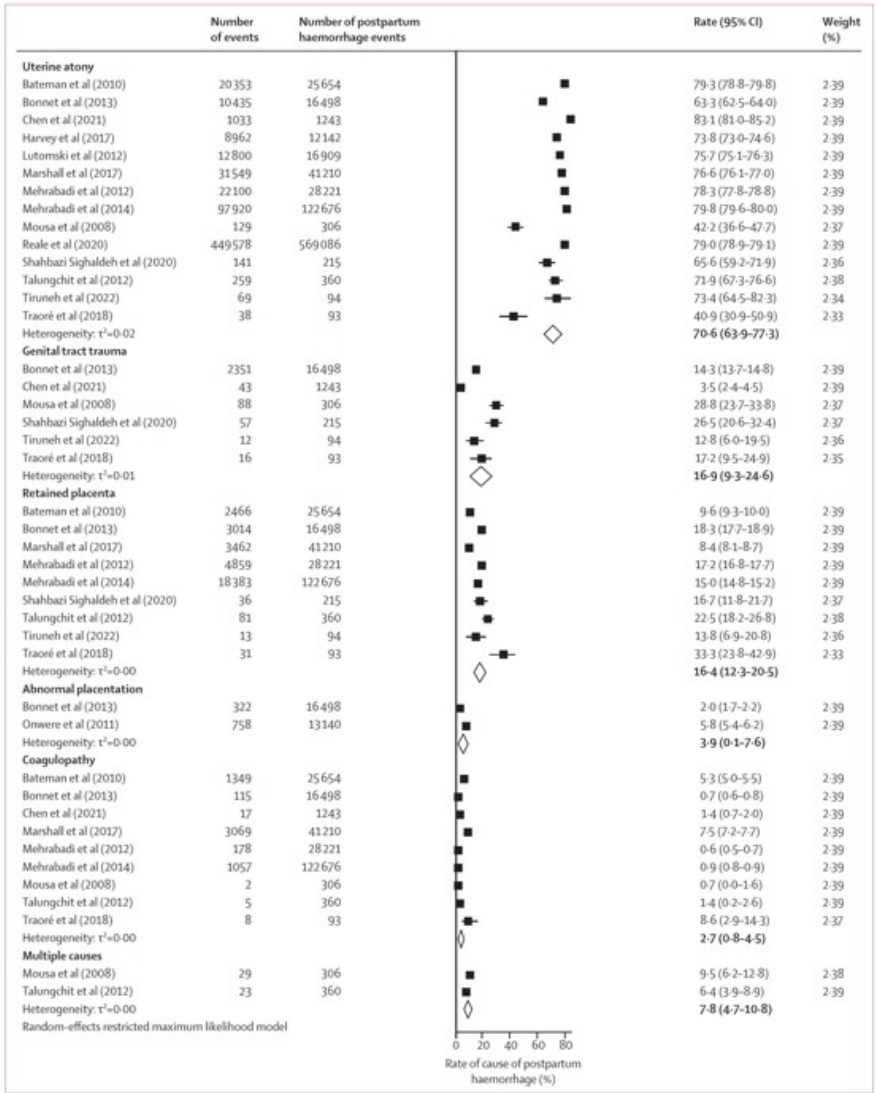

Figure 2: **Rates of causes of postpartum haemorrhage**

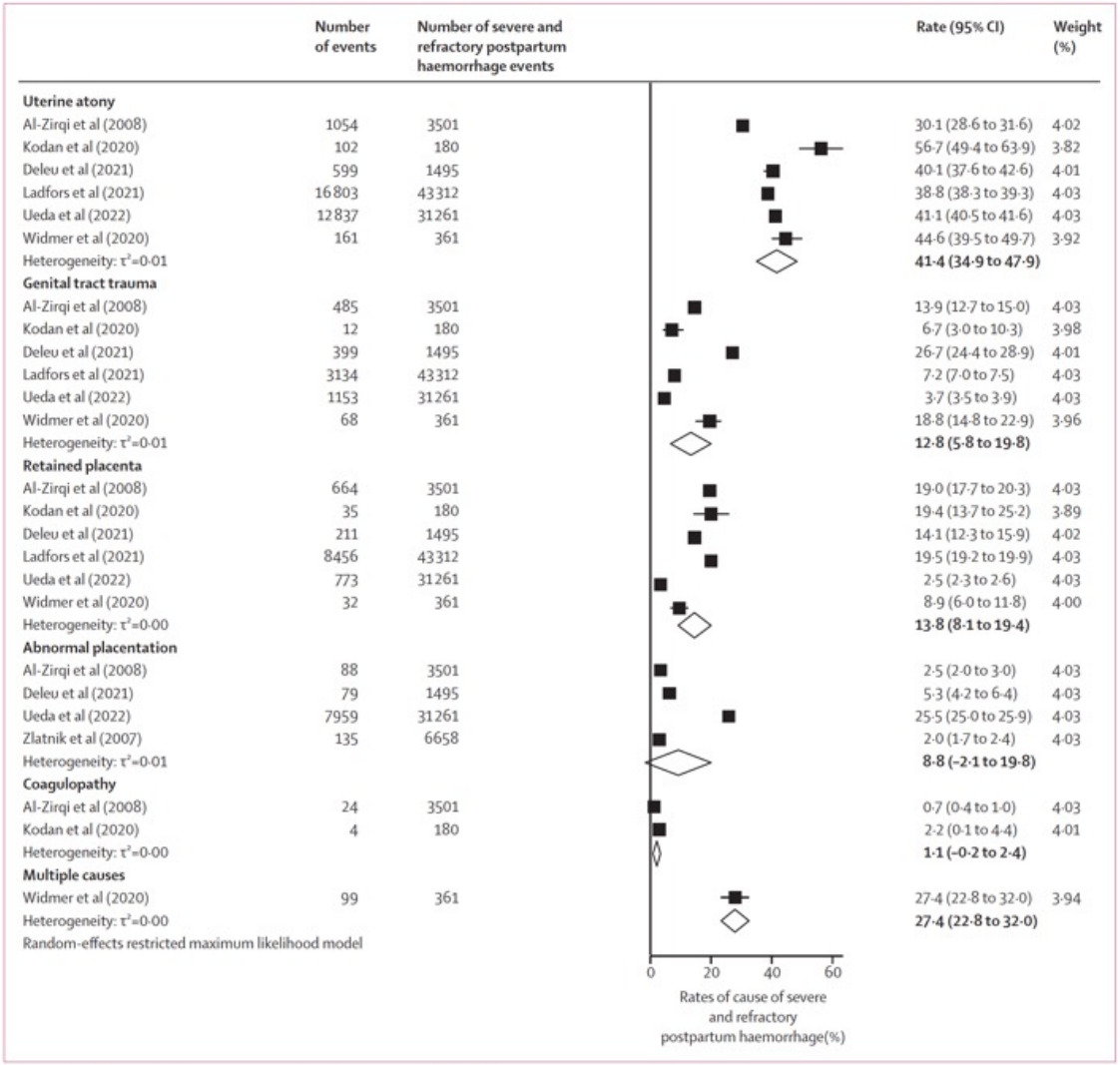

Figure 3: **Rates of causes of severe and refractory postpartum haemorrhage**

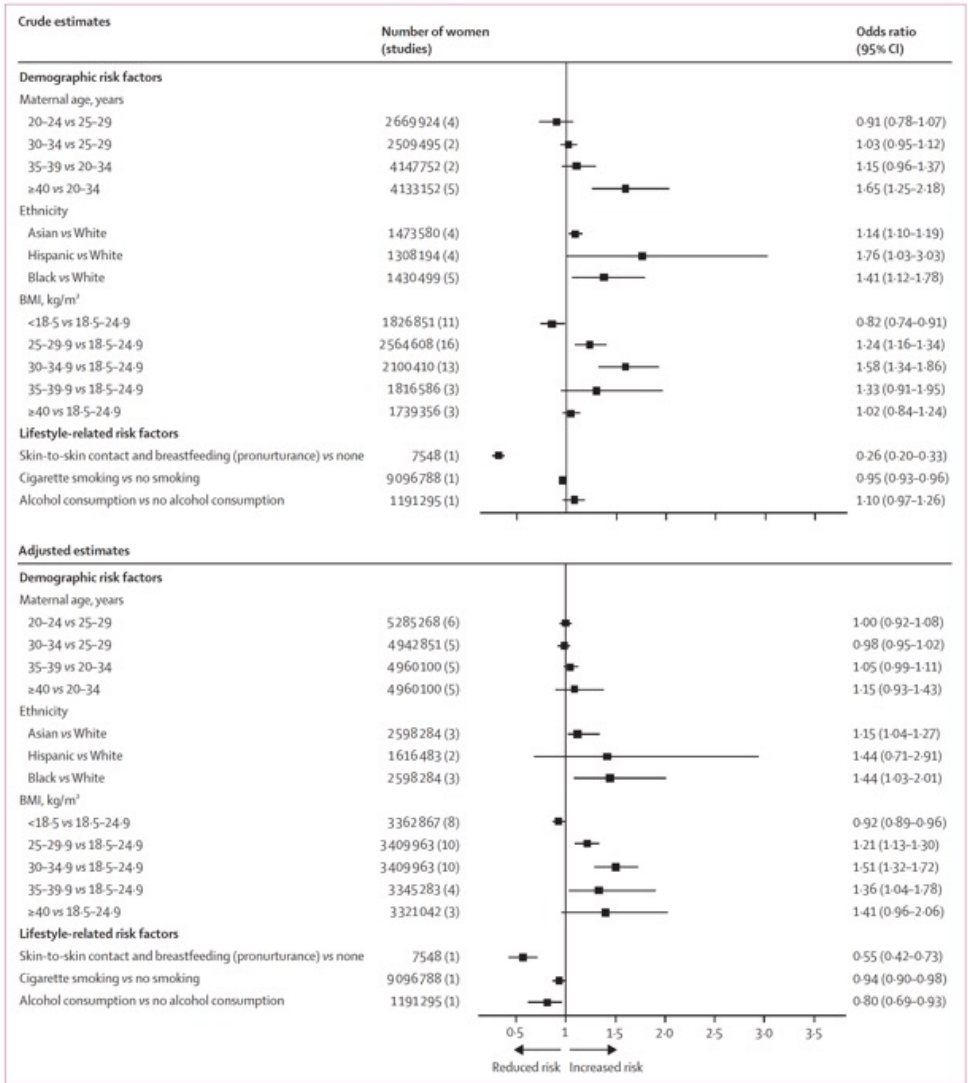

Figure 4: **Demographic and lifestyle-related risk factors for postpartum haemorrhage**

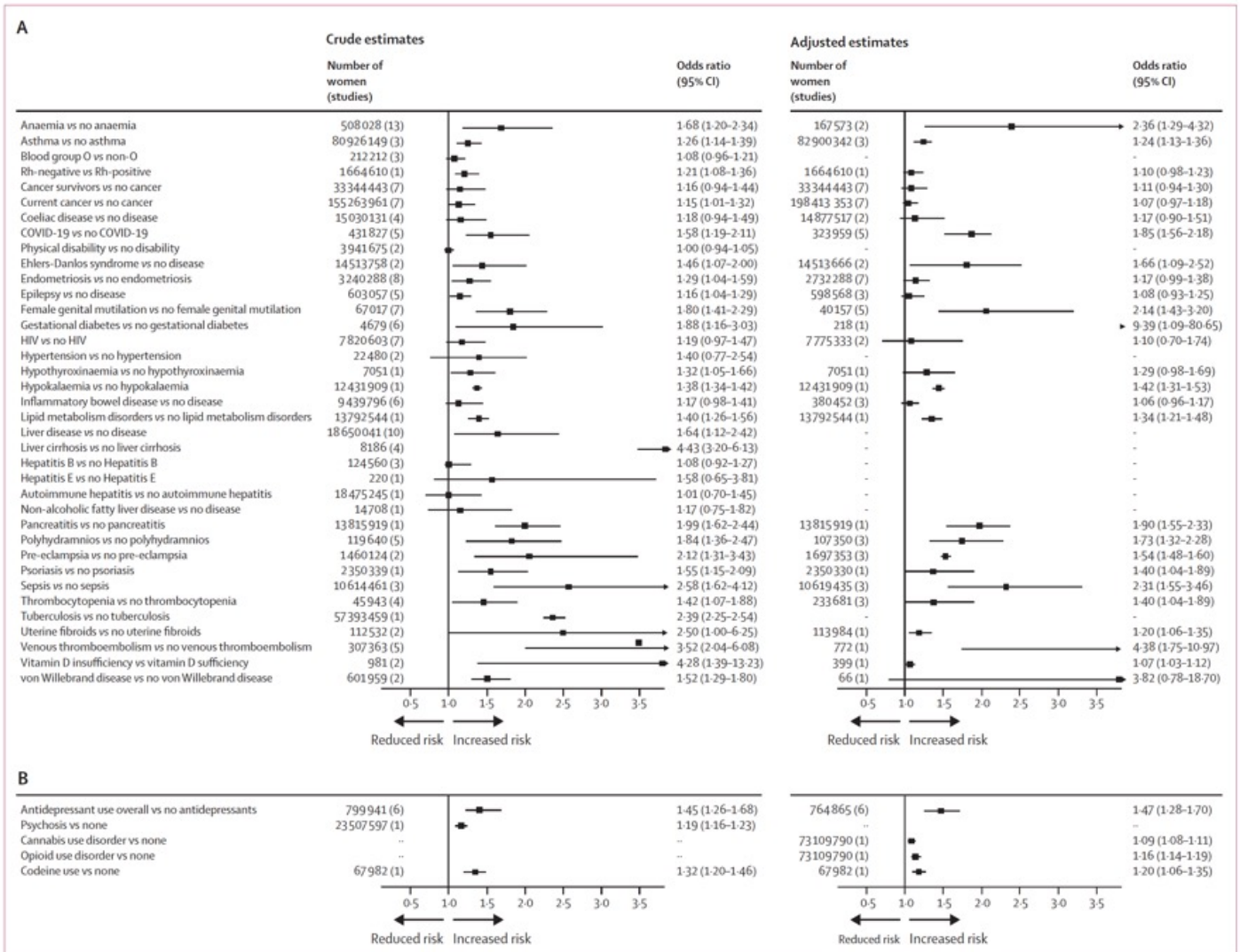

Figure 5: **Medical risk factors (A and B) for postpartum haemorrhage**

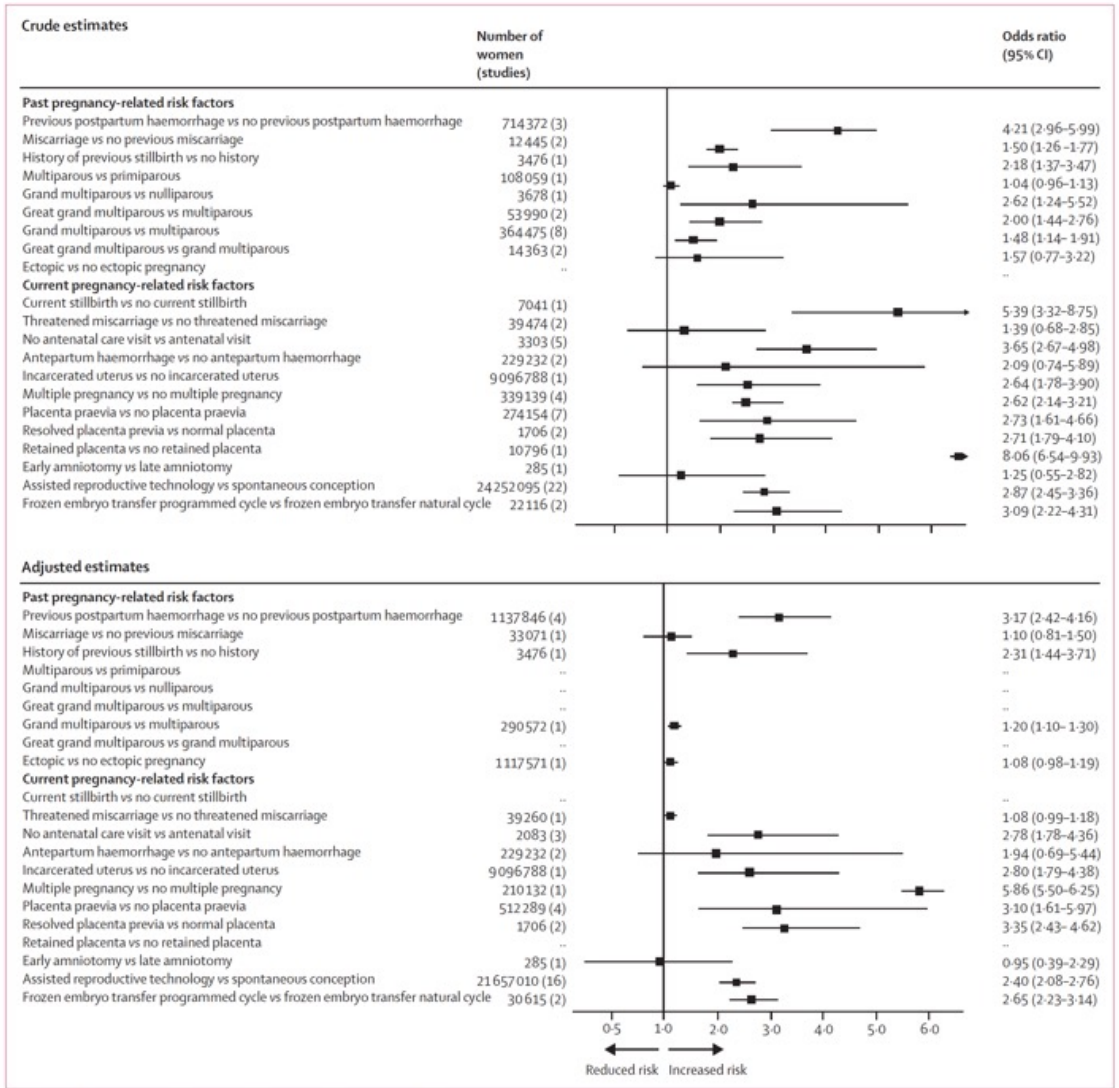

Figure 6: **Pregnancy-related risk factors for postpartum haemorrhage**

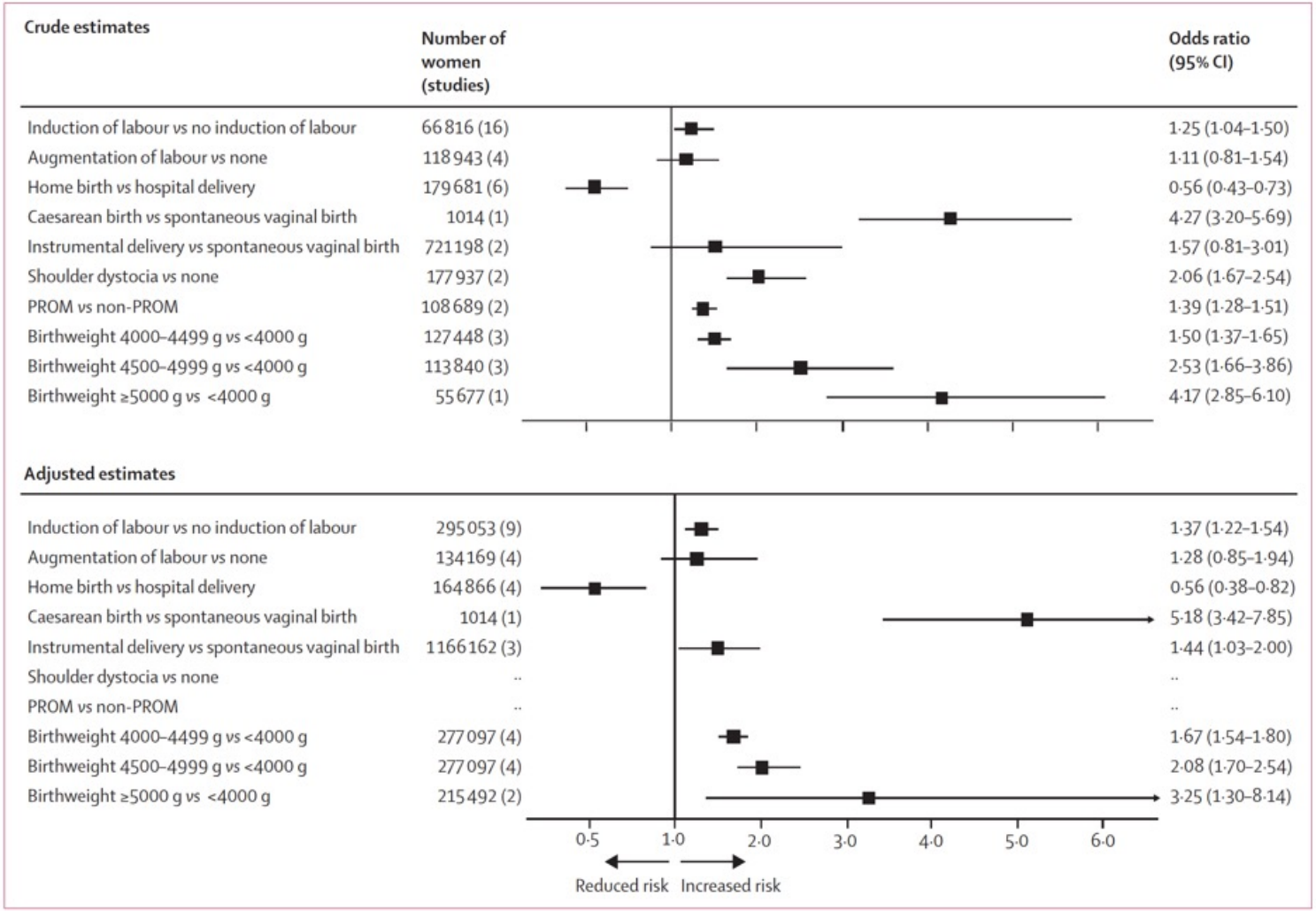

***Figure 7*: Labour and birth risk factors for postpartum haemorrhage**
PROM=premature rupture of membrane.

Research in context

Evidence before this study

Postpartum haemorrhage is a leading cause of maternal mortality worldwide. Updated synthesised data are needed to guide global policy on risk stratification and mitigation, as well as postpartum haemorrhage prevention and treatment. We searched MEDLINE, Web of Science, Embase, Cochrane Library, and Google Scholar from Jan 1, 1960, to Nov 30, 2024, without language restrictions, using the search term "postpartum haemorrhage" in the title and abstract, and as a MeSH term. We identified 22 studies for the rate of postpartum haemorrhage causes and 311 studies assessing risk factors for postpartum haemorrhage. Most of the included studies were of high methodological quality.

Added value of this study

Our systematic review and meta-analysis produced up-to-date evidence-based pooled rates of causes of postpartum haemorrhage, and severe and refractory postpartum haemorrhage. Uterine atony, which the majority of first-line postpartum haemorrhage treatments target, was the commonest cause. Other important causes were genital tract trauma, retained placenta, abnormal placentation, and coagulopathy. We highlighted the importance of multiple concurrent causes resulting in postpartum haemorrhage. A range of risk factors and their levels of association with postpartum haemorrhage were identified. Many of these are modifiable. Risk factors with a strong association with postpartum haemorrhage included anaemia, previous postpartum haemorrhage, caesarean birth, female genital mutilation, sepsis, no antenatal care, multiple pregnancy, placenta praevia, assisted reproductive technology use, fetal macrosomia with birthweight more than 4500 g, and shoulder dystocia.

Implications of all the available evidence

Knowledge of postpartum haemorrhage causes and risk factors can allow policy makers to promote effective prophylaxis and treatment, particularly for women at high risk for postpartum haemorrhage, and develop strategies to target the risk factors. Postpartum haemorrhage caused by multiple concurrent causes supports the use of treatment bundles. Practices associated with reduced risks of postpartum haemorrhage, such as skin-to-skin contact and breastfeeding, should be promoted.

Modern Stenting versus modern Bypass

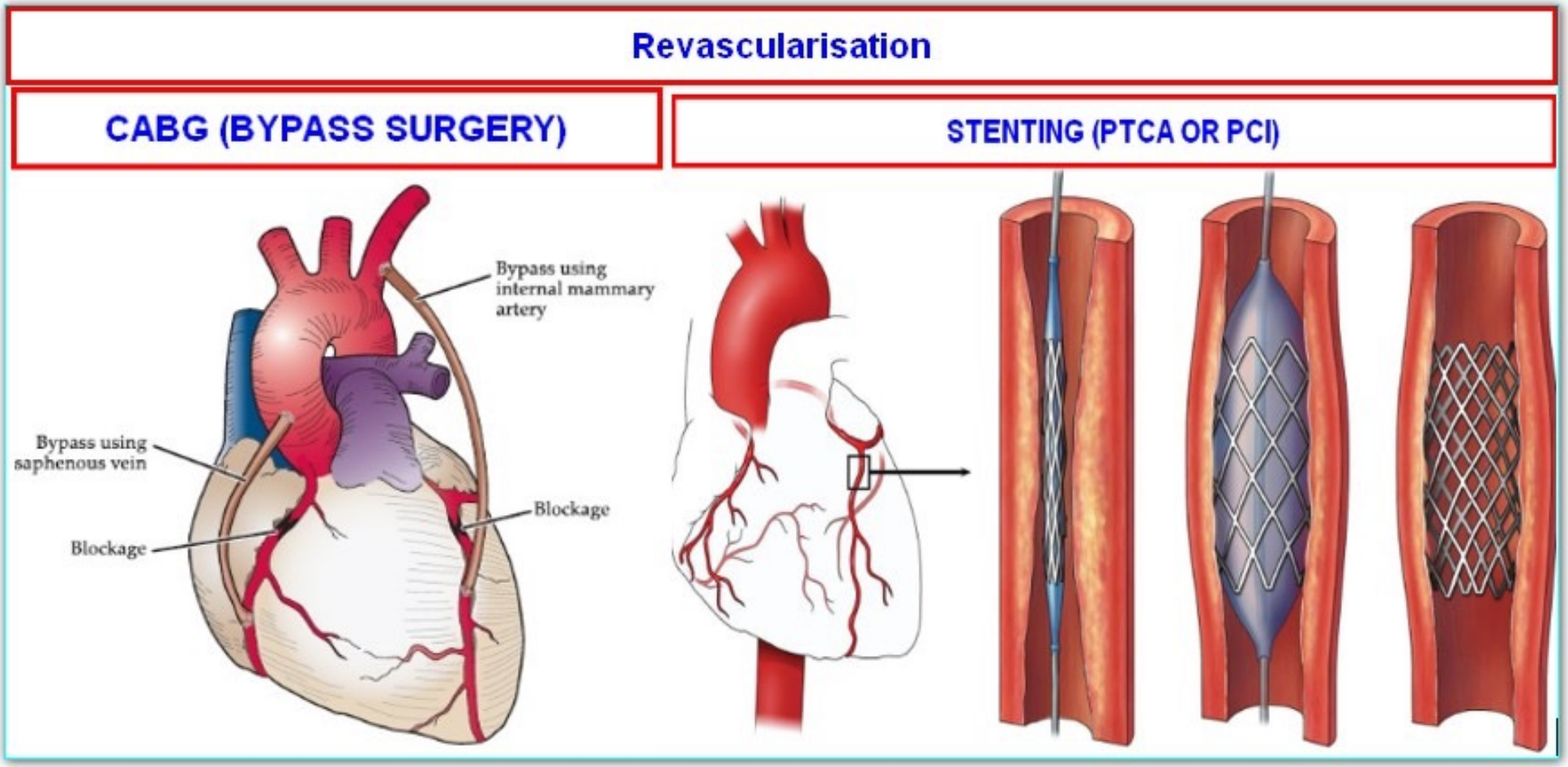

Outcomes after fractional flow reserve-guided percutaneous coronary intervention versus coronary artery bypass grafting (FAME 3): 5-year follow-up of a multicentre, open-label, randomised trial

Summary

Background Long-term outcomes following percutaneous coronary intervention (PCI) or coronary artery bypass grafting (CABG) might be changing because of improved techniques and better medical therapy. This final prespecified analysis of the Fractional Flow Reserve (FFR) versus Angiography for Multivessel Evaluation (FAME) 3 trial aimed to reassess their comparative effectiveness at 5 years.

Methods FAME 3 was a multicentre, randomised trial comparing FFR-guided PCI using current-generation zotarolimus-eluting stents versus CABG in patients with three-vessel coronary artery disease not involving the left main coronary artery. 48 hospitals in Europe, USA and Canada, Australia, and Asia participated in the trial. Patients (aged ≥21 years with no cardiogenic shock, no recent ST segment elevation myocardial infarction, no severe left ventricular dysfunction, and no previous CABG) were randomly assigned to either PCI or CABG using a web-based system. At 1 year, FFR-guided PCI did not meet the prespecified threshold for non-inferiority for the outcome of death, stroke, myocardial infarction, or repeat revascularisation versus CABG. The primary endpoint for this intention-to-treat analysis was the 5-year incidence of the prespecified composite outcome of death, stroke, or myocardial infarction. The trial was registered at ClinicalTrials.gov, NCT02100722, and is completed; this is the final report.

Findings Between Aug 25, 2014 and Nov 28, 2019, 757 of 1500 participants were assigned to PCI and 743 to CABG. 5-year follow-up was achieved in 724 (96%) patients assigned to PCI and 696 (94%) assigned to CABG. At 5 years, there was no significant difference in the composite of death, stroke, or myocardial infarction between the two groups, with 119 (16%) events in the PCI group and 101 (14%) in the CABG group (hazard ratio 1·16 [95% CI 0·89–1·52]; p=0·27). There were no differences in the rates of death (53 [7%] *vs* 51 [7%]; 0·99 [0·67–1·46]) or stroke (14 [2%] *vs* 21 [3%], 0·65 [0·33–1·28]), but myocardial infarction was higher in the PCI group than in the CABG group (60 [8%] *vs* 38 [5%], 1·57 [1·04–2·36]), as was repeat revascularisation (112 [16%] *vs* 55 [8%], 2·02 [1·46–2·79]).

Interpretation At the 5-year follow-up, there was no significant difference in a composite outcome of death, stroke, or myocardial infarction after FFR-guided PCI versus CABG, although myocardial infarction and repeat revascularisation were higher with PCI. These results provide contemporary evidence to allow improved shared decision making between physicians and patients.

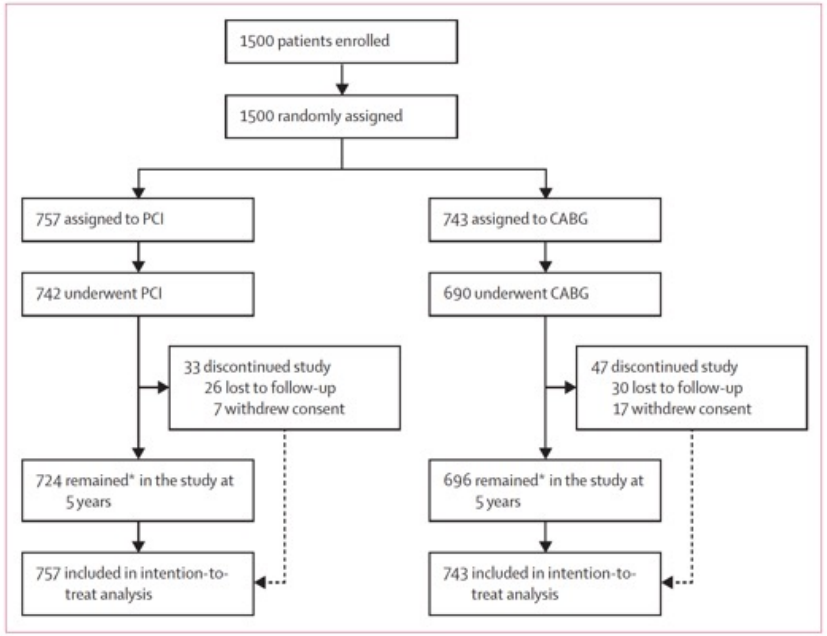

Figure 1: **Trial profile**
CABG=coronary artery bypass grafting. PCI=percutaneous coronary intervention. *Randomly assigned patients who had either completed follow-up within the protocol-specified timeframe or were deceased.

	PCI group (n=757)	CABG group (n=743)
Baseline characteristics		
Age, years	66 (59–72)	66 (59–71)
Sex		
Female	141 (19%)	124 (17%)
Male	616 (81%)	619 (83%)
Race or ethnicity*		
American Indian or Alaska Native	3 (<1%)	2 (<1%)
Asian	23 (3%)	30 (4%)
Black	12 (2%)	15 (2%)
Native Hawaiian or other Pacific Islander	2 (<1%)	4 (1%)
White	711 (94%)	686 (92%)
Hispanic or Latino	6 (1%)	6 (1%)
BMI, kg/m²	28·3 (25·2–31·4)	28·1 (25·6–31·0)
Diabetes	214 (28%)	214 (29%)
Insulin-dependent	55 (7%)	61 (8%)
Non-insulin-dependent	159 (21%)	153 (21%)
Hypertension	539/756 (71%)	557/741 (75%)
Dyslipidaemia	520/756 (69%)	530/741 (72%)
Smoking status		
Current tobacco user	146/756 (19%)	137/741 (18%)
Previous tobacco user	296/756 (39%)	296/741 (40%)
Family history of coronary artery disease	247/756 (33%)	215/740 (29%)
Previous myocardial infarction	253/756 (33%)	249/741 (34%)
Previous PCI	98/756 (13%)	104/741 (14%)
History of transient ischaemic attack or cerebrovascular accident	49/756 (6%)	56/741 (8%)
Estimated glomerular filtration rate <60 mL/min per 1·73 m²	37/756 (5%)	44/741 (6%)
Non-invasive test for ischaemia	311/756 (41%)	300/741 (40%)
Left ventricular ejection fraction ≤50%	137/753 (18%)	130/740 (18%)
Hospitalised with NSTE-ACS	300/756 (40%)	287/741 (39%)

(Table 1 continues in next column)

	PCI group (n=757)	CABG group (n=743)
(Continued from previous column)		
Angiographical and procedural characteristics		
Time to procedure, days	4 (1–13)	13 (6–26)
Procedure duration, min	87 (67–113)	197 (155–239)
Length of hospital stay, days	3 (1–7)	11 (7–16)
Number of lesions	4 (3–5)	4 (3–5)
At least one chronic total occlusion	157/755 (21%)	172/740 (23%)
At least one bifurcation lesion	525/755 (70%)	493/740 (67%)
SYNTAX score†	26·0 (7·1)	25·8 (7·1)
SYNTAX score category†		
Low (0–22)	237/734 (32%)	245/710 (35%)
Intermediate (23–32)	365/734 (50%)	343/710 (48%)
High (>32)	132/734 (18%)	122/710 (17%)
PCI characteristics		
Staged procedure	166/750 (22%)	NA
Number of stents	3 (2–5)	NA
Total length of stents placed, mm	80 (52–116)	NA
Intravascular imaging used	82/746 (11%)	NA
CABG characteristics		
Multiple arterial grafts	NA	179/704 (25%)
Number of distal anastomoses	NA	3 (3–4)
Left internal thoracic artery used as graft	NA	684/704 (97%)
Off-pump surgery	NA	167/697 (24%)

Data are n (%), median (IQR), mean (SD), or n/N (%), as of the final data lock on Jan 13, 2025. CABG=coronary artery bypass grafting. NA=not applicable. NSTE-ACS=non-ST-segment elevation acute coronary syndrome. PCI=percutaneous coronary intervention. SYNTAX=Synergy between Percutaneous Coronary Intervention with Taxus and Cardiac Surgery. *Race and ethnicity were self-reported by the patients. †Calculated by the core laboratory. Data were missing for 23 patients in the PCI group and 33 patients in the CABG group.

Table 1: **Baseline, angiographical, and procedural characteristics**

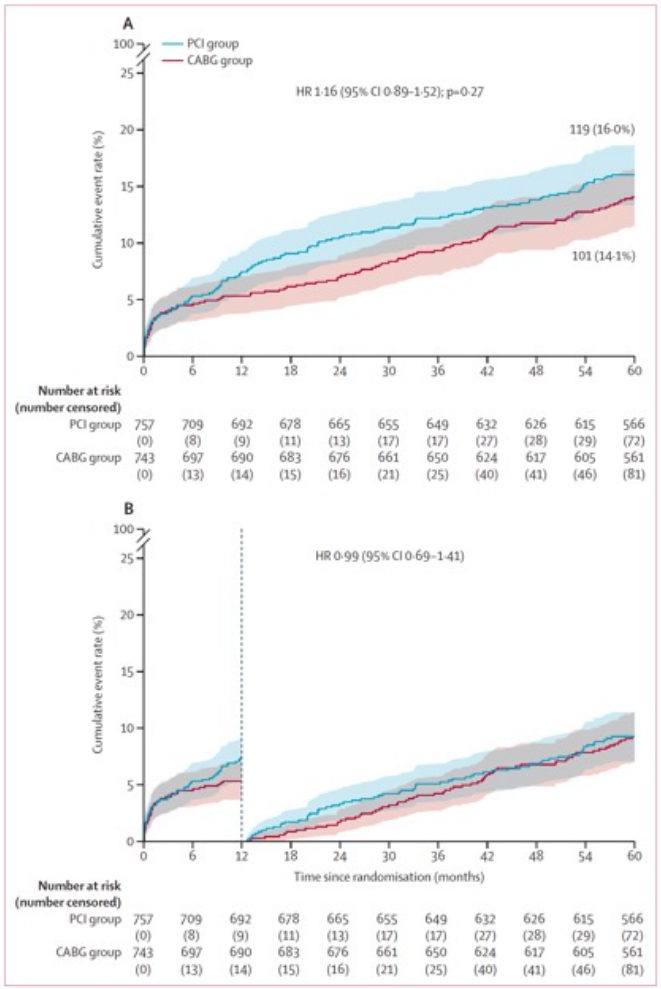

Figure 2: **Kaplan–Meier curves for the rate of the composite outcome of death, stroke, or myocardial infarction at 5 years**

(A) Kaplan–Meier curves for the rate of the composite outcome of death, stroke, or myocardial infarction at 5 years in the patients assigned to PCI compared with the patients assigned to CABG. (B) A landmark analysis comparing Kaplan–Meier curves for the rate of the composite of death, stroke, or myocardial infarction at 5 years in the patients assigned to PCI with those assigned to CABG, from 0 to 1 years and 1 to 5 years. CABG=coronary artery bypass grafting. HR=hazard ratio. PCI=percutaneous coronary intervention.

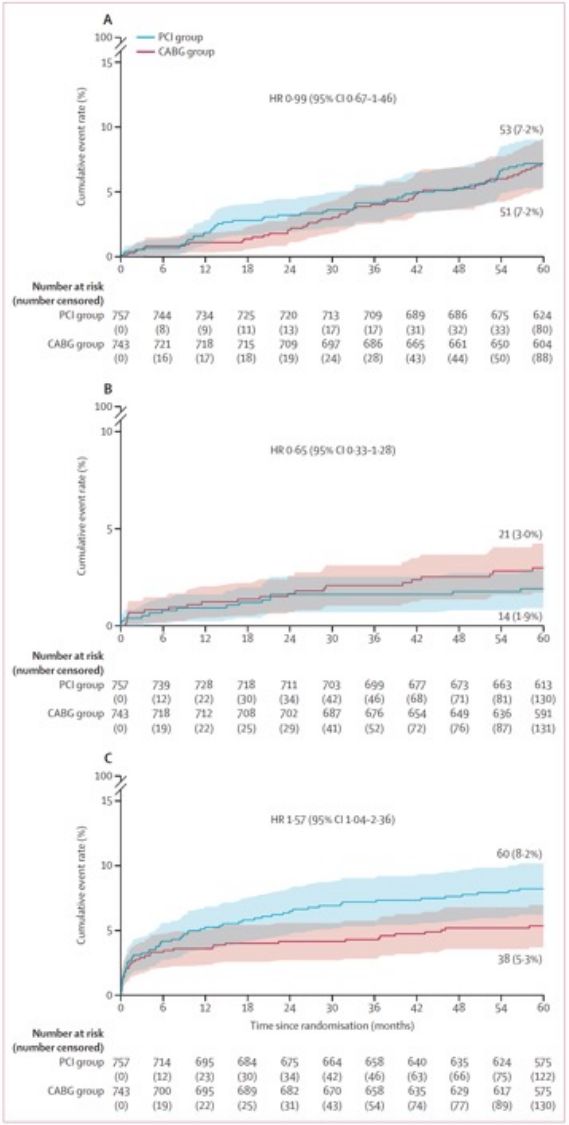

Figure 3: **Kaplan–Meier curves for death, stroke, and myocardial infarction at 5 years in the PCI *vs* CABG groups**

(A) Kaplan–Meier curves for the rate of death at 5 years. (B) Kaplan–Meier curves for the rate of stroke at 5 years. (C) Kaplan–Meier curves for the rate of myocardial infarction at 5 years. CABG=coronary artery bypass grafting. HR=hazard ratio. PCI=percutaneous coronary intervention.

	PCI group (n=757)	CABG group (n=743)	Hazard ratio (95% CI)	p value
Primary composite endpoint				
Death from any cause, stroke, or myocardial infarction	119 (16%)	101 (14%)	1·16 (0·89–1·52)	0·27*
Secondary endpoints†				
Death	53 (7%)	51 (7%)	0·99 (0·67–1·46)	..
Death from cardiac causes	15 (2%)	10 (1%)	..	..
Myocardial infarction	60 (8%)	38 (5%)	1·57 (1·04–2·36)	..
Spontaneous	46 (6%)	29 (4%)	..	..
Periprocedural	14 (2%)	9 (1%)	..	..
Stroke	14 (2%)	21 (3%)	0·65 (0·33–1·28)	..
Repeat revascularisation	112 (16%)	55 (8%)	2·02 (1·46–2·79)	..
PCI	98 (14%)	52 (7%)	..	..
CABG	14 (2%)	3 (<1%)	..	..
Death, myocardial infarction, stroke, or repeat revascularisation	188 (25%)	131 (18%)	1·44 (1·15–1·81)	..
Death, stroke, or myocardial infarction (as per SCAI criteria)	150 (20%)	172 (24%)	0·85 (0·69–1·07)	..

Data are n (%), except where otherwise specified. CABG=coronary artery bypass grafting. PCI=percutaneous coronary intervention. SCAI=Society for Cardiovascular Angiography and Interventions. Event rates were estimated from Kaplan–Meier survival curves based on an intention-to-treat analysis. *This p value was obtained from a prespecified test of superiority with respect to the primary endpoint. †CIs were not adjusted for multiplicity and should not be interpreted to inform definitive treatment effects.

Table 2: **Clinical endpoints at 5 years**

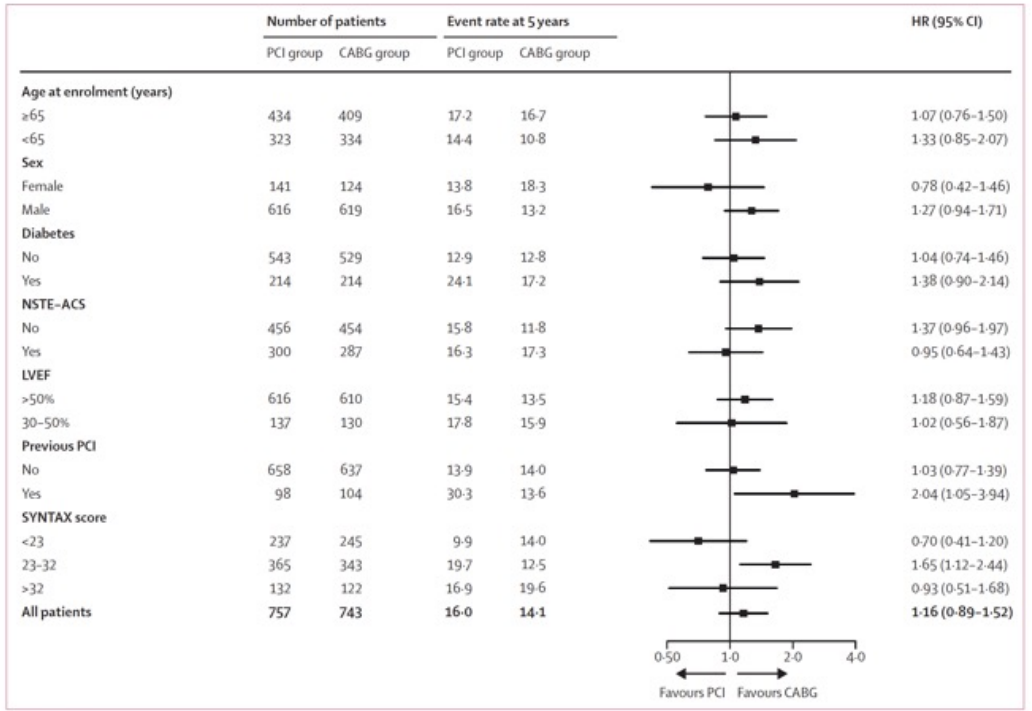

Figure 4: **Forest plot of estimated hazard ratios from subgroup analyses of the primary endpoint**
Event rates were estimated from Kaplan–Meier survival curves. SYNTAX scores were reported according to core laboratory analysed data. CABG=coronary artery bypass grafting. HR=hazard ratio. LVEF=left ventricular ejection fraction. NSTE-ACS=non-ST-segment elevation acute coronary syndrome. PCI=percutaneous coronary intervention. SYNTAX=Synergy between Percutaneous Coronary Intervention with Taxus and Cardiac Surgery.

Research in context

Evidence before this study

The optimal method of revascularisation—percutaneous coronary intervention (PCI) or coronary artery bypass grafting (CABG)—for patients with multivessel coronary artery disease (CAD) not involving the left main coronary artery remains uncertain given improvements in both techniques (eg, the use of current-generation drug-eluting stents [DES] and fractional flow reserve [FFR] improve outcomes from PCI, and improved patient selection and surgical technique have lowered short-term mortality after CABG). We searched PubMed, EMBASE, and the Cochrane Central Register of Controlled Trials databases from inception to Jan 15, 2025, with no language restrictions, for randomised trials comparing FFR-guided PCI with current-generation DES versus CABG in patients with multivessel CAD not involving the left main coronary artery. The search terms were "percutaneous coronary intervention", "coronary artery bypass graft", "revascularisation", "multivessel", and "randomised". Our search found one randomised study comparing PCI with current-generation DES without FFR guidance and CABG in patients with multivessel disease not involving the left main coronary artery (BEST trial). FAME 3 was the only randomised trial we found comparing FFR-guided PCI with current-generation DES versus CABG in patients with multivessel disease not involving the left main coronary artery, and it showed no significant difference in the composite outcome of death, stroke, or myocardial infarction at the 3-year follow-up.

Added value of this study

This prespecified 5-year follow-up of FAME 3 shows no significant differences in the composite outcome of death, stroke, or myocardial infarction in 1500 patients with three-vessel CAD not involving the left main coronary artery, although rates of myocardial infarction and repeat revascularisation remained higher with PCI. In addition, this final analysis of the trial showed no long-term accrual of benefit after CABG on a composite outcome of death, stroke, or myocardial infarction, which contradicts previous studies.

Implications of all the available evidence

The FAME 3 trial provides new data regarding outcomes after FFR-guided PCI with current-generation DES compared with CABG in patients with multivessel CAD; these data are distinctly different from earlier studies in this area and can facilitate more effective shared decision making between physicians and patients.

Fractional flow reserve versus IVUS

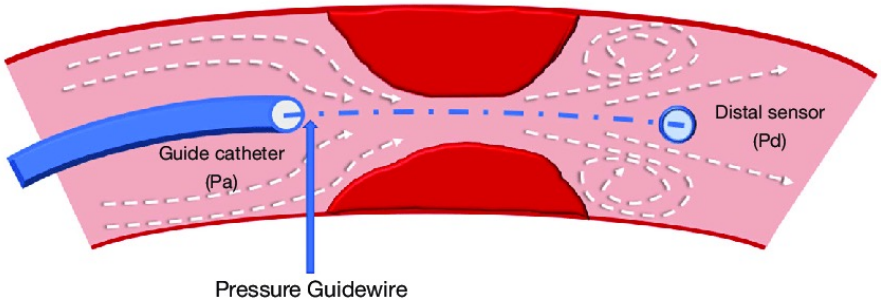

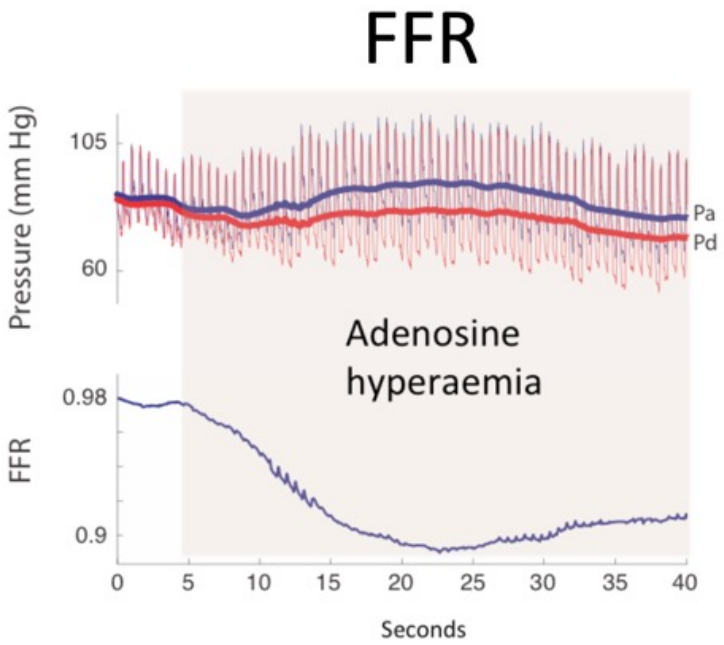

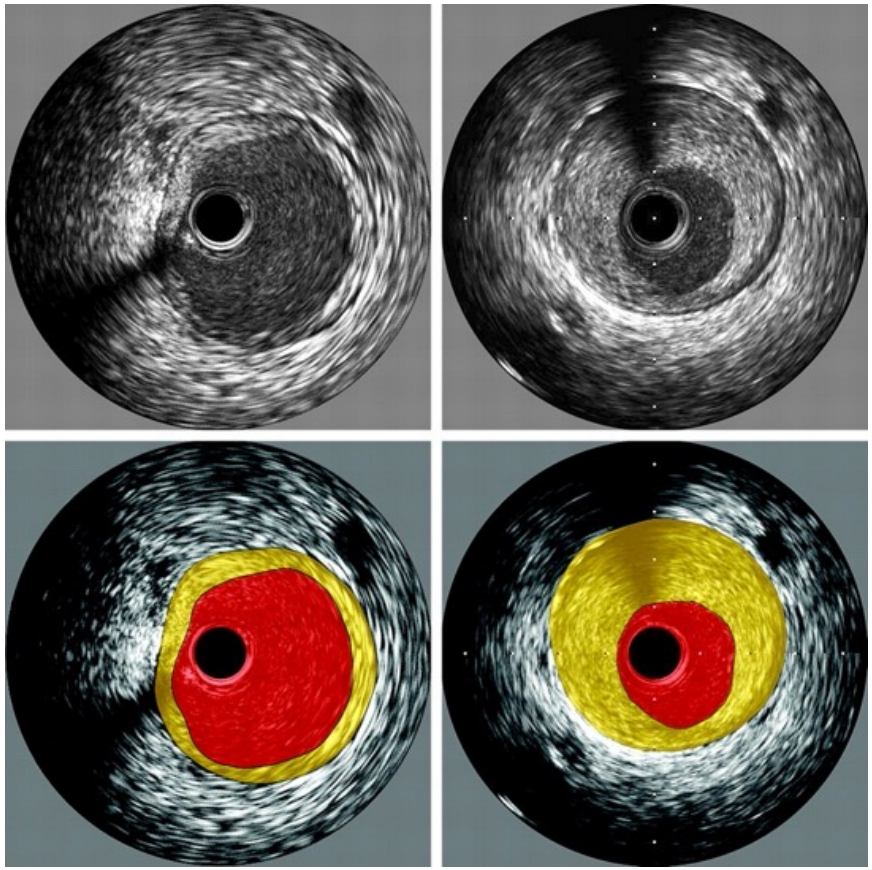

Angiography-derived fractional flow reserve versus intravascular ultrasound to guide percutaneous coronary intervention in patients with coronary artery disease (FLAVOUR II): a multicentre, randomised, non-inferiority trial

Summary

Background Revascularisation decisions based on angiography-derived fractional flow reserve (FFR) or optimisation of stent implantation with intravascular ultrasound yield superior clinical outcomes compared with percutaneous coronary intervention (PCI) guided by angiography alone. However, the differences in outcomes when a single approach is used for both purposes remain unclear. We aimed to assess the non-inferiority of angiography-derived FFR versus intravascular ultrasound guidance in terms of clinical outcomes at 12 months in patients with angiographically significant stenosis.

Methods This investigator-initiated, open-label, multicentre, randomised, non-inferiority trial, which was done in 22 centres in China, enrolled patients aged 18 years or older with suspected ischaemic heart disease and with at least 50% stenosis in epicardial coronary arteries measuring at least 2·5 mm by visual estimation on coronary angiography. Patients were randomly assigned (1:1) to undergo PCI guided by either angiography-derived FFR or intravascular ultrasound, including revascularisation decisions and optimisation of the stent implantations based on prespecified PCI criteria and optimal PCI goals. Use of both modalities simultaneously was not permitted. Randomisation as performed using a web-based program and stratified based on the trial centre and the presence or absence of diabetes. The primary outcome was a composite of death, myocardial infarction, or revascularisation at 12 months in the intention-to-treat population, and the non-inferiority margin was 2·5 percentage points. This trial is registered with ClinicalTrials.gov, NCT04397211; long-term follow-up is ongoing.

Findings Between May 29, 2020, and Sept 20, 2023, 1872 patients were enrolled. After 33 patients withdrew, 923 patients were randomly assigned to the angiography-derived FFR group and 916 to the intravascular ultrasound group. Median age of the study population was 66·0 years (IQR 58·0–72·0), and 1248 (67·9%) patients were male and 591 (32·1%) were female. Revascularisation was performed in 688 (69·5%) of 990 target vessels in the angiography-derived FFR group and 797 (81·0%) of 984 target vessels in the intravascular ultrasound group. At a median follow-up of 12 months (IQR 12–12), the primary outcome event occurred in 56 patients in the angiography-derived FFR group and 54 patients in the intravascular ultrasound group (6·3% *vs* 6·0%, absolute difference 0·2 percentage points [upper boundary of one-sided 97·5% CI 2·4], $p_{non\text{-}inferiority}$=0·022; hazard ratio 1·04 [95% CI 0·71 to 1·51]). Mortality did not differ between the two groups (1·8% in the angiography-derived FFR group *vs* 1·3% in the intravascular ultrasound group, absolute difference 0·4 percentage points [95% CI –0·7 to 1·6]; hazard ratio 1·34 [0·63 to 2·83], p=0·45). The incidence of recurrent angina was low in both groups: 26 (2·8%) of 923 patients in the angiography-derived FFR group and 35 (3·8%) of 916 patients in the intravascular ultrasound group.

Interpretation The angiography-derived FFR-guided comprehensive PCI strategy, encompassing revascularisation decision making and stent optimisation, was non-inferior to intravascular ultrasound guidance. This finding might have implications for future guidelines on its role and application.

Funding National Natural Science Foundation of China, The Key R & D Projects of Zhejiang Province, and the RCT Program from The Second Affiliated Hospital of Zhejiang University School of Medicine.

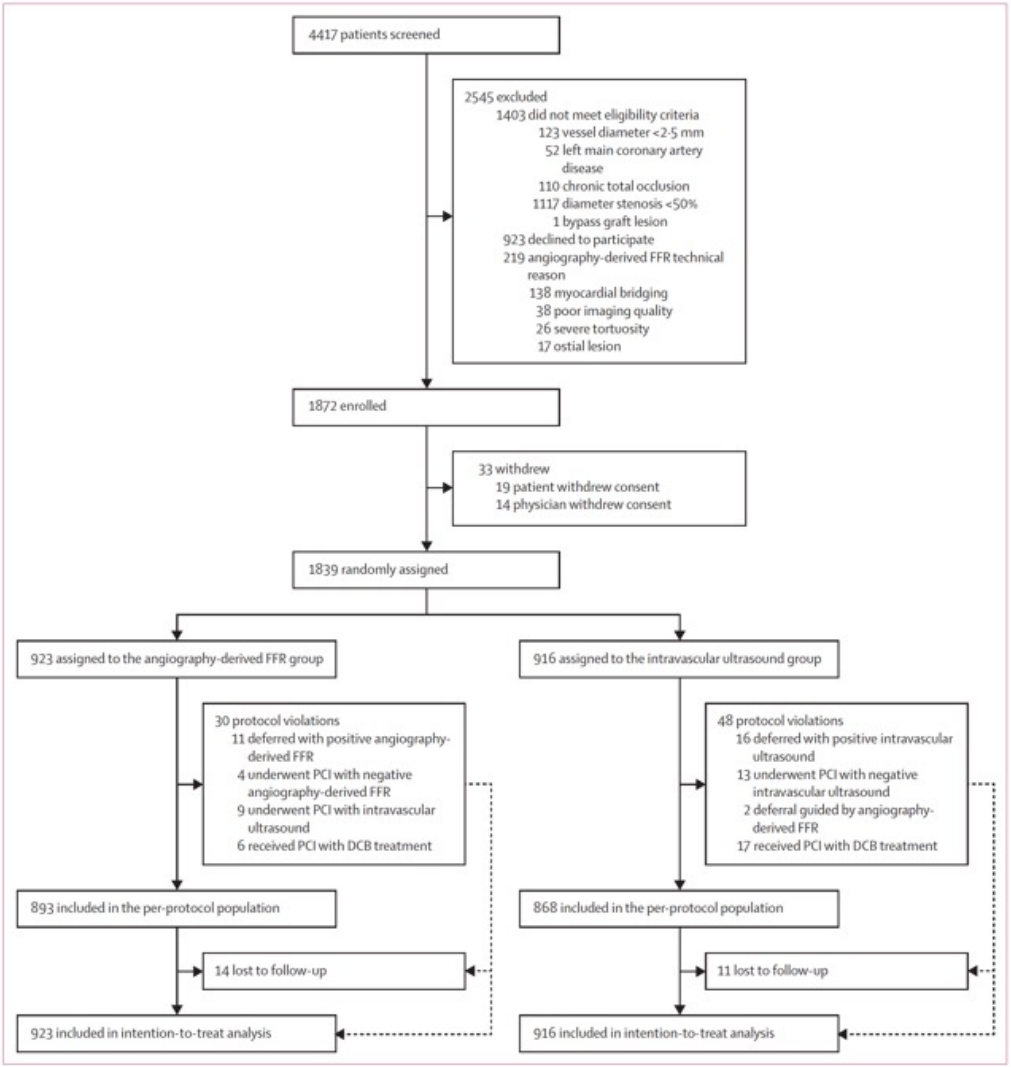

Figure 1: **Trial profile**
DCB=drug-coated balloon. FFR=fractional flow reserve. PCI=percutaneous coronary intervention.

	Total (n=1839)	Angiography-derived FFR group (n=923)	Intravascular ultrasound group (n=916)
Demographics			
Age, years	66·0 (58·0–72·0)	66·0 (58·0–72·0)	66·0 (58·0–72·0)
Sex			
Male	1248 (67·9%)	624 (67·6%)	624 (68·1%)
Female	591 (32·1%)	299 (32·4%)	292 (31·9%)
BMI, kg/m²	24·1 (22·2–26·4)	24·2 (22·2–26·4)	24·1(22·2–26·5)
Diagnosis			
Chronic coronary syndrome	736 (40·0%)	371 (40·2%)	365 (39·8%)
Acute coronary syndrome	1087 (59·1%)	545 (59·0%)	542 (59·2%)
STEMI	18 (1·0%)	9 (1·0%)	9 (1·0%)
NSTEMI	81 (4·4%)	48 (5·2%)	33 (3·6%)
Others*	16 (0·9%)	7 (0·8%)	9 (1·0%)
Medical history			
Diabetes	569 (30·9%)	279 (30·2%)	290 (31·7%)
Hypertension	1243 (67·6%)	615 (66·6%)	628 (68·6%)
Dyslipidaemia	1230 (66·9%)	616 (66·7%)	614 (67·0%)
Chronic kidney disease†	447 (24·3%)	210 (22·8%)	237 (25·9%)
Current smoking	477 (25·9%)	242 (26·2%)	235 (25·7%)
Previous myocardial infarction	255 (13·9%)	129 (14·0%)	126 (13·8%)
Previous PCI	559 (30·4%)	300 (32·5%)	259 (28·3%)
Left ventricular ejection fraction, %	64·6% (60·0–69·2)	64·9% (60·0–69·3)	64·0% (60·0–69·1)
Laboratory data			
White blood cell count, cells per uL	6·2 (5·2–7·4)	6·1 (5·1–7·2)	6·3 (5·3–7·5)
Haemoglobin, mg/dL	135·0 (124·0–146·0)	134·0 (123·0–145·0)	136·0 (125·0–146·0)
Creatinine, mg/dL	0·9 (0·7–1·0)	0·8 (0·7–1·0)	0·9 (0·7–1·0)
Total cholesterol, mg/dL	152·0 (124·9–186·4)	151·6 (125·3–186·4)	152·7 (123·7–185·6)
HDL, mg/dL	42·2 (35·6–49·1)	42·2 (35·7–49·1)	41·8 (35·6–49·5)
LDL, mg/dL	82·8 (62·3–109·8)	82·8 (62·3–109·2)	82·4 (62·3–110·6)
Triglycerides, mg/dL	119·6 (85·9–168·3)	120·5 (85·9–170·1)	117·8 (85·9–167·4)

Data are median (IQR) or n (%). We did not collect race or ethnicity data. FFR=fractional flow reserve. NSTEMI=non-ST-elevation myocardial infarction. PCI=percutaneous coronary intervention. STEMI=ST-elevation myocardial infarction. *Other diagnoses included heart failure (in seven patients), syncope (four patients), atypical chest pain (four patients), and valvular heart disease (one patient). †Chronic kidney disease was defined as a history of chronic kidney disease or an estimated glomerular filtration rate of less than 60 mL/min per 1·73 m² of body-surface area.

Table 1: **Baseline characteristics**

	Total (n=1839)	Angiography-derived FFR group (n=923)	Intravascular ultrasound group (n=916)	p value
Angiographic findings				
Patients who underwent PCI	1443 (78·5%)	682 (73·9%)	761 (83·1%)	<0·0001
Stent data				
Total number per patient	1·14 (0·91)	1·06 (0·90)	1·22 (0·92)	<0·0001
Total number per patient	1 (1–2)	1 (0–2)	1 (1–2)	<0·0001
Total length per patient, mm	29·9 (24·7)	27·6 (24·5)	32·3 (24·6)	<0·0001
Total length per patient, mm	28 (15–41)	24 (0–38)	29 (18–44)	<0·0001
Total number per patient who underwent PCI, mm	1 (1–2)	1 (1–2)	1 (1–2)	0·63
Total length per patient who underwent PCI, mm	33 (24–50)	30 (23–48)	33 (24–50)	0·054
SYNTAX score*				
At baseline	9 (5–15)	10 (5–15)	9 (5–15)	0·66
After PCI	5 (0–9)	5 (0–9)	5 (0–8)	0·92
Additional procedures due to suboptimal conditions†	291/1443 (20·2%)	126/682 (18·5%)	165/761 (21·7%)	0·15
Target vessel findings				
Number of target vessels	1974	990	984	..
Target vessel PCI	1485/1974 (75·2%)	688/990 (69·5%)	797/984 (81·0%)	<0·0001
Location	..	..	..	0·12
Left anterior descending coronary artery	1171/1974 (59·3%)	565/990 (57·1%)	606/984 (61·6%)	..
Left circumflex coronary artery‡	276/1974 (14·0%)	146/990 (14·8%)	130/984 (13·2%)	..
Right coronary artery	527/1974 (26·7%)	279/990 (28·2%)	248/984 (25·2%)	..
Quantitative coronary angiography findings				
Lesion length, mm	19·7 (12·9–30·3)	19·0 (12·5–29·8)	20·3 (13·2–30·5)	0·083
Reference vessel diameter, mm	3·0 (2·6–3·3)	2·93 (2·61–3·30)	2·96 (2·65–3·35)	0·16
Minimal lumen diameter, mm	1·11 (0·83–1·39)	1·10 (0·82–1·38)	1·12 (0·83–1·39)	0·49
Diameter stenosis, %	62·2% (54·3–70·6)	62·3% (53·8–70·9)	62·2% (54·7–70·0)	0·94
Minimal stent diameter, mm	2·64 (2·38–2·96)	2·61 (2·35–2·93)	2·66 (2·42–2·96)	0·022
Residual diameter stenosis, %	10·7% (7·1–14·5)	10·9% (7·3–15·0)	10·3% (6·8–14·4)	0·13
Stent data				
Total number per stented vessels	1 (1–2)	1 (1–2)	1 (1–2)	0·80
Total length per stented vessels, mm	32·0 (24·0–48·0)	31·5 (23·0–48·0)	33·0 (24·0–48·0)	0·21
Diameter per stented vessels, mm	3·08 (0·42)	3·05 (0·41)	3·1 (0·43)	0·028
Diameter per stented vessels, mm	3·00 (2·75–3·50)	3·00 (2·75–3·50)	3·00 (2·75–3·50)	0·044
Intravascular ultrasound findings				
Onsite				
Minimal luminal area, mm²	NA	NA	2·68 (2·19–3·35)	NA
Plaque burden, %	NA	NA	76·0% (70·0–81·0)	NA
Post-PCI minimal stent area, mm²	NA	NA	6·76 (5·49–8·57)	NA
Core laboratory	NA	NA		NA
Minimal luminal area, mm²	NA	NA	2·55 (2·07–3·36)	NA
Plaque burden, %	NA	NA	76·1% (69·7–81·2)	NA
Post-PCI minimal stent area, mm²	NA	NA	5·80 (4·72–7·25)	NA

(Table 2 continues on next page)

(Continued from previous page)

	Total (n=1839)	Angiography-derived FFR group (n=923)	Intravascular ultrasound group (n=916)	p value
Angiography-derived FFR findings				
Onsite				
At baseline	NA	0·73 (0·56–0·84)	NA	NA
After PCI	NA	0·96 (0·93–0·98)	NA	NA
Core laboratory				
At baseline	0·74 (0·58–0·84)	0·74 (0·57–0·86)	0·74 (0·61–0·80)	0·11
After PCI	0·95 (0·92–0·97)	0·95 (0·93–0·97)	0·95 (0·92–0·97)	0·21

Data are n (%), mean (SD), median (IQR), or n/N (%) unless otherwise stated. We did not collect race or ethnicity. FFR=fractional flow reserve. NA=not applicable. PCI=percutaneous coronary intervention. SYNTAX=Synergy between Percutaneous Coronary Intervention with Taxus and Cardiac Surgery. *The SYNTAX score reflects a comprehensive angiographic assessment of the coronary vasculature; a higher score denotes higher anatomical complexity, and a score of 32 or less typically indicates low or intermediate anatomical complexity of coronary artery disease. †In the angiography-derived FFR group, 120 patients underwent optimisation with non-compliant balloons, with additional stent implantation performed in six patients; following the optimisation procedure, 113 patients met the optimal criteria. In the intravascular ultrasound group, 165 patients underwent optimisation with non-compliant balloons, with additional stent implantation performed in one patient; after optimisation, 95 patients met the optimal criteria. ‡The left circumflex coronary artery included large obtuse marginal branches and ramus.

Table 2: **Procedural findings**

	Angiography-derived FFR group (n=923)	Intravascular ultrasound group (n=916)	Absolute difference (95% CI)*, percentage points	Hazard ratio (95% CI)	p value for hazard ratio
Primary outcome†					
Death from any cause, myocardial infarction, or revascularisation	56 (6·3%)	54 (6·0%)	0·2 (−2·0 to 2·4)‡	1·04 (0·71 to 1·51)	0·85
Secondary outcomes†					
Target vessel failure (death from cardiac cause, target vessel myocardial infarction, or target vessel revascularisation)	21 (2·4%)	17 (1·9%)	0·4 (−0·9 to 1·8)	1·24 (0·65 to 2·35)	0·51
Death					
Any	16 (1·8%)	12 (1·3%)	0·4 (−0·7 to 1·6)	1·34 (0·63 to 2·83)	0·45
From cardiac cause	6 (0·7%)	4 (0·4%)	0·2 (−0·5 to 0·9)	1·49 (0·42 to 5·29)	0·54
Myocardial infarction					
Any	6 (0·7%)	4 (0·4%)	0·2 (−0·5 to 0·9)	1·49 (0·42 to 5·28)	0·54
Target vessel	0	1 (0·1%)	−0·1 (−0·3 to 0·1)	..	..
Non-fatal myocardial infarction					
Periprocedural	4 (0·4%)	2 (0·2%)	0·2 (−0·3 to 0·7)	1·97 (0·36 to 10·78)	0·43
Non-periprocedural	0	0	..	..	..
Stent thrombosis					
Any	2 (0·2%)	1 (0·1%)	0·1 (−0·3 to 0·5)	1·99 (0·18 to 21·94)	0·58
Definite	0	1 (0·1%)	−0·1 (−0·3 to 0·1)	..	..
Probable	0	0	..	..	..
Possible	2 (0·2%)	0	0·2 (−0·1 to 0·5)	..	..
Revascularisation					
Any	36 (4·1%)	41 (4·7%)	−0·6 (−2·5 to 1·4)	0·88 (0·56 to 1·37)	0·56
Ischaemia driven	25 (2·8%)	29 (3·3%)	−0·4 (−2·0 to 1·2)	0·86 (0·50 to 1·47)	0·59
Target vessel	15 (1·7%)	14 (1·6%)	0·1 (−1·1 to 1·3)	1·08 (0·52 to 2·23)	0·84
Non-target vessel	21 (2·4%)	27 (3·1%)	−0·7 (−2·2 to 0·8)	0·78 (0·44 to 1·38)	0·39
Stroke§					
Any	6 (0·7%)	9 (1·0%)	−0·3 (−1·2 to 0·5)	0·67 (0·24 to 1·89)	0·45
Ischaemic	4 (0·4%)	6 (0·7%)	−0·2 (−0·9 to 0·5)	0·67 (0·19 to 2·37)	0·53
Haemorrhagic	2 (0·2%)	2 (0·2%)	−0·0 (−0·4 to 0·4)	1·00 (0·14 to 7·13)	1·00
Procedural outcome					
PCI achieved optimisation criteria¶	606/682 (88·9%)	430/761 (56·5%)	..	..	<0·0001
Device success‖	688/688 (100%)	797/797 (100%)	..	..	1·00
Lesion success**	683/688 (99·3%)	791/797 (99·2%)	..	..	1·00

FFR=fractional flow reserve. PCI=percutaneous coronary intervention. *The between-group difference was measured in the angiography-derived FFR group versus the intravascular ultrasound group. The widths of the 95% CIs have not been adjusted for multiplicity and cannot be used to infer treatment effects. †Data are n (Kaplan-Meier-estimated %). Primary and secondary outcomes were evaluated in the intention-to-treat population at 12 months after randomisation. Detailed definitions of the outcomes are provided in the appendix (p 22). ‡For the between-group difference in the primary outcome, the upper boundary of the one-sided 97·5% CI was 2·4 percentage points ($p_{non\text{-}inferiority}$=0·022). §One stroke of unknown cause was classified as neither ischaemic nor haemorrhagic. ¶Data are n/N (%). The PCI optimisations were counted according to prespecified definitions: a post-procedural angiography-derived FFR of at least 0·88 or a difference in the angiography-derived FFR across the stent of less than 0·05 in the angiography-derived FFR group; or a plaque burden at the stent edge of 55% or less and a minimal stent area of 5·5 mm² or more or a minimal stent area that was equal to or larger than the distal reference lumen area in the intravascular ultrasound group. ‖Data are n/N (%). Device success was defined as residual diameter stenosis of less than 30% at the in-stent segment without device failure or malfunction. **Data are n/N (%). Lesion success was defined as in-stent segment diameter stenosis of less than 30% with normal coronary flow and no more than a type C dissection.

Table 3: **Primary and secondary outcomes**

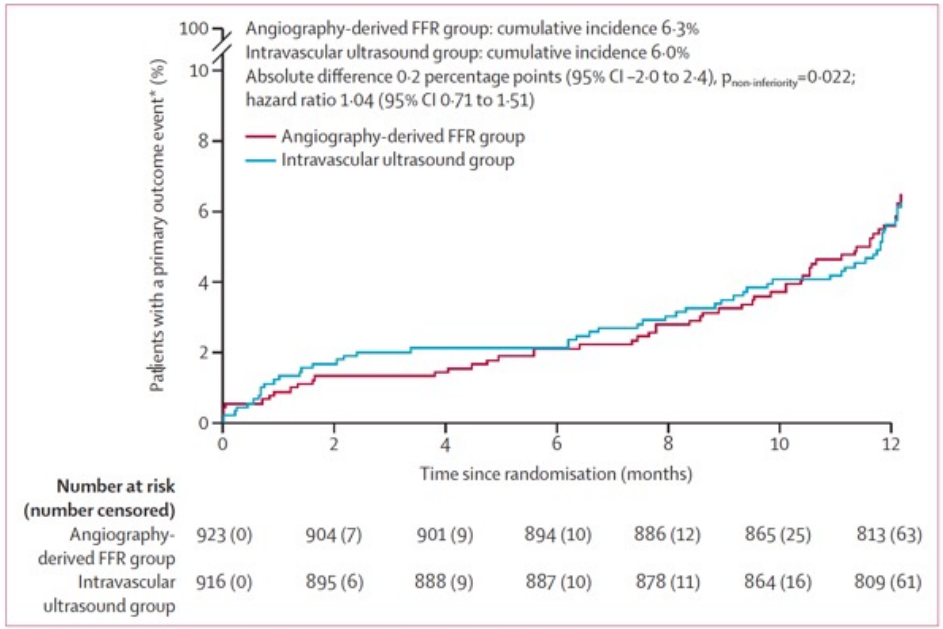

Figure 2: **Cumulative incidence of the primary outcome at 12 months**
FFR=fractional flow reserve. *The primary outcome was a composite of death from any cause, myocardial infarction, or revascularisation at 12 months after randomisation among patients who underwent a procedure guided by angiography-derived FFR or intravascular ultrasound.

	Angiography-derived FFR group (n=923)	Intravascular ultrasound group (n=916)
Heart failure	6 (0·7%)	8 (0·9%)
Recurrent angina	26 (2·8%)	35 (3·8%)
Rehospitalisation due to coronary artery disease follow-up	22 (2·4%)	18 (2·0%)
Valvular disease	1 (0·1%)	2 (0·2%)
Arrhythmia	7 (0·8%)	8 (0·9%)
Cardiac tamponade	1 (0·1%)	0
Aortic dissection	0	1 (0·1%)
Peripheral vascular disease	2 (0·2%)	1 (0·1%)
Bleeding	6 (0·7%)	3 (0·3%)
Pulmonary embolism	0	1 (0·1%)
Renal insufficiency	2 (0·2%)	1 (0·1%)

Data are n (%). FFR=fractional flow reserve.

Table 4: **Cardiovascular disease-related adverse events at 12 months**

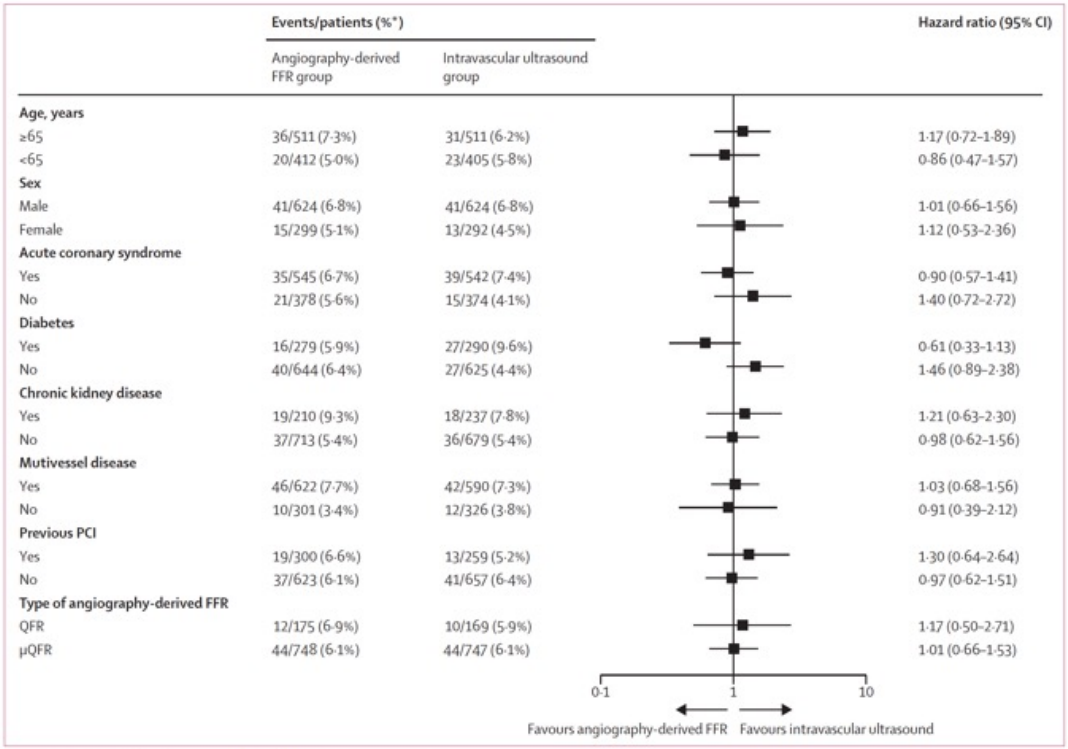

Figure 3: **Prespecified subgroup analysis of the primary outcome**
The widths of the CIs were not adjusted for multiplicity; therefore, they should not be used to infer the definitive treatment effects for the primary outcome. FFR=fractional flow reserve. PCI=percutaneous coronary intervention. QFR=quantitative flow ratio. μQFR=Murray law-based quantitative flow ratio. *Percentages are cumulative incidences at 12 months.

Research in context

Evidence before this study

Decision making for percutaneous coronary intervention (PCI) and optimisation of PCI procedures are crucial for patients with coronary artery disease who are referred to the catheterisation laboratory. Angiography-derived fractional flow reserve (FFR), a wire-free computational physiological index obtained directly from angiography (European Society of Cardiology Class IB recommendation), has been shown in previous trials to outperform angiography alone but has not demonstrated non-inferiority to conventional wire-based FFR in decision making for PCI. Intravascular ultrasound (Class IA recommendation) is the most widely used intravascular imaging tool for optimising stent implantation and has been associated with better clinical outcomes than angiography-guided PCI. Beyond current guideline recommendations, angiography-derived FFR also has applications for PCI procedure optimisation, whereas intravascular ultrasound facilitates pre-PCI lesion characterisation for decision making. However, whether a comprehensive strategy, encompassing both PCI decision making and procedural optimisation, performs similarly when guided by angiography-derived FFR or intravascular ultrasound remains uncertain. On Feb 13, 2025, we searched PubMed, without language restrictions, for articles using the terms "angiography-derived fractional flow reserve", "quantitative flow ratio", "intravascular ultrasound", "randomised", and "clinical outcome". Our search revealed no randomised trials comparing an angiography-derived FFR-guided comprehensive strategy, including PCI decision making and procedure optimisation, with the refined PCI strategy guided by intravascular ultrasound.

Added value of this study

To our knowledge, FLAVOUR II is the first large-scale, randomised, controlled trial to compare the clinical outcomes of PCI strategies, encompassing decision making and procedure optimisation, guided by angiography-derived FFR and intravascular ultrasound. In this trial, the angiography-derived FFR-guided PCI strategy was non-inferior to intravascular ultrasound-guided strategy in terms of a composite of death, myocardial infarction, or revascularisation at 12 months. Additionally, angiography-derived FFR guidance was associated with a lower rate of revascularisation, leading to fewer stent implantations and less frequent use of dual antiplatelet therapy.

Implications of all the available evidence

The results of FLAVOUR II provide clinical evidence that, in patients with non-complex coronary artery disease, a computational physiological technique can perform as effectively as the most commonly used invasive intravascular imaging technique when used as a comprehensive strategy. These findings have further defined and expanded the use of angiography-derived FFR and might have implications for future guidelines regarding its role and application.

The 2025 report of the *Lancet* Countdown to 2030 for women's, children's, and adolescents' health: tracking progress on health and nutrition

Executive summary

In line with previous progress reports by Countdown to 2030 for Women's, Children's, and Adolescents' Health, this report analyses global and regional trends and inequalities in health determinants, survival, nutritional status, intervention coverage, and quality of care in reproductive, maternal, newborn, child and adolescent health (RMNCAH) and nutrition, as well as country health systems, policies, financing, and prioritisation. The focus is on low-income and middle-income countries (LMICs) where 99% of maternal deaths and 98% of child and adolescent deaths (individuals aged 0–19 years) occur, with special attention to sub-Saharan Africa and South Asia.

Recognising the urgency of reaching the Sustainable Development Goal (SDG) for health, SDG 3, and health-related targets by 2030, the report assesses whether the momentum needed to reach these goals has been sustained, accelerated, stagnated, or regressed in comparison with the Millennium Development Goal (MDG) period (2000–15). Although most health and health-related indicators continue to show progress, there has been a notable slowdown in the rate of improvement after 2015, falling well short of the pace needed to achieve the 2030 SDG targets. This deceleration in pace contrasts sharply with the aspired grand convergence in health, characterised by drastic reductions in mortality and RMNCAH inequalities, which was expected to occur during the SDG period based on the assumption that the spectacular progress achieved during the MDG period would continue unabated. Multiple threats, external and internal to the RMNCAH health community, must be addressed to safeguard the gains in RMNCAH and nutrition and to accelerate progress. Furthermore, a large gap between sub-Saharan Africa, especially West and Central Africa, and other parts of the world persists for many indicators, necessitating further prioritisation of this region.

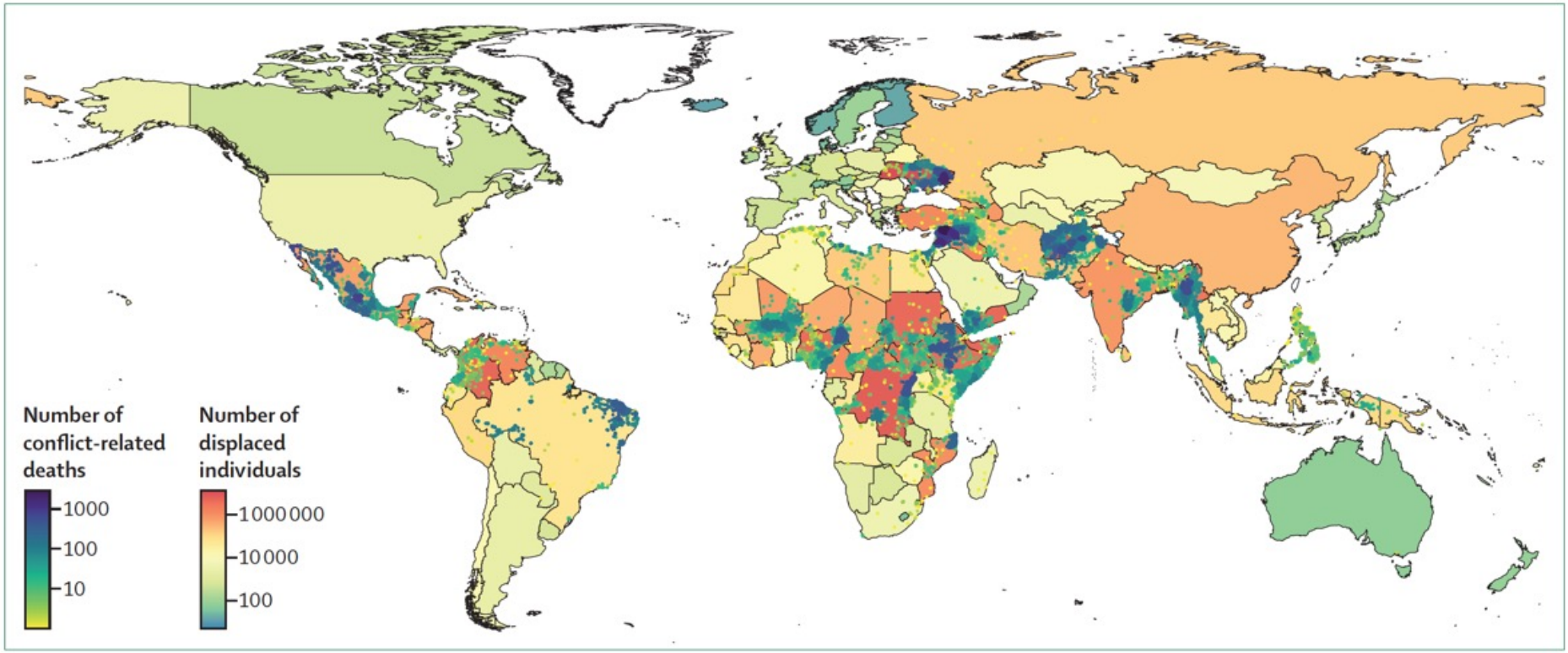

Figure 3: **Number of individuals displaced by country of origin in the most recent year (country shading), and the localisation of events (dots) that were associated with at least 25 battle-related deaths in a year during 2016–22**

Data sourced from Uppsala Conflict Data Program,[93] UN High Commissioner for Refugees,[95] and International Displacement Monitoring Centre.[96]

Women's, children's, and adolescents' health must remain central

To conclude, no matter what phase of the mortality and fertility transition a country is in, adequate investments in the health of women, children, and adolescents should be a clear and consistent priority of governments and development partners. Making and following through on such commitments are essential to secure the future of the current generation and for the strength and resilience of societies overall.[145,213,293] By working collectively across sectors and stakeholders, including civil society, to address systemic barriers and leverage emerging opportunities, major progress can be achieved.

The mid-point assessment of progress of the MDG period, circa 2008, was a case in point. An assessment at that time would have shown similarly discouraging results for many indicators. Although not all targets were eventually reached by 2015, major gains were achieved in the second half of the MDG period, propelled by a strong global commitment and country focus, increased resources, and enhanced accountability mechanisms. This history should inspire confidence that a similar acceleration is possible in the second half of the SDGs. There is an urgent need for a collective focus on RMNCAH and nutrition to prevent backsliding and put the world on course to achieve its commitments to women, children, and adolescents everywhere.

The cellular basis for middle-age spread

Age-specific adipocyte progenitors drive visceral adipose tissue expansion in middle age

Body fat in humans tends to increase in middle age (approximately 40 to 65 years old), with a preferential expansion of visceral adipose tissue (VAT) around internal organs in the abdominal cavity rather than subcutaneous adipose tissue (SAT) that is stored just beneath the skin. This increase in VAT-selective deposits is linked to declines in insulin sensitivity and a heightened risk of metabolic diseases. Total energy expenditure in humans remains relatively stable from ages 20 to 60 years old. However, if caloric expenditure is roughly constant, it is unclear how VAT continues to grow with age. On page 378 of this issue, Wang *et al.* report that a population of adipocyte progenitor cells (APCs) emerges in middle-aged VAT that drives adipogenesis. This APC subpopulation exhibits a high potential for differentiation into adipocytes, which suggests that adipose tissue in middle age is biologically primed for spread.

Distinct adipose progenitor cells emerging with age drive active adipogenesis

INTRODUCTION: Adipose tissue plays a crucial role in regulating various hormonal and metabolic processes and demonstrates substantial compositional and phenotypic plasticity. From middle age to early aging, adults often experience a notable increase in visceral adipose tissue mass. Visceral adiposity is believed to be an important risk factor for various metabolic disorders. The accumulation of adipose tissue occurs through two primary mechanisms: adipocyte hypertrophy and adipogenesis. However, the mechanisms by which early aging contributes to adipose tissue accumulation remain poorly understood.

RATIONALE: Adipogenesis is the process by which new adipocytes are generated through the proliferation and differentiation of adipose progenitor cells (APCs). Previous reports suggested that APCs exhibit a reduced capacity for adipogenesis in aged humans or rodents in an in vitro, two-dimensional (2D) culture setting. In this work, we used in vivo lineage tracing mouse models, 3D profiling of APC transplants to monitor adipogenesis of APCs up to middle age, and single-cell RNA sequencing to identify distinct types of APCs generated during this life stage. Functional assessments of these age-specific APCs provide insights into how adipogenesis contributes to visceral adipose tissue accumulation during middle age and early aging.

RESULTS: At 12 months old, male mice gained body weight due to increased adipose tissue mass, especially in the visceral site. By contrast, female mice only had moderate body weight gain. Tracking adipogenesis in lineage-tracing mouse models revealed that in contrast to the low turnover rate of adipocytes in young adults, more than 80% of adipocytes were newly generated in the visceral adipose tissue of 12-month-old male mice fed a standard chow diet. Along with this massive adipogenesis, middle-aged mice developed adipocyte hypotrophy, visceral adiposity, reduced energy expenditure, and insulin resistance. 3D profiling of APC transplants quantitatively showed that APCs in middle-aged mice had a much higher adipogenic rate than those in young mice, indicating that these APCs cell-autonomously obtain higher adipogenic potential. Single-cell RNA sequencing of APCs then identified a new committed preadipocyte population that is age enriched (CP-A), both in mice and humans. CP-As displayed high proliferation and differentiation capacities, both in vitro and in vivo. The number of CP-As in the visceral adipose tissue increased-when mice were 9 months old, peaked when they were 12 months old, and then sharply declined when they were 18 months old. Leukemia inhibitory factor receptor (LIFR) was identified as a functional marker of CP-A. Pharmacological inhibition and genetic manipulations indicated that LIFR is indispensable for CP-A adipogenesis. The inhibition of LIFR did not affect the adipogenesis of young APCs, indicating that LIFR signaling is specifically required for CP-As. Lastly, chronic treatment with a LIFR inhibitor during early aging prevented the expansion of visceral fat in mice.

CONCLUSION: Integrating in vivo lineage-tracing, 3D profiling of transplants, and single-cell RNA sequencing, our work reveals that adipogenesis of APCs contributes greatly to the visceral adipose tissue expansion during middle age. The discovery of CP-A as an age-specific APC population, along with the validation of its high adipogenic capacity both in vitro and in vivo, and the identification of LIFR signaling as a CP-A–specific adipogenic mechanism enhance our understanding of the early aging process in fat tissue. A key finding from our work is that despite the low turnover rate of adipocytes in young adults, adipogenesis is unlocked during middle age. The increase of adipogenic capacity in APCs distinguishes these cells from most other adult stem cells, which typically exhibit a reduced capacity to proliferate and differentiate with age. Moreover, as the enhancement of adipogenesis and emergence of the CP-A population happens primarily in the male visceral adipose tissue and only during middle age and early aging, these events are location, stage, and sex specific. Our findings offer a fundamental understanding of the pathophysiology of age-related metabolic disorders, which may have critical implications for preventing and treating age-related diseases, thereby promoting healthy aging.

The Leukemia Inhibitory Factor Receptor (LIFR) is a transmembrane protein that serves as the receptor for the leukemia inhibitory factor (LIF) and other cytokines like oncostatin M, ciliary neurotrophic factor, and cardiotrophin-1.

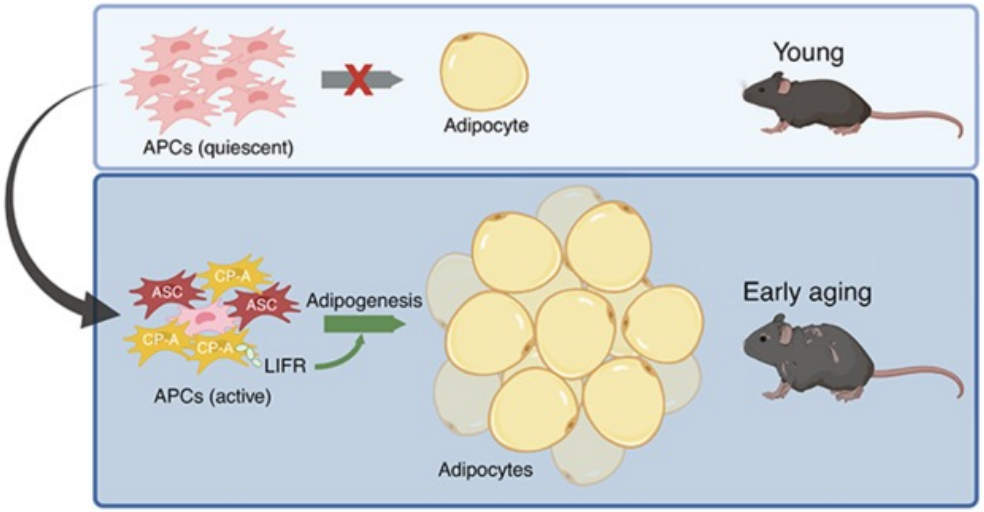

Adipogenesis contributes to age-related visceral adipose tissue accumulation. Male mice gain a large amount of body weight during middle age owing to increased visceral adipose tissue mass. APCs in young adult mice exhibit low adipogenesis activity unless stimulated by metabolic stresses. However, adipogenesis in visceral adipose tissue becomes markedly active during middle age. APCs from middle-aged mice display a cell-autonomous increase in adipogenic potential, generating a distinct committed preadipocyte population that is age enriched (CP-A). CP-As possess high proliferation and differentiation capabilities. LIFR serves as a functional marker that is essential for CP-A adipogenesis. ASC, adipocyte stem cell. [Figure created with BioRender.com]

At 77, she's as fit as a 25-year-old. What her body tells us about aging.

158 cm; 43 kg; BMI 19
Marathon 42,2 km.
Zeit 3,5 h.

Rice is 5 feet 2 inches tall and weighs 95 pounds. Her physiology is so striking that her maximal oxygen uptake (VO_2 max) — a measure that reflects her aerobic fitness and endurance capacity — equals that of a 25-year-old woman, according to lab tests in the days after her World Record performance (3 hours, 33 minutes and 27 seconds) in last year's London Marathon.

The tests were part of a case study of Rice published in the Journal of Applied Physiology.

Researchers are studying Rice to understand how humans can stay fit as they age, regardless of natural ability and the reduced physical activity often seen in older people, said Bas Van Hooren, assistant professor in nutrition and movement sciences at Maastricht University in the Netherlands and one of the study authors.

Among numerous tests, Van Hooren and Michele Zanini, then a doctoral researcher at Loughborough University (now a lecturer in exercise science at the Open University in England) had Rice run on a treadmill with increasing intensity while measuring her oxygen consumption and heart rate. They also drew blood to assess levels of lactate, a chemical produced when cells break down carbohydrates.

Lactate levels can be used to assess the transition from a "sustainable" effort to a "more strenuous" one, Van Hooren said. Researchers also analyzed body fat, muscle structure and capacity to use oxygen at her specific marathon running speed.

They found that Rice's "exceptional" VO2 max suggested "outstanding" cardiovascular fitness, pointing out — for comparison purposes — that the VO2 max of most untrained women between ages 70 and 79 typically is 45 percent to 65 percent lower than that of Rice.

"Her unique physiology allows her to be extremely competitive in any distance running event from the track to the road, a rare feat at the world-class level," Zanini said.

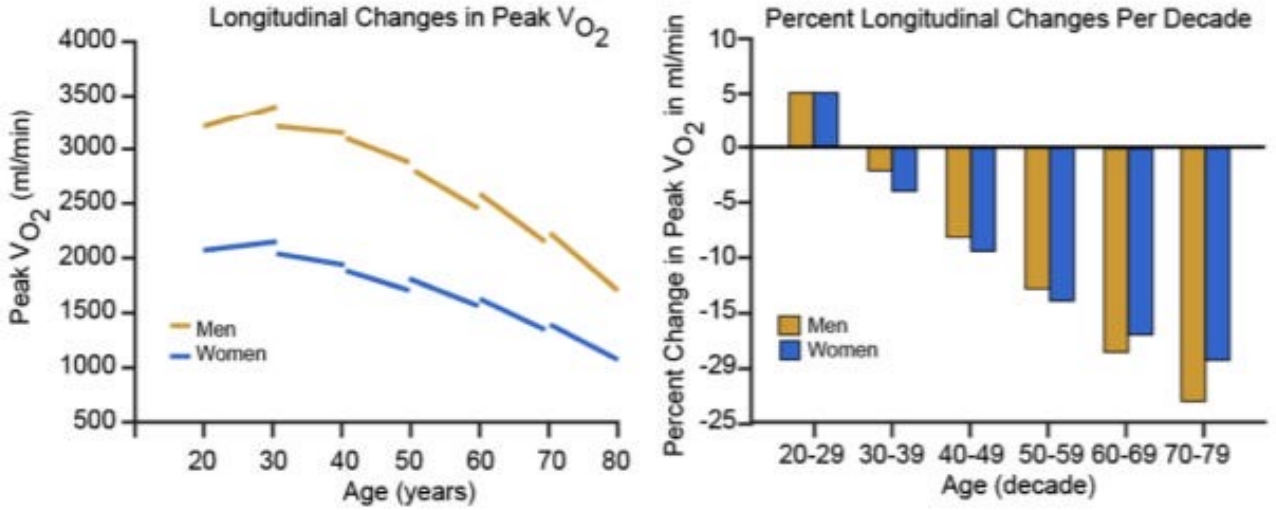

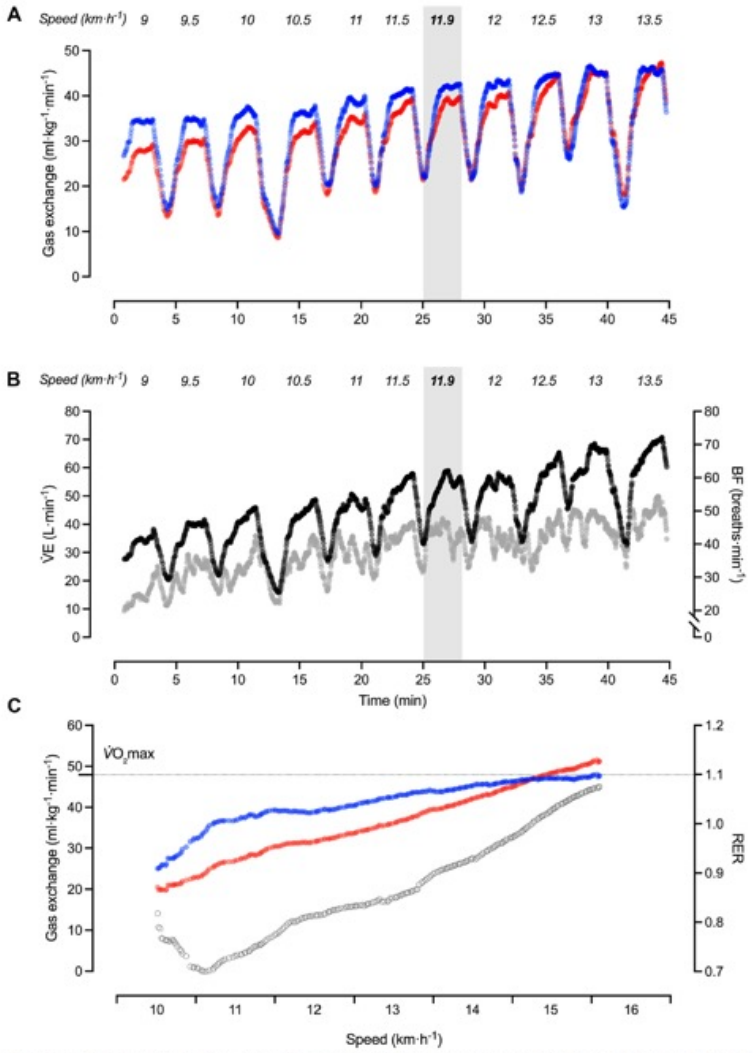

Figure 1. Physiological response during the laboratory submaximal (*A* and *B*) and maximal assessments (*C*). The dots indicate: $\dot{V}O_2$ (blue), $\dot{V}CO_2$ (red), ventilation ($\dot{V}E$; black), breathing frequency (BF; light grey), and respiratory exchange ratio (RER; open black). In *A* and *B*, the speed corresponding to each stage is indicated above the graphs, with the speed of the marathon world record in bold and highlighted in light gray. In *C* the dotted line represents the highest 30 s $\dot{V}O_2$ average during the test.

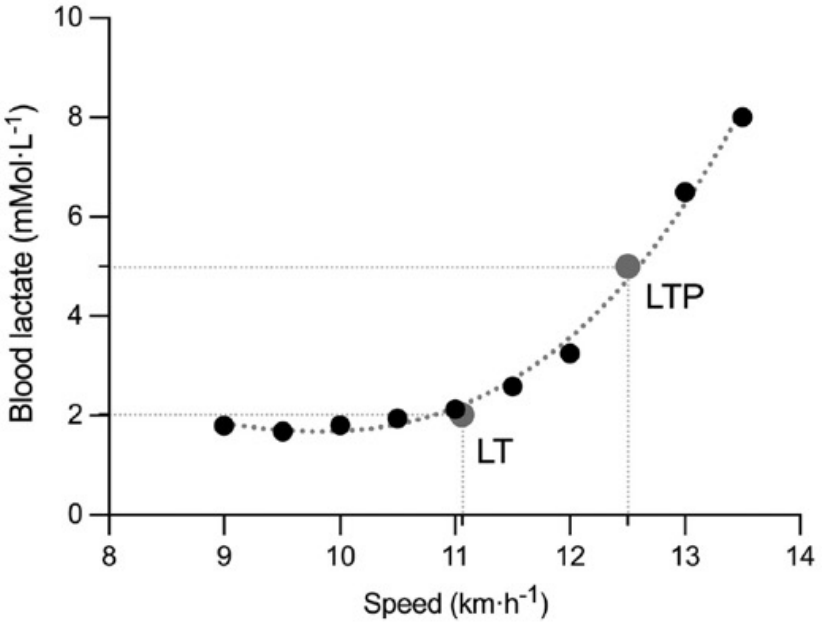

Figure 2. Blood lactate (BLa) accumulation during the submaximal test. The black dots indicate lactate samples collected; the dotted line depicts the third-order polynomial regression on the lactate samples; and the gray dots highlight the speed and BLa corresponding to lactate threshold (LT) and lactate turnpoint (LTP).

VO_2max was 47.9 mL·kg 1·min 1, and HRmax was 180 beats·min 1.
(about 2000 ml/min)